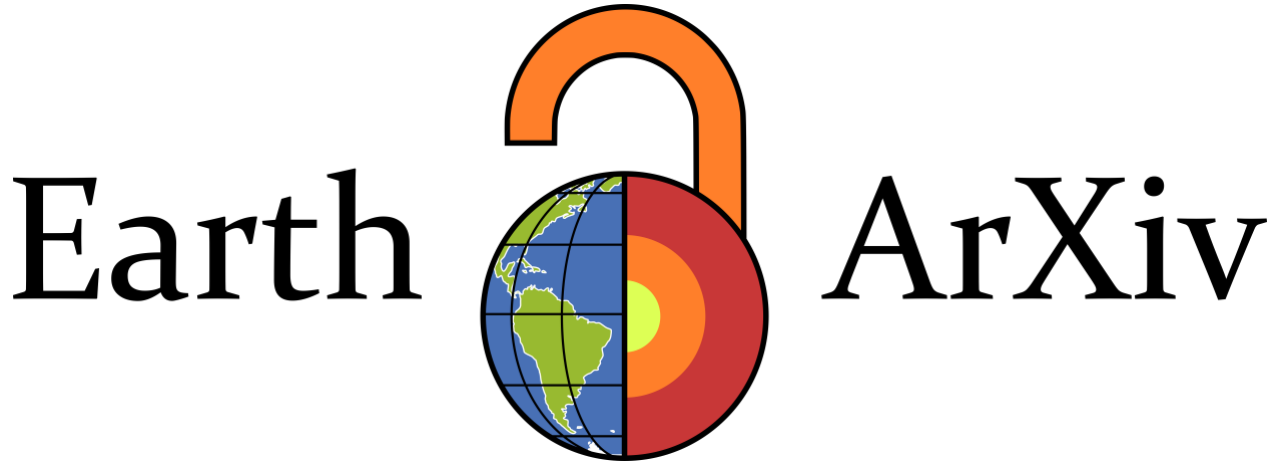

Last Interglacial shoreline successions in southeastern Australia: A framework for identifying a waning mantle upwelling, neotectonic movements and sea-level change

Nicolas Flament[1] and Colin V. Murray-Wallace[1]

[1]Environmental Futures, University of Wollongong, Northfields Avenue 2522 Australia

Highlights:

- MIS 5e sea level reached 4 ± 1 m above present sea level in southeastern Australia.
- There is no evidence for two sea-level peaks during MIS 5e times in southeastern Australia.
- Elevated Tasmanian MIS 5e successions relate to the waning Cosgrove mantle upwelling.
- Volcanism caused differential uplift of the Woakwine Range, on the Coorong coastal plain since MIS 5e times.
- Neotectonic movements are evident on Fleurieu Peninsula, southern Mount Lofty Ranges.

Abstract

Relict shoreline successions are critically important for investigations of recent tectonism, as they are commonly amenable to dating and may provide information about surface displacement and changes in sea level since their deposition. In this study, Last Interglacial (MIS 5e; 128–116 ka) shoreline successions from 47 locations across southeastern Australia are reviewed. The surface displacement of shoreline successions since their deposition is inferred from their present-day elevation and paleosea levels derived from sedimentary lithofacies and molluscan faunal assemblages. The paleosea levels suggest that marine isotope stage (MIS) 5e sea level peaked at 4 ± 1 m above present sea level in southeastern Australia, about two metres lower than the commonly assumed global sea level maximum. Although this remains to be investigated with models, we speculate that this difference could be explained by glacial isostatic adjustment and topography associated with mantle convection in the region. There is no evidence for two MIS 5e sea-level peaks in paleoshoreline successions from southeastern Australia.

The inferred uplift since MIS 5e is largest in Tasmania (up to 31 m at Stumpys Bay), where it is likely caused by the waning Cosgrove mantle upwelling. Seismic tomographic models and MIS 5e shoreline data suggest that the Cosgrove mantle upwelling is centred presently under northeastern Tasmania, farther east than previously proposed. Volcanism above a steep gradient in lithospheric thickness caused about 10 m of eastward, upward tilt of the Woakwine Range on the Coorong coastal plain since MIS 5e time. On the Fleurieu Peninsula, 6.5 m of upward displacement of the block to the southeast of the Willunga Fault is inferred. In contrast, the Gawler Craton stands out as tectonically stable, with possible limited local subsidence. The careful characterisation of shoreline successions is a powerful way to define subtle geodetic changes.

Keywords

Last Interglacial; MIS 5e; Sea level change; Paleoshoreline successions; neotectonics; mantle plumes; volcanism; stratigraphy; amino acid racemization; residual topography; dynamic topography; coastal landscape evolution

1. Introduction

Australia has traditionally been regarded as a tectonically highly stable continent (Ollier, 1978; Ollier, 1986; Twidale, 2007). Apart from its northern margin, the continent is situated within an intraplate setting, remote from plate boundaries. Indicators of tectonic stability include the absence of recent volcanism, low seismicity, the lowest topographical relief of all continents, deeply eroded fold belts and regionally extensive erosion surfaces, as well as the antiquity of drainage systems, landscapes, relict soils, and regolith. Despite these regionally distinctive landscape characteristics, subtle evidence for neotectonism has been documented from across the continent, particularly in the coastal realm (Gardner et al., 2009; Murray-Wallace and Belperio, 1991; Quigley et al., 2010; Sandiford, 2003; Whitney and Hengesh, 2015).

In a global context, relict shoreline successions and landforms have become increasingly important for investigations of recent tectonism, as they are commonly amenable to dating and may provide critical information about geodetic changes through time, based on well-defined paleosea level indicators and marine oxygen isotope evidence for former sea levels based on ice volumes (Lisiecki and Raymo, 2005). The present-day elevation of relict shorelines indicates the cumulative eustatic and relative sea-level changes since their formation (e.g. Pedoja et al., 2014; Rovere et al., 2023). Paleoshorelines in tectonically active regions have been commonly used to infer rates of tectonic uplift (Bordoni and Valensise, 1999; Chappell, 1974; Saputra et al., 2022) and in tectonically quiescent regions can be used to examine the

92 interplay between eustatic (ice-equivalent) sea-level change and large-scale processes such as
93 glacial isostatic adjustment (GIA) and mantle dynamic topography (Dutton et al., 2015). Here
94 we focus on the Last Interglacial period that corresponds with Marine Isotope Substage 5e
95 (MIS 5e; c. 128–116 ka ago), during which marine foraminifers had lighter $\delta^{18}O$ values (e.g.
96 Shackleton et al., 2002), and eustatic sea level was higher than in the present Holocene
97 interglacial (Hallmann et al., 2021; Muhs, 2022; Murray-Wallace and Woodroffe, 2014),
98 possibly with two sea level peaks during that period (Kopp et al., 2009; Kopp et al., 2013). In
99 this work, the Last Interglacial coastal record for a portion of the southern Australian passive
100 continental margin at the trailing edge of a fast-moving plate is reviewed. A regional data set
101 is used to infer the geographical extent of the Cosgrove mantle upwelling, as well as other
102 processes responsible for neotectonism along the continental margin.

103 Southeastern Australia comprises tectonically quiescent provinces such as the Gawler
104 Craton (Fig. 1), regions presenting neotectonic activity such as the Mount Lofty and Flinders
105 Ranges of the Adelaide Fold Belt (Bourman and Lindsay, 1989; Rajabi et al., 2017; Sandiford,
106 2003; Fig. 1) or volcanic activity between ~7.9 Ma and ~800 ka in the Newer Volcanic
107 Province (Heath et al., 2020) and as recently as ~5,000 years ago at Mount Gambier and Mount
108 Schank (Barbetti and Sheard, 1981; Murray-Wallace, 2011; Robertson et al., 1996). This
109 volcanic activity is located close to the southern termination of Earth's longest continental
110 hotspot track (Davies et al., 2015). The Cosgrove hotspot track links volcanic centres
111 presenting decreasing ages (from ~33 Ma to ~9 Ma) over ~2,000 km from north to south, which
112 is consistent with reconstructed motions of the Australian plate over a stationary mantle
113 upwelling (Davies et al., 2015).

114 The elevation of Last Interglacial shoreline successions in southeastern Australia has been
115 studied extensively (e.g., Gardner et al., 2009; Goodwin et al., 2023; Kiernan and Lauritzen,
116 2001; Murray-Wallace, 2002), making it possible to investigate the relationship between

117 tectonic or geodynamic environments and paleoshoreline elevations across different geological
118 provinces. Besides the confident identification and dating of these sedimentary successions,
119 sufficient time has elapsed since their deposition to quantify even slow rates of geodetic
120 change.

121 The geotectonic processes responsible for the differential elevations of Last Interglacial
122 coastal successions in southeastern Australia, and their inferred paleosea levels are reviewed
123 in this work. Accordingly, several attributes are explored to identify the basis for differential
124 paleoshoreline elevations, including earthquake and fault data, the distribution of volcanism at
125 the continental scale, as well as continental-scale models of crustal and lithospheric thickness,
126 and residual and dynamic topography. A representative value for ice-equivalent MIS 5e sea
127 level is also defined for the region. This synthesis is based on our previously published
128 research, as well as our more recent field observations, integrated with the wider literature.

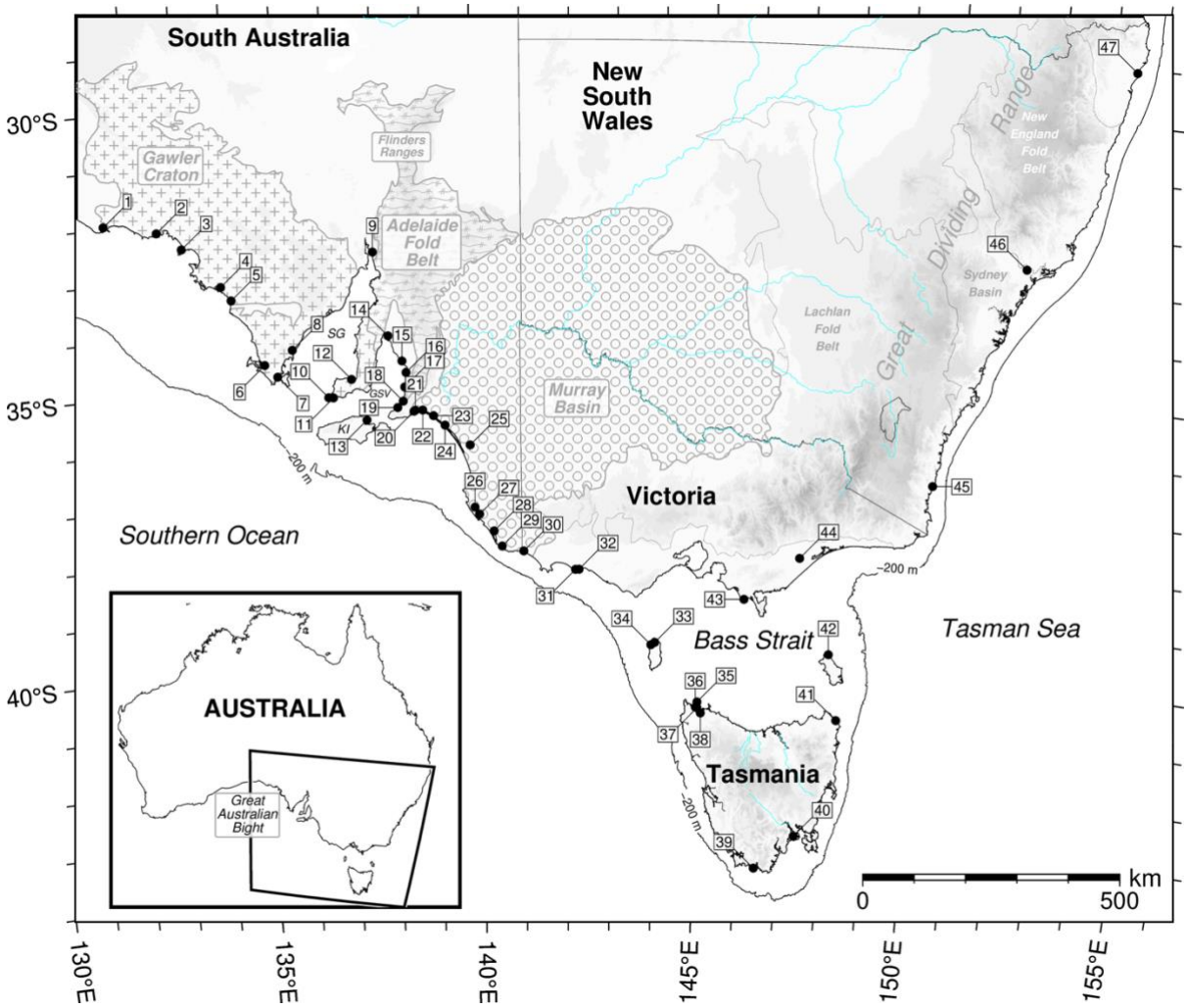

Figure 1. Locations of Last Interglacial shoreline successions in southeastern Australia reviewed in this work. Digital Elevation Model (Geoscience Australia, 2019) and Last Interglacial shoreline successions at 47 locations (Table 1): 1. Fowlers Bay, 2. Tourville Bay, 3. Smoky Bay, 4. Venus Bay, 5. Lake Newland, 6. Coffin Bay, 7. Port Lincoln, 8. Tumby Bay, 9. Redcliff, 10. Pondalowie Bay, 11. Marion Lake, 12. Point Turton - Hardwicke Bay, 13. Rolls Point (Kangaroo Island), 14. Port Wakefield, 15. Port Gawler, 16. Port Adelaide, 17. Port Stanvac, 18. Sellicks Beach, 19. Normanville, 20. Chiton Rocks, 21. Victor Harbor, 22. Hindmarsh Island, 23. Mark Point, 24. Bonney Reserve, 25. Salt Creek, 26. Lake Hawdon South, 27. McCourt Cutting (Woakwine Range), 28. Lake Bonney, 29. Nene Valley, 30. Nelson, 31. Goose Lagoon, 32. Warrnambool, 33. Egg Lagoon (King Island), 34. Yellow Rock River (King Island), 35. Robbins Island, 36. Montagu, 37. Mowbray Swamp, 38. Broadmeadows, 39. New River Lagoon Sea Caves, 40. Mary Ann Bay, 41. Stumpys Bay, 42. North East River (Flinders Island), 43. Liptrap, 44. Sale, 45 Gillard's Beach, 46. Largs, 47. Evans Head. The Gawler Craton, Adelaide Fold Belt, Murray Basin regions are shown in grey with symbols and thick outlines, and the Lachlan Fold Belt, Sydney Basin, and New England Fold Belt regions are outlined with thin dotted black lines, all at the 1:5 million scale (Blake, 1998). State boundaries are shown as thin dark grey lines. Main rivers are shown in cyan, and the -200 m isobath (GEBCO Compilation Group, 2020) is shown as a black line. 'GSV': Gulf St Vincent; 'KI': Kangaroo Island; 'SG': Spencer Gulf. The inset shows the map area in the context of Australian coastlines.

Table 1. Locations, age, upper bounding surface elevation, inferred paleosea level, inferred surface displacement and paleosea level indicator for Last Interglacial shoreline successions in southeastern Australia. Paleosea levels are inferred from sedimentary facies. Last interglacial shoreline elevations and inferred paleosea levels APSL (m) are based on molluscan fossil assemblages. 'APSL': above present sea level; 'SA': South Australia; 'VIC': Victoria; 'TAS': Tasmania; NSW: New South Wales.

Location number and name	Latitude and Longitude	Age	Elevation of upper bounding surface of sedimentary unit (m APSL)*	Inferred MIS 5e sea level (m APSL)	Inferred surface displacement (m)	Paleosea level indicator	Reference
1. Fowlers Bay, SA	S31°57'06.9" E132°20'40.6"	113±8 ka U-Series‡	0.16	2.1±0.5	-1.74	Relict back-barrier lagoonal sandflat facies with *Katelysia rhytiphora* and *Anadara trapezia*†	Murray-Wallace et al. (2016)
2. Tourville Bay, SA	S32°08'14.5" E133°25'52.0"	MIS 5e AAR#	2.55	4±0.5	2.55	Relict intertidal sandflat facies with *Katelysia rhytiphora* and *Anadara trapezia.*†	Belperio et al. (1995); Murray-Wallace et al. (2016)
3. Smoky Bay, SA	S32°27'31.4" E133°55'24.4"	MIS 5e AAR	1.9	3.4±0.5	1.3	Intertidal to shallow subtidal mud flat facies with *Katelysia* sp., *Batillaria* sp.	Murray-Wallace et al. (2016)
4. Venus Bay, SA	S33°10'09.8" E134°40'55.7"	Correlation by litho- and biostratigraphy	2.0	3.5±0.5	1.5	Intertidal shelly facies beneath calcrete	Belperio et al. (1995)
5. Lake Newland, SA	S33°25'13.4" E134°52'55.8"	112±10 ka U-Series‡ *Anadara trapezia* MIS 5e AAR	1.9	3.5±0.5	1.4	Intertidal lagoon facies with *Anadara trapezia*† and *Katelysia* sp. beneath calcrete	Murray-Wallace et al. (2016)

6. Coffin Bay, SA	S34°35’55.80” E135°30’9.08”	Correlation by litho- and biostratigraphy	2.0	3.5±0.5	1.5	Intertidal shelly sandflat facies beneath calcrete	Belperio et al. (1995)
7. Port Lincoln, SA	S34°49’5.70” E135°45’51.44’	Correlation by litho- and biostratigraphy	1.0	2±0.5	-1	Intertidal shelly sands beneath calcrete	Belperio et al. (1995)
8. Tumby Bay, SA	S34°21’39.12” E136°6’24.36”	Correlation by litho- and biostratigraphy	0.5	2±0.5	-1.5	Intertidal shelly sands beneath calcrete	Belperio et al. (1995)
9. Redcliff, northern Spencer Gulf, SA	S32°41’39.38” E137°54’2.78”	Correlation by litho- and biostratigraphy	2.0	4±1	2	Intertidal to shallow subtidal facies with *Anadara trapezia*† and *Marginopora vertebralis*† in Redcliff Core Red 51.	Belperio et al. (1995)
10. Pondalowie Bay, SA	S35°13’58.0” E136°49’53.0”	Correlation by litho- and biostratigraphy	1.5	4±1	1.5	Shallow subtidal facies with *Eucrassatella* sp., *Venerupis* sp., and *Thalotia* sp., beneath calcrete	This study
11. Marion Lake, SA	S35°14’28.10” E136°56’6.70”	Correlation by litho- and biostratigraphy	2.5	4±1	2.5	Intertidal shelly facies beneath calcrete	Belperio et al. (1995)
12. Point Turton, Hardwicke Bay, SA	S34°55’47.8” E137°20’26.5”	127.3±2.1 to 115±5.4 ka U-Series & AAR	2.9	4.8±1	3.7	Upward deepening transition from intertidal to shallow subtidal facies with *Batillaria* sp., *Katelysia* sp., and *Amesodesma angusta*.	Pan et al. (2018)
13. Rolls Point, Kangaroo Island, SA	S35°39’37.59” E137°38’3.35”	122±1 ka U-Series	3.4	3.1±0.04	2.5	Shingle beach facies	Nicholas et al. (2019)
14. Port Wakefield, SA	S34°11’10.9” E138°09’24.3”	MIS 5e AAR	3–4.6	3±1	3.6	Top of laminar calcrete on gravel beach ridges with *Anadara trapezia.*†	Murray-Wallace and Belperio (1991); Belperio et al. (1995)
15. Port Gawler, SA	S34°38’21.93” E138°26’11.94”	Correlation by litho- and biostratigraphy	2.0	3±0.5	1	Shelly intertidal facies beneath calcrete	Belperio et al. (1995)

16. Port Adelaide, SA	S34°50'53.27" E138°30'55.45"	Correlation by litho- and biostratigraphy	-1.2–2.1	2±0.5	0.1	Intertidal shelly sands beneath calcrete	Ludbrook (1976)
17. Port Stanvac, SA	S35°6'8.18" E138°28'36.74"	Correlation by litho- and biostratigraphy	3.8	4±1	3.8	Intertidal to shallow subtidal shelly facies beneath calcrete	Belperio et al. (1995)
18. Sellicks Beach, SA	S35°21'09.8" E138°26'07.5"	MIS 5e AAR	5.5	4±1	5.5	Bevelled platform surface with overlying fossiliferous shingle-gravel beach facies	Murray-Wallace and Bourman (2002)
19. Normanville, SA	S35°27'43.54" E138°18'34.27"	MIS 5e AAR	12	4±1	12	Shelly embayment fill facies	Bourman et al. (1999)
20. Chiton Rocks, SA	S35°32'10.0" E138°39'39.6"	MIS 5e AAR	8.0	3±1	7	Relict estuarine facies with *Anadara* sp.†	Murray-Wallace et al. (2010)
21. Victor Harbor, SA	S35°31.33'.43" E138°41'15.40"	MIS 5e AAR	6.0	3±1	5	Relict estuarine facies with *Anadara* sp.†	Murray-Wallace et al. (2010)
22. Hindmarsh Island, SA	S35°31'12.31" E138°50'56.49"	MIS 5e AAR	1.0	3±0.5	0	Estuarine intertidal facies with *Katelysia scalarina* beneath calcrete	Murray-Wallace et al. (2010)
23. Mark Point, SA	S35°37'37.01" E139°4'45.27"	MIS 5e AAR	1.9	3±0.5	0.9	Planar and trough cross bedded lower foreshore facies with *in situ Donax deltoides*	Murray-Wallace et al. (2010)
24. Bonney Reserve, SA	S35°47'58.72" E139°19'19.16"	Correlation by litho- and biostratigraphy	3.8	3±0.5	2.8	Planar and trough cross bedded lower foreshore facies with *in situ Donax deltoides*	(Bourman et al., 2000)
25. Salt Creek, SA	S36°09'40.1" E139°51'30.6"	MIS 5e AAR	4.6	3±0.5	3.6	Relict beach facies of Woakwine Range with transported *Anapella* sp.	Murray-Wallace and Cann (2007); Murray-Wallace (2018)
26. Lake Hawdon South, SA	S37°15'44.4" E139°56'10.7"	MIS 5e AAR	5–7.0	3±0.5	6	Back-barrier intertidal to subtidal lagoon facies of Woakwine Range	Murray-Wallace (2018)
27. McCourt Cutting, Woakwine Range, SA	S37°15'43.8" E139°56'12.6"	117±8 ka TL MIS 5e AAR	6.4 to 11.6	3±0.5	11.6	Transgression from 6.4 to 11.6 m APSL. Upper surface of back-barrier lagoon facies with	Murray-Wallace et al. (1999)

						articulated *Katelysia* sp. in growth position.	
28. Lake Bonney, SA	37°41'24.45" E140°20'58.22"	Correlation by litho- and biostratigraphy	13	3±0.5	12	Intertidal shelly facies beneath calcrete of Glanville Formation	Murray-Wallace et al. (1996a)
29. Nene Valley, SA	S37°59'55.04" E140°33'42.86"	Correlation by litho- and biostratigraphy	18	≥3±1	17	Top of shelly facies of Glanville Formation	Murray-Wallace et al. (1996a)
30. Nelson, VIC	S38°2'58.92" E141°0'25.42"	Correlation by litho- and biostratigraphy	4	3±0.5	3	Lithified Intertidal shelly sands	Murray-Wallace et al. (1996a)
31. Goose Lagoon, VIC	S38°22'50.30" E142°9'52.19"	101±2.6 ka U/Th 110±17 ka Pa/Th MIS 5e by AAR	3.7–4.2	3±1	3.2	Intertidal to shallow subtidal molluscan shell bed with *Katelysia rhytiphora* and *Batillaria (Zeacumantus) diemenensis*	Sherwood et al. (1994)
32. Warrnambool, VIC	S38°22'42" E142°14'34"	Correlation by Litho-and Biostratigraphy	7.5	3±1	6.5	Marine molluscs including *Ninella torquata* in Port Fairy Calcarenite immediately above a shore platform cut on Port Campbell Limestone	Gill (1988)
33. Egg Lagoon, King Island, TAS	S39°39'22.87" E143°58'34.88"	MIS 5e AAR & ESR	6	4±1	6	Intertidal to shallow subtidal shelly sands with *Katelysia rhytiphora* and *K. scalarina*	Murray-Wallace and Goede (1995)
34. Yellow Rock River, King Island, TAS	S39°41'58.46" E143°53'32.07"	MIS 5e AAR and ESR^	3.5	4.5±0.5	4	Intertidal to shallow subtidal bioclastic shelly sands with *Katelysia rhytiphora* and *K. scalarina*	Murray-Wallace and Goede (1995)
35. Remarkable Banks beach ridge plain, Robbins Island, TAS	S40°41'7.87" E144°59'10.28"	OSL	11	5.75±0.5	12.75	Intertidal beach facies seaward of each relict beach ridge	Goodwin et al. (2023)
36. Montagu, TAS	S40°46'39.45" E144°57'9.87"	MIS 5e AAR and ESR	12	4±1	12	Mella Sand, Shallow subtidal embayment fill	Murray-Wallace and Goede (1995)
37. Mowbray Swamp, TAS	S40°47'28.74" E144°59"32.61'	MIS 5e AAR and ESR	12	4±1	12	Mella Sand, Shallow subtidal embayment fill	Murray-Wallace and Goede (1995)

38. Broadmeadows, TAS	S40°52.7'7.49" E145°4'30.56"	MIS 5e AAR and ESR	13	4±1	13	Mella Sand, Shallow subtidal embayment fill	Murray-Wallace and Goede (1995)
39. New River Lagoon Sea Caves, TAS	S43°29'07" E146°35'13"	121.76 +6.07 -5.80 ka U-Series	<10	>3	7	Coastal sourced gravels and shingle beneath speleothem and stalagmite in Bahaus Cave	Kiernan and Lauritzen (2001)
40. Mary Ann Bay, TAS	S42°58'28.18" E147°23'47.75"	MIS 5e AAR and ESR	24.5	≥2	22.5	Lower shoreface sands with shell rich planar cross beds	Murray-Wallace and Goede (1995)
41. Stumpys Bay, TAS	S40°53'39.08" E148°13'26.59"	Inferred MIS 5e	32	3±1	31	Relict quartz beach ridges of the Stumpys Bay Sand	Bowden and Colhoun (1984)
42. North East River, Flinders Island, TAS	S39°44'43.36" E147°57'22.53"	MIS 5e AAR and ESR	4.5	4±1	4.5	Intertidal to shallow subtidal bioclastic shelly sands with *Katelysia rhytiphora* and *K. scalarina* and *Batillaria (Zeacumantus) diemenensis*	Murray-Wallace and Goede (1995)
43. Liptrap, VIC	S38°50'48.69" E145°58'30.89"	OSL	7.25	(3.45±1)	6.7	(Average of sea level at all other locations)	Gardner et al. (2009)
44. Lake Wellington Main Drain, West of Lake Melanyara, Sale, VIC	S38°04'35" E147°10'45"	125 ka on *Neotrogonia* sp. U-Series	7.6	3±1	6.6	Estuarine shell bed with *Ostrea sinuata* and *Anadara trapezia*.	Schornick (1973); Jenkin (1988)
45. Middle Lagoon at Gillard's Beach, NSW	S36°39'02" E150°00'24"	114±15 ka 126±13 ka TL	4.8	3	3.8	Beach facies with cobbles and stringers of pebbles	Young et al. (1993)
46. Largs, Hunter Valley, NSW	S32°42'14.62" E151°36'23.44'	MIS 5e AAR	4–5	5.5±0.5	6.5	Intertidal estuarine shell bed with *Anadara trapezia*†	Thom and Murray-Wallace (1988); Murray-Wallace et al. (1996b)
47. Evans Head, NSW	S28°04' E153°27'	112±9 to 127±18 ka U-Series	c. 0	5±1	1	Corals *Montipora* sp. *Platygyra lamellina* *Acropor a* sp. *Pocillopora damicornis*	Marshall and Thom (1976)

*APSL: above present sea level; ‡Uranium-series ages; † Warm-water indicators, extralimital species; # AAR: amino acid racemization; ^ESR: Electron spin resonance.

2. Geological and geophysical context

2.1. Tectonic setting

Southeastern Australia consists of several geotectonic provinces defined based on their distinctive bedrock and structural characteristics, tectonic history, and regional assemblages of landforms (Murray-Wallace, 2002; Preiss et al., 2002). The Gawler Craton extends across the western study area, covering all of Eyre Peninsula, Spencer Gulf and Yorke Peninsula. The regional bedrock has been tectonically stable since the last deformation event 1.5 Ga ago (Fanning et al., 2007; Preiss et al., 2002). The low relief, gently undulating landscapes of the Gawler Craton have developed on late Archean greenstone belts, high-grade metamorphic rocks and felsic volcanics, and Paleoproterozoic and early Mesoproterozoic orogenic belts subjected to deformation and magmatism (Preiss et al., 2002).

The eastern boundary of the Gawler Craton corresponds with the Torrens Hinge Zone, which defined a transitional area of rifting from the craton to the Adelaide Rift Complex (formerly termed Adelaide Geosyncline) during its depositional history (Preiss et al., 2002). The elongate, north-south trending upland region of the Mount Lofty and Flinders Ranges, defines the limit of a fault-bound, deeply eroded Neoproterozoic–Cambrian age fold belt. The eastern margin of Eyre Peninsula, Spencer Gulf, Yorke Peninsula, Gulf St Vincent, and the Mount Lofty and Flinders Ranges are fault-bound landscapes with notable seismic activity along the regional faults that define these features. The gulfs, peninsulas and the Mount Lofty and Flinders Ranges, represent graben and horst structures respectively. Faults and earthquakes represented at the regional scale reveals that the most significant seismicity occurs in the Adelaide Fold Belt, with some activity in the southeastern part of the mainland, which is well established (e.g., Rajabi et al., 2017; Sandiford, 2003).

The Paleogene–Neogene Murray Basin is an epicratonic marine basin immediately to the east of the Mount Lofty Ranges. The basin fill was initiated some 45 Myr ago during the

separation of Antarctica and southern Australia. The Murray Lakes (lakes Alexandrina and Albert) and River Murray mouth area, adjacent the Mount Lofty Ranges, is a zone of subsidence in the southwestern Murray Basin in response to sediment accumulation within the failed delta area of the River Murray (Murray-Wallace et al., 2010) and uplift farther north associated with reverse faulting of Cambrian Kanmantoo metasedimentary rocks over Miocene limestones and Quaternary fanglomerates on the Millendella Fault (Bourman and Lindsay, 1989). Epeirogenic uplift involving differential tilting is evident across the Coorong Coastal Plain as shown by an emergent series of interglacial coastal barriers having formed over the past 1 Myr (Murray-Wallace, 2018).

The Lachlan Fold Belt (Cambrian to Early Carboniferous), Sydney Basin (Late Carboniferous to Middle Triassic) and New England Fold Belt (Silurian to Triassic) encompass the region from western Victoria to northern New South Wales and define the limit of this investigation. Collectively, these regions confer a high degree of tectonic stability to the coastal landscapes developed within these geotectonic provinces, as illustrated by the absence of emergent shoreline complexes.

2.2. Geological and geophysical data

Digital datasets were used to place last interglacial successions in their geological and geophysical context. Topographical relief was based on continental-scale digital elevation models with resolution ~435 m (Geoscience Australia, 2019) and regional-scale models with resolution ~30 m (NASA JPL, 2013). The location and magnitude of 416 earthquakes between 1973 and 2024 with magnitudes greater than 2.5 were obtained from the Geoscience Australia Earthquake Catalogue (Geoscience Australia, 2024) on 9 September 2024. The magnitude of events was defined using either Richter magnitude (282 events), body wave magnitude (129 events), moment magnitude (four events), or coda magnitude (one event).

Quaternary volcanic formations were represented at the 1:1 million scale (Geoscience Australia, 2012), faults at the 1:2.5 million scale (Raymond, 2023), and the Gawler Craton and Adelaide Fold Belt at the 1:5 million scale (Blake, 1998). The upper surface of the Oligo-Miocene Gambier Limestone was digitised from Figure 4.9 of Murray-Wallace (2018), and the outline of the Mount Gambier uplift was digitised from Figure 9 of Sprigg (1952). Reconstructions of the Cosgrove hotspot track by Davies et al. (2015) and by Seton et al. (2019) were obtained from the corresponding authors of these articles.

Continental crustal thickness was represented by an interpolated discrete global model (Stephenson et al., 2024) at 0.25 degree resolution. Lithospheric thickness was represented using the model of Hoggard et al. (2020), residual topography using the model of Stephenson et al. (2024) and dynamic topography using the model of Davies et al. (2019) that considers the structure of the lithosphere. Sub-lithospheric mantle structure was based on tomographic models PRI-S05 (Montelli et al., 2006), REVEAL (Thrastarson et al., 2024) and UU-P07 (Amaru, 2007).

3. Nature and Age of Last Interglacial coastal successions in southeastern Australia (locations 1–32)

3.1. General context

Last Interglacial coastal sedimentary successions and landforms are particularly well-preserved along the cool water, temperate carbonate realm of southern Australia (Belperio et al., 1995; Murray-Wallace and Belperio, 1991). In this region, extensive pedogenic calcrete development has provided a protective carapace to the underlying fossiliferous carbonate successions, reducing their susceptibility to erosion. Last Interglacial coastal successions occur landward of Holocene coastal complexes and reflect a higher relative sea level than in the present, Holocene interglacial. The intertidal and shallow subtidal, estuarine-lagoonal back-

barrier facies (open ocean coastline), and peritidal sand and mudflat facies (protected gulfs) have been mapped as the Glanville Formation (Belperio et al., 1995). Correlative interdigitated bioclastic carbonate dune facies (aeolianites) have been mapped as the Upper Member of the Bridgewater Formation (Sprigg and Boutakoff, 1953). An overview of the literature on the Pleistocene Bridgewater Formation is provided elsewhere (Murray-Wallace, 2018).

Regionally extensive and emergent coastal sedimentary successions have been described in southeastern Australia for well over a century. Woods (1862; later publishing as Tenison-Woods), Tate (1879a), Tate (1879b), Tate (1882), Howchin (1888) and Greenway and Phillipps (1902) identified distinctive shelly limestones cropping out along extensive sectors of the southern Australian coastline that were potentially of equivalent age and representing an 'upheaval of the land' (Tate, 1879a, p. lxviii). Many workers have since documented the field relationships of numerous occurrences of lithologically and palaeontologically similar sedimentary successions, now assigned to the Glanville Formation (Belperio et al., 1995; Blakemore et al., 2015; Bourman et al., 2016; Ludbrook, 1984; Murray-Wallace and Belperio, 1991; Murray-Wallace et al., 2016; Nicholas et al., 2019; Pan et al., 2021; Pan et al., 2018).

3.2. The Glanville Formation

The Glanville Formation *sensu* Firman (1966) was first described in the Adelaide region of Gulf St Vincent, in an excavation for Fletcher's Graving Dock at Glanville, in the Inner Harbor at Port Adelaide (Howchin, 1888; Ludbrook, 1976; Fig. 1). Within the depth interval of 10.05–11.27 m below the ground surface, the section revealed calcareous sand with a diverse molluscan fauna beneath a prominent calcrete representing the top of the formation and a subaerial exposure surface. Most of the fossil marine mollusc species have modern equivalents. The presence of some extra-limital northern, warmer-water species no longer living in the coastal waters of South Australia, such as the Sydney Blood cockle *Anadara*

trapezia (originally termed *Arca trapezia*; Howchin 1888; Tate, 1882), Shark Bay pearl oyster *Pinctada carchariarum*, the Rosemouth star shell *Astralium rhodostomum*, conical-fusiform gastropod *Euplica bidentata*, and the benthic foraminifers *Marginopora vertebralis* (originally termed *Orbitolites complanata*; Howchin 1888) and *Quinqueloculina polygona*, led several researchers to describe the faunal assemblages as 'Sub-Recent' or 'Sub-fossil' (Howchin, 1888; Ludbrook, 1984; Tate, 1879a). The shallow depth of the formation below present sea level at the Glanville Graving Dock indicates that the Glanville Formation at this locality represents a transgressive succession before the culmination of sea-level rise after the penultimate glacial period (MIS 6). Post-depositional subsidence of the Adelaide Plains since the Last Interglacial may also have contributed to the lower topographical level of the succession (Belperio, 1993).

In the terminology of Sequence Stratigraphy (Coe, 2003), the Glanville Formation represents a parasequence, reflecting the interplay of sediment supply and the production of sedimentary carbonate in relation to changes in accommodation space associated with relative sea-level changes during MIS 5e. In Spencer Gulf and Gulf St Vincent, the base of the Glanville Formation is commonly represented by an unconformable contact (a thin transgressive facies or flooding surface) with underlying Middle Pleistocene alluvial successions such as the Hindmarsh Clay, representing distal alluvial fans of the Mount Lofty and Flinders Ranges (Firman, 1966; Hails et al., 1984). The calcreted top of the Glanville Formation, representing a subaerial exposure surface, is characteristically overlain by contemporaneous Upper Pleistocene or unconformably, by younger successions of the alluvial Pooraka Formation, or coastal facies of the Holocene St Kilda Formation (Bourman et al., 2010; Cann and Gostin, 1985). Marine vibracores from Gulf St Vincent show that the calcrete developed on the upper-most portion of the Glanville Formation dips gently towards the central portion of the gulf, revealing an antecedent topography defined by this calcareous hardground surface, and

285 influencing the geometry of younger Late Pleistocene and Holocene successions (Murray-
286 Wallace et al., 2021).

287 Before the application of geochronological methods, the Glanville Formation was
288 presumed to be of Last Interglacial age based on distinctive warmer-water fossil assemblages
289 and lithological properties not evident in younger successions (Belperio et al., 1995). The
290 Glanville Formation can be traced laterally for over 1,500 km along the coastline of South
291 Australia including Hindmarsh (location 22) and Kangaroo islands (location 13). The western-
292 most location of the formation is at the Head of the Great Australian Bight at Yalata Swamp,
293 where richly fossiliferous shelly limestones containing *Anadara trapezia*, capped by a 23 cm
294 thick calcrete, crop out up to 2 m above present sea level (APSL) (Tate, 1879b).
295

296 **3.3. Gawler Craton to Yorke Peninsula (locations 1–15)**

297 The Glanville Formation occurs from near the modern coastline up to several
298 kilometres inland on depositional coasts, or within coastal cliffs on eroding coasts (Belperio et
299 al., 1995; Bourman et al., 2016; Murray-Wallace, 2018; Pan et al., 2026; Pan et al., 2018). On
300 western Eyre Peninsula, the Glanville Formation occurs as back-barrier estuarine-lagoonal
301 successions and at Fowlers Bay (location 1) was also deposited in the lee of Middle Pleistocene
302 barrier complexes (Murray-Wallace et al., 2016; Figs 2–3). On the northern Adelaide plains,
303 the Glanville Formation indicates minor subsidence of this region associated with the continued
304 neotectonic uplift of the Mount Lofty Ranges to the east, along Range-bounding faults such as
305 the Para Fault and the Eden-Burnside Fault (Belperio et al., 1995; Preiss, 2019). At Sandy Point
306 near the apex of Gulf St Vincent, the top of the Glanville Formation occurs between c. 1.5–2 m
307 APSL. In the Port Wakefield Proof Range area near Sandy Point (location 14), some 10 km
308 south of Port Wakefield, former intertidal flats of the Glanville Formation, up to 600 m wide
309 in cross-section, now represent supratidal environments of the current, Holocene interglacial

(Belperio, 1985; Fig. 4). The relict, calcrete-capped and cemented clay-rich to micrite biocalcarenite sediments are partially karstified. The intertidal flat sediments of the Glanville Formation and the alluvial successions of the Middle Pleistocene Hindmarsh Clay represent an antecedent topography that has severely restricted the space available for the deposition of Holocene coastal sediments within the region.

Figure 2. Detached block (Sample EP#2 of Murray-Wallace et al., 2016) of Last Interglacial Glanville Formation sediment (coquina) at Fowlers Bay, western Eyre Peninsula, southern Australia (location1). Sample EP#2 was collected 7 km inland from the modern coastline, from back-barrier estuarine-lagoonal facies. The back-barrier sediments include a shell assemblage dominated by articulated specimens of the cockle *Katelysia* sp. The general character of the sediment is representative of many back-barrier facies of the Glanville Formation in South Australia.

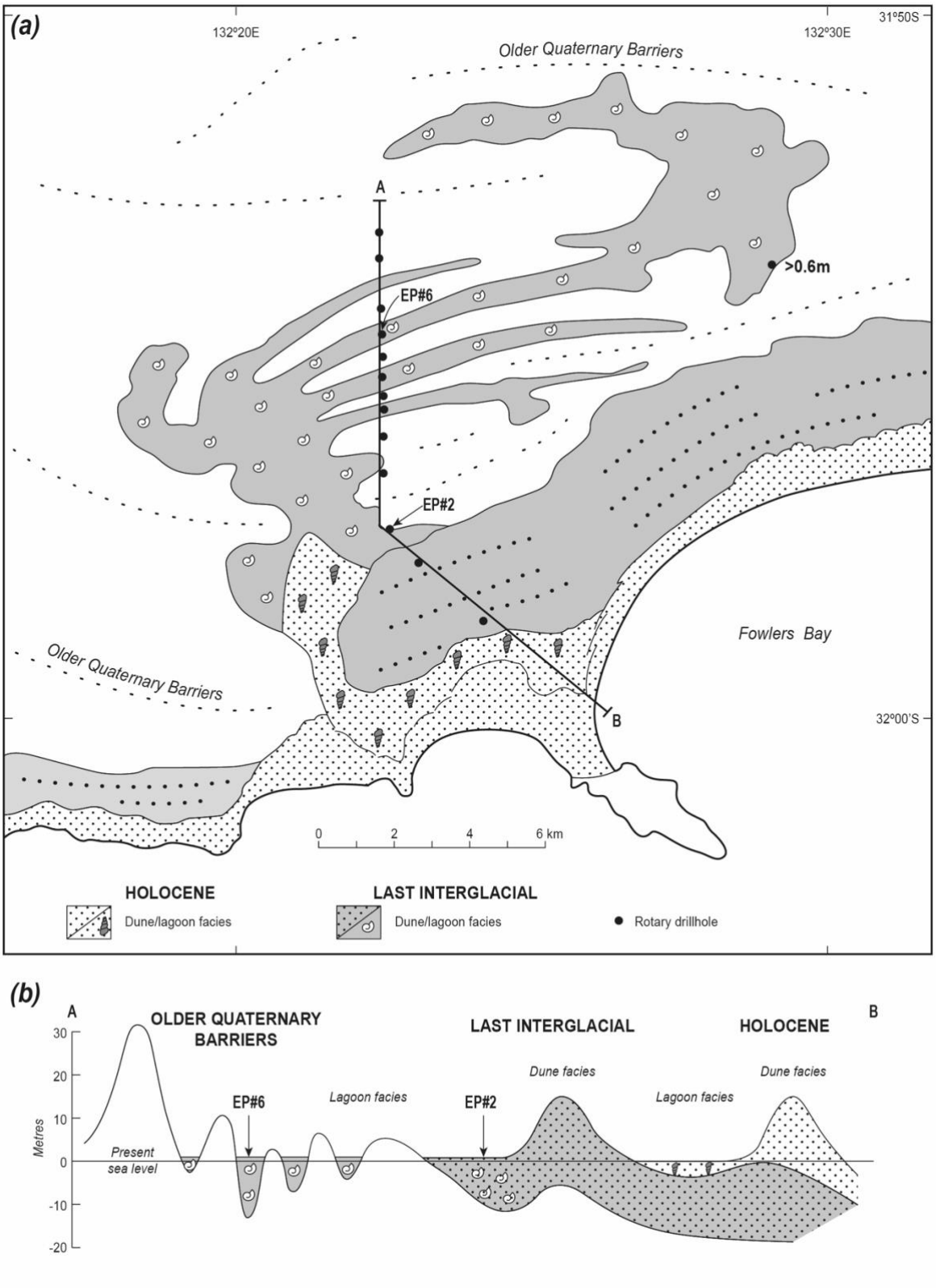

Figure 3. Map (a) and stratigraphical cross-section (b) of Fowlers Bay, western Eyre Peninsula, southern Australia (location 1). Sample EP#2 (Figure 2) is located on the landward side of the Last Interglacial barrier. The higher sea level of the Last Interglacial (MIS 5e) resulted in a marine incursion in the lee of four Middle Pleistocene aeolianite barriers (source: Murray-Wallace et al., 2016; published with the permission of the Geological Society of Australia).

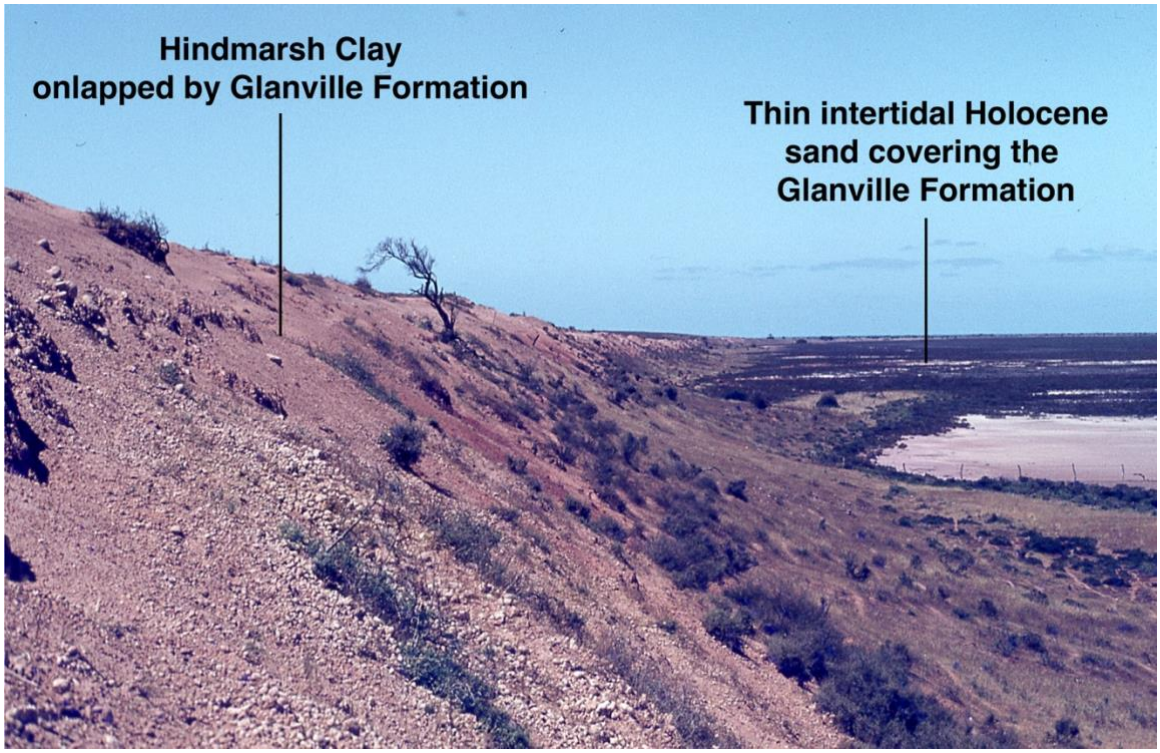

Figure 4. View looking south across relict intertidal flats of the Last Interglacial (MIS 5e) Glanville Formation at Sandy Point (location 14), near the apex of Gulf St Vincent, southern Australia. The modern surface at 1.5 m to 2 m APSL on the right-hand side of the image, represents the landward limit of Holocene supratidal flats, which have formed on the calcreted and karstified pavement surface of the Last Interglacial Glanville Formation. Minimal accommodation space was available for Holocene coastal sedimentation with only a thin sediment veneer covering the Glanville Formation. The backing cliff up to 4 m high has formed on distal alluvial fan sediments of the Middle Pleistocene Hindmarsh Clay (Belperio, 1985). The succession comprises stiff mottled sandy clay with calcrete accumulations.

3.4. Fleurieu Peninsula (locations 16–21) and Coorong Coastal Plain (locations 22–30)

Emergence of the Glanville Formation is evident at several sites on Fleurieu Peninsula. At Sellicks Beach (location 18), an emergent shingle-gravel beach deposit on a marine eroded bench, occurs at a 5.5 m APSL (Murray-Wallace and Bourman, 2002). At Normanville (location 19), 23 km SW of Sellicks Beach, a shelly sand, embayment fill succession occurs at 12 m APSL (Bourman et al., 1999). Emergent coastal successions of MIS 5e age also occur on the eastern side of Fleurieu Peninsula, at Chiton Rocks and Victor Harbor (locations 20–21) occurring at 8 m and 6 m APSL m, respectively. The Glanville Formation with a well-

352 developed calcrete surface above a shell coquina also occurs on Dudley Peninsula, Kangaroo
353 Island (Nicholas et al., 2019; Fig. 5f).

354 Last Interglacial shoreline successions and coastal landforms are particularly well-
355 represented in southern South Australia, extending from the River Murray mouth region
356 adjacent to Fleurieu Peninsula (De Mooy, 1959; Ryan, 2015; Sprigg, 1959), across Hindmarsh
357 Island (location 22; Murray-Wallace et al., 2010) and south-eastwards towards Mount Gambier
358 and Mount Schank (Hossfeld, 1950; Murray-Wallace et al., 1996a; Murray-Wallace et al.,
359 2016; Fig. 1). Along this coastal sector, there is a progressive rise of the surface elevation of
360 the Glanville Formation from 0.17–2.94 m at Goolwa (Ryan, 2015), 1 m APSL on Hindmarsh
361 Island (location 22), 1.9 m APSL at Mark Point (location 23; Fig. 5c), 15 km SE of Hindmarsh
362 Island, 3.8 m at Bonney Reserve (location 24), 4.6 m at Salt Creek (location 25), 5–7 m at Lake
363 Hawdon South (location 26), 6.4–11.6 m at McCourt Cutting (location 27), 13 m at Lake
364 Bonney (location 28), rising to 18 m APSL at Nene Valley (location 29; Murray-Wallace et
365 al., 1996a; Table 1).
366

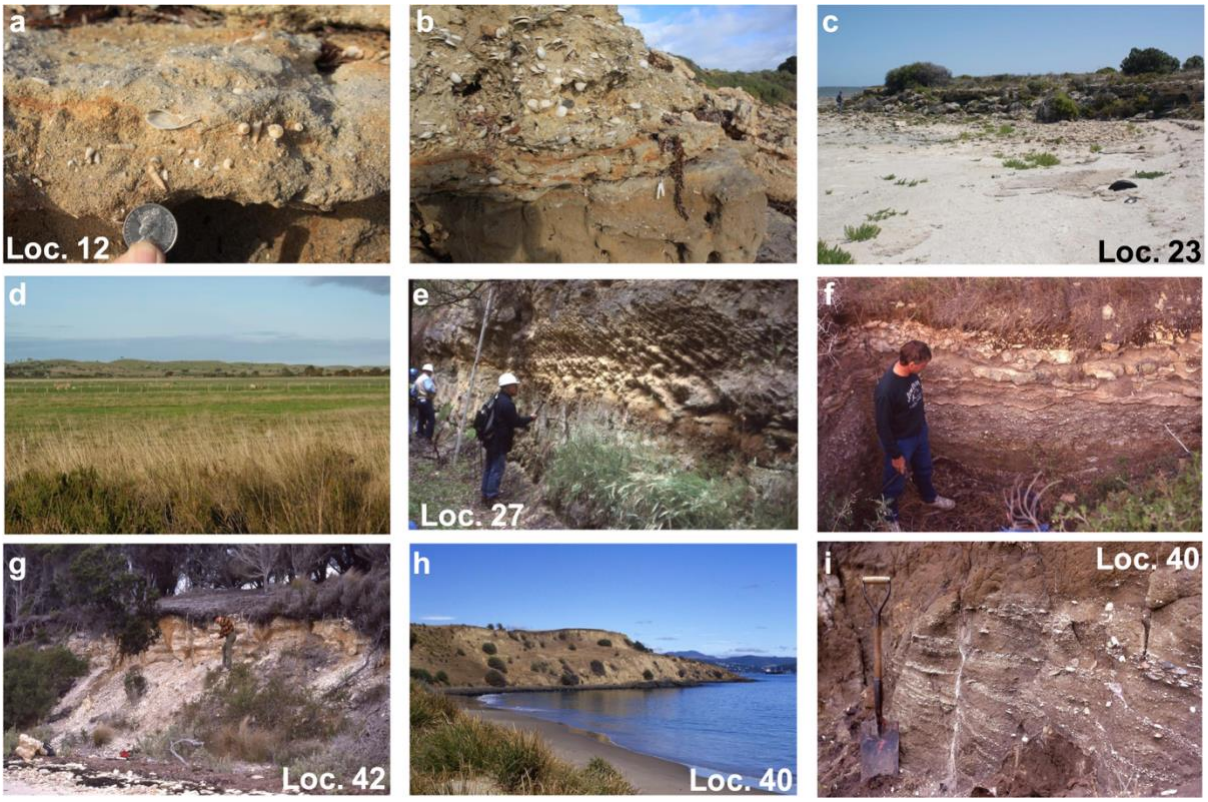

Figure 5. Last Interglacial (MIS 5e; 128–116 ka) coastal sedimentary successions and landforms in southeastern Australia. **a**, Indurated intertidal sandflat facies with the upper-bounding surface evident, Point Turton, southern Yorke Peninsula (location 12). The turreted gastropod *Batillaria (Zeacumantus) diemenensis* in life position, formerly grazing immediately below the sediment-water interface. The former sandflat surface is 2.5 m APSL. **b**, Shallow subtidal shelly facies overlying intertidal sandflat facies approximately 70 m west of photo site 2a at Point Turton. The condensed shell bed represents a mixed concentration of *in situ* articulated and disarticulated bivalve molluscs dominated by *Katelysia scalarina* which frequents the shallow subtidal to lower intertidal zone of sandflats. The succession signifies a relative rise in sea level. The upper bounding surface of the shelly unit is 2.4 m APSL suggesting that sea level reached up to 4.8 ± 1 m APSL at the time of sedimentation. **c**, Strongly indurated, seaward dipping lower- to upper foreshore facies up to 2 m APSL at Mark Point, northern Coorong Lagoon (location 23). The laminar calcrete capped unit crops out on the landward side of the Holocene/modern Coorong Lagoon 18 km SE of the River Murray Mouth. **d**, View looking north towards the landward side of the Woakwine Range, a coastal barrier complex with relict dune surfaces reaching up to 50 m APSL. **e**, Planar cross-bedded (foreset beds) of transgressive aeolian dunes overriding back-barrier estuarine-lagoonal facies in the lee side of the Woakwine Range in the McCourt Cutting near Beachport (location 27). **f**, Small exposure of the Last Interglacial Glanville Formation 2 km east of Pelican Lagoon, Dudley Peninsula, Kangaroo Island, showing an *in situ* shelly assemblage overlain by laminar, blocky and rubbly calcrete. **g**, Shell beds dominated by *Katelysia rhytiphora* overlying oyster mounds at North East River, Flinders Island, Bass Strait, Tasmania (location 42). **h**, Emergent shelly sands up to 24.5 m APSL at Mary Ann Bay, southern Tasmania (location 40). The succession is capped by aeolian sands and overlies a bench on Jurassic dolerite. **i**, Detail of the low angle planar cross-stratified shelly sands at Mary Ann Bay (location 40), with whole, disarticulated valves of the molluscs *Pecten meridionalis* and *Fulvia tenuicostata*.

3.5. The Woakwine Range (locations 22–29)

The principal Last Interglacial coastal landform in this region is the Woakwine Range, a partially lithified coastal barrier which extends uninterrupted along the landward side of the Coorong Lagoon (Fig. 5d-e). The dune range is a prominent structure (30–35 m high and 1–2 km wide) extending southeasterly for over 370 km from the River Murray mouth area to Nelson in western Victoria (locations 22 to 30; Murray-Wallace et al., 1996a). To the south of Mount Gambier, the barrier was termed the MacDonnell Range by Sprigg (1952) and has been dated to 124±10 ka by OSL on quartz sand (Blakemore et al., 2014). The only interruption in the continuity of the Woakwine Range is between Cape Jaffa and Kingston SE, where the dune range bifurcates to form an easterly trending spit or 'hook' (Benson's Hook; Fig. 6). The spit formed within a partially protected marine corridor between the Woakwine Range and Reedy Creek, an older barrier of MIS 7 age, due to longshore drift in the lower wave energy, lee side of the Woakwine Range at southern Lacepede Bay. During the Last Interglacial, a 20–25 km wide marine corridor existed between the actively forming Woakwine Range and the older, more landward and consolidated Reedy Creek Range (MIS 7; Fig. 6). Low-energy estuarine-lagoonal successions containing *Anadara trapezia* were deposited between these dune ranges, representing the *Anadara* High Sea Level of Crocker and Cotton (1946) and (Sprigg, 1952) and correlated here with the Last Interglacial (MIS 5e). The basis for the break in the lateral continuity of the Woakwine Range at southern-most Lacepede Bay remains unresolved, however, it is noted that it coincides with the northern limit of the Paleogene–Neogene Gambier Embayment and may relate to subtle differences in the bathymetry of southern Lacepede Bay.

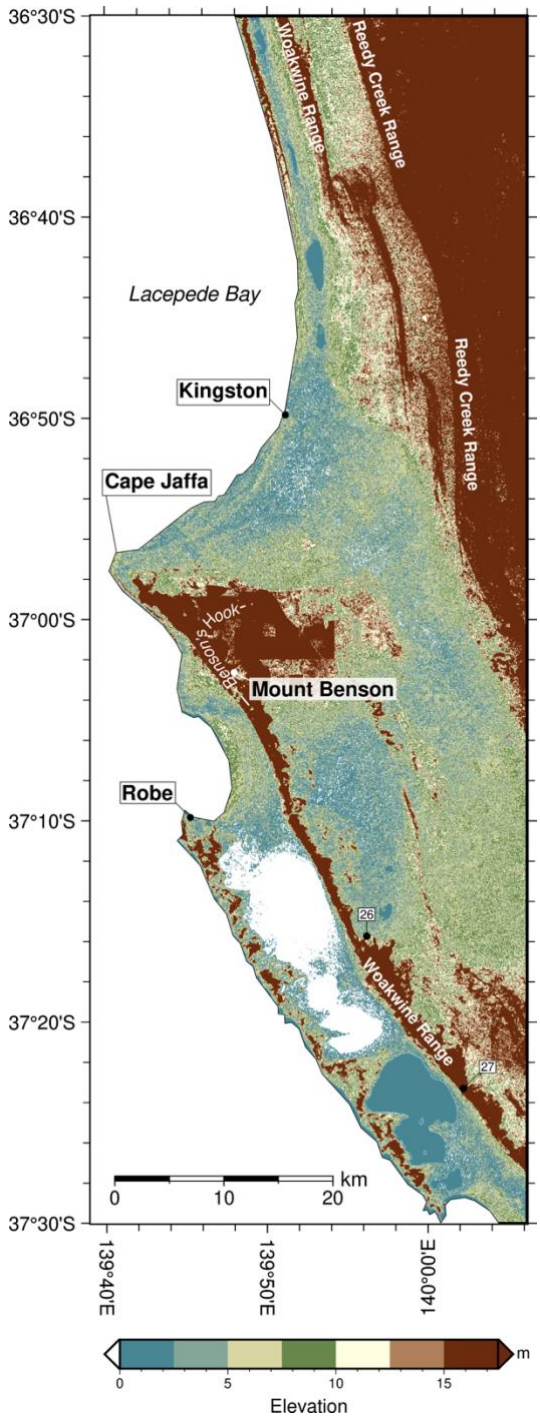

Figure 6. Digital Elevation Model (NASA JPL, 2013) of the Coorong Coastal Plain around Kingston and Robe. The map illustrates a portion of the Last Interglacial coastal barrier, Woakwine Range. The map reveals that the Woakwine Range bifurcates at southern Lacepede Bay with the development of Benson's Hook to the east of Cape Jaffa. Back-barrier estuarine-lagoonal sediments of MIS 5e age, formed between the Woakwine Range, an aeolianite coastal barrier also of MIS 5e age and Reedy Creek, a barrier of MIS 7 age. The former coastal water way was 20–25 km wide.

3.6. Age of the Glanville and Bridgewater Formations in South Australia

The Last Interglacial age of the coastal successions reported in this study, and their correlation with MIS 5e is based on uranium-series dating, thermoluminescence (TL), optically stimulated luminescence (OSL), amino acid racemization (AAR), and electron spin resonance (ESR). The Last Interglacial age of the Glanville Formation has been established from several sites based on uranium-series dating, supplemented by regional correlation using AAR. Daniel (2002) reported a uranium-series age of 124 ± 9 ka on a specimen of the coral *Goniopora* sp., from the Glanville Formation at Flagstaff Landing, Streaky Bay, western Eyre Peninsula. Although the uranium-series dating of fossil marine molluscs remains problematic (Kaufman et al., 1971; McLaren and Rowe, 1996), specimens of the robust cockle, *Anadara trapezia* from Tourville Bay, western Eyre Peninsula (location 2), were dated at 120 ± 10 ka based on multi-collector, inductively coupled plasma mass spectrometry (MC-ICP-MS; Eggins et al., 2005). At Point Turton, southern Yorke Peninsula (location 12), uranium-series ages of 128.3 ± 2.5 ka, 127.3 ± 2.1 ka, and 121.4 ± 2.4 ka have been reported for corals within consolidated bioclastic sands of the Glanville Formation (Pan et al., 2018; Fig. 5a). A uranium-series age of 125 ± 10 ka was obtained on aragonitic fossil molluscs from back-barrier, estuarine-lagoonal sediments of the Woakwine Range near Robe in southern South Australia (Schwebel, 1984).

Luminescence analyses on quartz sands from aeolianite of the Bridgewater Formation have contributed to defining the geographical extent of the Last Interglacial shoreline in southern Australia. Although the analytical precision is lower than more recently derived uranium-series ages, the TL and OSL ages consistently fall within the age range of 132 ± 9 to 117 ± 8 ka (see overview in Murray-Wallace, 2018).

Amino acid racemization has been used for regional stratigraphical correlation, to confirm the time equivalence of geographically widely separated, lithologically similar successions, otherwise presumed to be of Last Interglacial age based on fossil biota and

similarity of morphostratigraphical setting (Murray-Wallace, 2000). Electron spin resonance analyses of fossil shells have been undertaken as an additional framework to evaluate the results of the AAR method (Murray-Wallace and Goede, 1991, 1995).

3.7. Nature and basis for age of MIS 5e successions in Victoria

Correlative stratigraphical successions to the Glanville Formation (MIS 5e) of South Australia have been described from Victoria (Gill, 1988; Jenkin, 1988; Sherwood et al., 1994), New South Wales (Bryant et al., 1997; Murray-Wallace et al., 1996b; Thom and Murray-Wallace, 1988; Young et al., 1993), and Tasmania and the Bass Strait Islands (Bowden and Colhoun, 1984; Goodwin et al., 2023; Murray-Wallace and Goede, 1995; Table 1). Sedimentary successions along the eastern coastline of Victoria and New South Wales are dominantly of terrigenous-clastic origin with few calcium carbonate bioclasts.

Estuarine-lagoonal shelly successions of MIS 5e age indicating a relative sea level of up to 4.2 m APSL, have been described at Goose Lagoon, 13 km west of Warrnambool (location 31), where specimens of the marine gastropod *Turbo* (*Ninella*) *torquatus* were dated at 101±2.6 ka ($^{230}Th/^{234}U$) and 110±17 ka ($^{231}Pa/^{235}U$) and correlated with other MIS 5e shelly successions by AAR (Sherwood et al., 1994). At Warrnambool (location 32), a relative sea level of 7.5 m APSL is indicated by shelly successions within the Port Fairy Calcarenite resting on a shore platform (Gill, 1988).

The Gippsland coastal plain to the east of Wilson Promontory in eastern Victoria, represents an extensive lowland, landward of the arcuate shaped Holocene coastal barrier of Ninety Mile Beach. The region is backed by differentially block-faulted terrain with warped and tilted marine terraces (Jenkin, 1968; Jenkin, 1988). Residual beach sands and gravels within and on terrace surfaces preserve little or no marine fossils. A shell bed exposed in Lake Wellington Main Drain (location 44), west of Lake Melanyara near Sale, containing fossil

478 oysters of *Ostrea sinuata, Anadara trapezia* and *Noetrigonia margaritaea* were dated at 101 ka
479 (average age) based on uranium-series dating (Schornick, 1973). The shelly succession occurs
480 up to 7.6 m APSL.

481 Farther east, Quaternary marine terraces indicating coastal emergence have been
482 described from Cape Liptrap, 47 km NW of Wilson Promontory in Victoria (location 43;
483 Gardner et al., 2009). The marine abrasion platform surfaces range in elevation from 1.2 m
484 APSL at Morgan's Beach, west of Cape Liptrap, to 7.25 m APSL at Walkerville South in
485 Waratah Bay. The NE trending Waratah Fault has differentially elevated the latter shoreline
486 through a scissor movement. This is illustrated by a decrease in shoreline angle, a marine
487 eroded junction between the cliff face and landward limit of the shore platform, in a NE
488 direction from 7.25 m to 3.2 m APSL over 2 km, parallel with the Waratah Fault. Quartz sand
489 from a marine pebble-cobble conglomerate at Walkerville North, 10 km NE of Cape Liptrap
490 was dated at 132±9 ka by OSL and horizontal to wavy bedded fine-grained sands overlying a
491 marine abrasion platform at Morgan's Beach was dated at 122±9 ka by OSL, both successions
492 correlating with MIS 5e (Gardner et al., 2009). The lower terrace elevation at Morgan's Beach
493 may be associated with down-faulting on the western side of a parallel trending fault, 2 km
494 west of the Waratah Fault. Faulting and varied elevations of MIS 5e paleoshoreline successions
495 at Cape Liptrap suggest neotectonic motions since MIS 5e times, which is consistent with
496 seismic activity and the present-day stress field of Australia (Rajabi et al., 2017; Sandiford,
497 2003).

498

499 **3.8. Nature and basis for age of MIS 5e successions in New South Wales**

500 Although coastal barrier landforms are well-developed along sectors of the New South
501 Wales coastline, shell-rich, estuarine successions representing valuable paleosea level
502 information are less common due to removal of former interglacial sedimentary records by

503 fluvial erosion within confined bedrock valleys at times of low sea level (Nichol and Murray-
504 Wallace, 1992). Nevertheless, three critical sites for documenting relative sea level during MIS
505 5e exist in New South Wales, including Gillard's Beach along the southern coastline (location
506 45; Young et al., 1993), Largs, Hunter Valley (location 46; Murray-Wallace et al., 1996b;
507 Thom and Murray-Wallace, 1988) and Evans Head (location 47; Marshall and Thom, 1976).
508 A relict cobble-pebble beach facies at Gillard's Beach (location 45) yielded TL ages of 114±15
509 ka and 126±13 ka, indicating a relative sea level of up to 4.8 m APSL (Young et al., 1993). At
510 Largs (location 46), an MIS 5e estuarine shell bed was deposited near the inland limit of a
511 proto-estuary of the Hunter River some 30 km inland from the present coastline (Thom and
512 Murray-Wallace, 1988). An MIS 5e age is based on AAR dating of *Anadara trapezia* and other
513 fossil molluscs (Murray-Wallace et al., 1996b). At Evans Head (location 47), fossil corals
514 collected from an exposure within a relict coastal barrier were dated at 114±9 to 127±18 ka,
515 suggesting a paleosea level of 5±1 m APSL (Marshall and Thom, 1976).
516

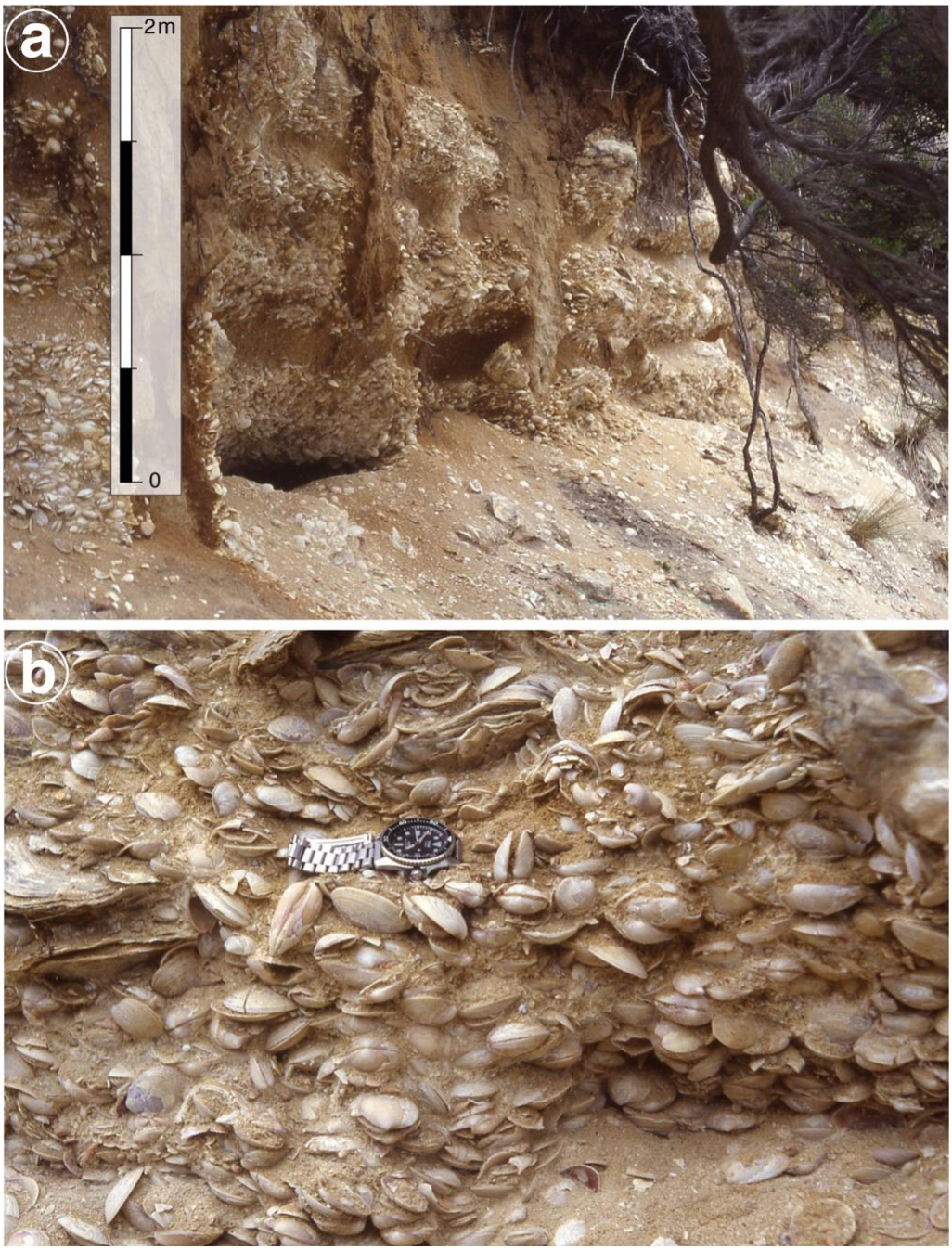

Figure 7. **a**. Last Interglacial (MIS 5e) estuarine-lagoonal sediments exposed in an eroding embankment of the North East River, northern Flinders Island, Bass Strait, Tasmania (location 42). The three shelly successions (photographed in 1990) are dominated by abundant articulated cockles in life position of the shallow water mollusc *Katelysia rhytiphora* interbedded with depauperate sandy beds. *K. rhytiphora* lives gregariously in subtidal waters immediately below low water datum and characteristically form coquina accumulations. The upper bounding surface of the deposit is 4.5 m APSL. A Last Interglacial age has been established by amino acid racemization and electron spin resonance dating (Murray-Wallace and Goede, 1995). The vertical face above the scree is 2 m high. **b**. Detail of a portion of the lowest Last Interglacial shelly succession at North East River, Flinders Island, Bass Strait, featured in **a**. The shelly succession (coquina) is dominated by articulated and *in situ Katelysia rhytiphora* with five individuals of the oyster *Ostrea angasi* also present, both species indicating shallow subtidal conditions at the time of sedimentation.

3.9. Nature and basis for age of MIS 5e successions in Tasmania

Hypothesised last interglacial (MIS 5e) coastal successions in Tasmania include a shallow water, estuarine succession at Mary Ann Bay near Hobart (location 40; Fig. 5h-i), embayment fill successions at Broadmeadows, Montagu and Mowbray Swamp (locations 36–38) on the north-western coastline of the island, and a succession of quartz-rich relict beach ridges at Stumpys Bay (location 41) in north-eastern Tasmania (Bowden and Colhoun, 1984; Colhoun et al., 1982a; Murray-Wallace and Goede, 1991; Murray-Wallace and Goede, 1995; Table 1). Last interglacial successions on the Bass Strait Islands include successions at Yellow Rock River (location 34) and Egg Lagoon (location 33) on King Island (Jennings, 1959; Murray-Wallace and Goede, 1995) and a succession in the North East River Estuary on Flinders Island (location 42; Sutherland and Kershaw, 1971; Figs 5g and 7a-b). Coastal shingle deposits covered by speleothems in relict sea caves at New River Lagoon, SW Tasmania, also indicate a higher relative sea level during MIS 5e and local uplift since that time, as they occur up to 10 m APSL (Kiernan and Lauritzen, 2001).

Several lines of evidence have led to a last interglacial age being inferred for these successions in Tasmania. The elevation of the successions above present sea level (APSL) is generally too high for them to be regarded as Holocene (i.e. typically >11 m APSL). In addition, radiocarbon ages for peat and marl that overlie marine shelly sands, and on fossil molluscs from the coastal successions, yielded ages older than Holocene. In general, radiocarbon dating of the Pleistocene materials yielded ‘finite’ ages close to the practical limits of the radiocarbon method (Colhoun et al., 1982b; Gill and Banks, 1956; Van de Geer et al., 1986). A minimum radiocarbon age of >52 ka (GrN-9743) on peat from Mowbray Swamp (location 37) overlying fossiliferous, shallow marine sands in northwestern Tasmania (Van de Geer et al., 1986) indicates that the previously reported ‘finite’ ages reflect contamination by varying amounts of ^{14}C with a higher activity (yielding a younger apparent age) that could not

556 be removed during sample pre-treatment. Other evidence consistent with a Late Pleistocene
557 age centres on the morphostratigraphical, biostratigraphical and diagenetic character of the
558 strata (Bowden and Colhoun, 1984) in conjunction with records of Late Quaternary glacio-
559 eustatic sea-level changes (Lambeck and Chappell, 2001).

560 A 9.6 m thick succession of tabular cross-stratified shelly sands rests unconformably
561 on an eroded bench of Jurassic dolerite at Mary Ann Bay, South Arm Peninsula (location 40),
562 adjacent to the Derwent Estuary in south-eastern Tasmania (Fig. 5h-i). The shelly sedimentary
563 succession is an erosional remnant of a formerly more widespread shallow subtidal, mixed-
564 quartz bioclastic succession. A distinct partitioning is evident in the cross-stratification
565 represented by higher-energy pulses of whole shells, shell fragments and bioclastic sand,
566 interbedded with quartz sand reflecting lower energy during tidal cycles, and in water depths
567 above fair-weather wave base (Fig. 5i). The shallow subtidal estuarine sands are
568 unconformably overlain by an aeolian cover sand of Last Glacial age, representing part of an
569 undulating dune landscape of South Arm Peninsula.

570 The mollusc-rich succession has long been of interest in view of its physical setting, a
571 stepped coastal cliff which extends up to 24.5 m APSL. The shell-rich succession is significant
572 in terms of the relative sea level and neotectonic history of the region (Bowden and Colhoun,
573 1984; Lambeck and Chappell, 2001; Murray-Wallace and Goede, 1991; Murray-Wallace and
574 Goede, 1995; Van de Geer et al., 1986). The shelly sands contain a thanatocenose assemblage
575 of 49 species of fossil marine molluscs (Colhoun et al., 1982a; Slee et al., 2012), many of the
576 species signifying shallow water deposition in an estuarine environment with good tidal
577 exchange, similar to the modern Derwent Estuary. Some mollusc species are extra-limital in
578 their geographical range, indicating marginally warmer conditions at the site of deposition than
579 prevail today, and are now found in more northerly parts of Tasmania (e.g. *Chlamys aktinos*,
580 *Mactra Jacksonensis*, *Notocallista kingi*, and *Scutellastra chapmani*, Slee et al. 2012). Twelve

581 species of benthic foraminifers as well as the planktonic species *Globigerina bulloides* are
582 present in the shelly succession (Lewis and Quilty, 2009).

583 A Last Interglacial age (MIS 5e) for the shelly successions at Mary Ann Bay has been
584 established based on AAR and ESR dating of the marine molluscs *Fulvia tenuicostata*, and
585 *Pecten meridionalis* (Murray-Wallace and Goede, 1991; Murray-Wallace and Goede, 1995;
586 Slee et al., 2012). More recently, the age and origin of the shelly sand succession have been
587 questioned based on thermoluminescence ages of 30.7±1.9 ka and 30.3±3.7 ka (McIntosh et
588 al., 2013; Murray-Wallace et al., 2013; Slee et al., 2012), and OSL ages of 25±3 ka and 31±3 ka
589 (Shin, 2013) on quartz sand, host to the marine fossil assemblage. While '*lithostratigraphy is*
590 *the basis of all other stratigraphy…(sedimentary units) … should be defined on the basis of*
591 *lithological character only, and not on any inference as to mode of origin or age.*' (Bowen,
592 1985, p. 86) and hence the younger luminescence ages have no bearing on the lithostratigraphy
593 at Mary Ann Bay. The disparity between the AAR and ESR ages compared with the
594 luminescence results remains unresolved. Subsequent luminescence-based investigations will
595 require higher density spatial resolution for quantifying *in situ* field dosimetry down the
596 sedimentary profile, as the dispersion noted in Equivalent Dose values by Shin (2013) for a
597 sample from Mary Ann Bay (Sample MA02) implies down-profile translocation of quartz
598 grains contributing to younger numeric ages.

599 A spectacular succession of relict foredunes (beach ridges) is preserved on Remarkable
600 Banks, a coastal plain trending NNE on Robbins Island (location 35), northwestern Tasmania
601 (Bowden and Colhoun, 1984; Goodwin et al., 2023). Minimal erosional truncation of
602 individual ridges, reflecting a relatively low-energy depositional environment, has also
603 preserved the seaward intertidal facies for each ridge, critical for paleosea level interpretations
604 (Goodwin et al., 2023). The progradational sequence of approximately 140 relict foredunes are
605 found from 11 m to 4 m APSL across a 7 km long coastal plain, with OSL ages ranging

606 seawards from 130.3 to 117.5 ka for these beach ridges (Goodwin et al., 2023). Relative sea
607 level during this period is represented by three discrete phases: Goodwin et al. (2023)
608 concluded that sea level fell from 7 m to 6 m APSL between 130–126 ka, a stillstand occurred
609 at 5.75 ± 0.5 m APSL from 126–121 ka, and that a fall in sea level occurred between 119–
610 114 ka. The Robbins Island MIS 5e sea level history is important for its longer time-series
611 record than what is available from many other sites in southern Australia. Notably, the beach
612 ridge succession does not record the higher MIS 5e relative sea levels documented from
613 mainland Tasmania (Murray-Wallace et al., 1990; Murray-Wallace and Goede, 1991; Murray-
614 Wallace and Goede, 1995).
615

616 ## 4. MIS 5e sea surface from paleoshoreline elevations

617 The Last Interglacial coastal sedimentary record of southern Australia is fragmentary, with
618 most successions preserving only a limited portion of the interglaciation. Fewer examples of
619 relatively complete records, spanning the interval 128–116 ka have been identified. In broad
620 view, the MIS 5e Glanville Formation in South Australia is 1–3 m thick (Belperio et al., 1995;
621 Murray-Wallace et al., 2016; Pan et al., 2018). The upper bounding surface of the formation is
622 defined by pedogenic calcrete, resulting from subaerial exposure of the coastal successions
623 accompanying a fall in sea level (forced regression – basinward movement of the shoreline into
624 lower topographical situations) at the end of MIS 5e. Although the upper bounding surfaces of
625 all the MIS 5e sedimentary units reported in this study signify a cessation in deposition, it is
626 unlikely that they represent substantial deflation surfaces, as the thickness of the sedimentary
627 successions are marine limited, having been defined by a common elevation of paleosea level
628 during MIS 5e, and regionally, a common thickness of the formations is noted. Based on global
629 records of Late Quaternary sea-level changes, all the successions reported here have remained
630 above sea level since the end of MIS 5e (Murray-Wallace and Woodroffe, 2014). The calcrete

631 profiles on the Glanville Formation suggest limited erosion and exhumation of the primary
632 sedimentary units, notwithstanding that they might not originally have represented the entire
633 interglacial sea level highstand. Accordingly, surface uplift mostly represents rock (crustal)
634 uplift of much of the original sedimentary units (England and Molnar, 1990).

635 Most of the Last Interglacial successions reported in this investigation record deposition
636 since the culmination of sea-level rise in the early portion of MIS 5e, based on their facies
637 architecture in relation to the onset of the highstand following the penultimate interglacial
638 Exceptions include the Woakwine Range in South Australia, which chronicles the latest portion
639 of sea-level rise and a falling stage sea level during the interglacial, possibly linked to hydro-
640 isostasy (Murray-Wallace et al., 1999). The upward deepening succession at Point Turton,
641 southern Yorke Peninsula (location 12), also documents a relative sea-level rise during MIS 5e
642 without evidence for two sea level highstands (Pan et al., 2018). The prograded beach ridge
643 plain on Robbins Island also records relative sea-level changes during MIS 5e from c. 129–
644 114 ka (Goodwin et al., 2023).

645
646 **4.1. Basis for relative sea-level observations from the sedimentary facies**

647 In this work, relative paleosea levels (Table 1) have been determined primarily from
648 sedimentary lithofacies and their contained molluscan faunal assemblages, particularly where
649 species occur within a narrow range of tidal datum. Molluscan species identification follows
650 Ludbrook (1984). Characteristic sedimentary facies from which paleosea level has been
651 determined include beach (lower foreshore), and back-barrier estuarine-lagoonal facies.
652 Paleosea levels have been inferred based on the location and elevation of sea-level indicators
653 and their relation to a former tidal datum at the time of sedimentation (sea-level index point
654 sensu Shennan, 2015 and Rovere et al., 2023). Accordingly, modern tidal ranges across the
655 field sites were considered in the determination of paleosea level. In South Australia, tides are
656 micro-tidal, semidiurnal with Spring tides extending up to 2 m on the open ocean coastlines

and increase in range northwards within Gulf St Vincent to 3 m at the apex of the gulf, and 3.8 m at Port Augusta at the apex of northern Spencer Gulf. Along the coastline of Victoria, tides are microtidal, of semidiurnal–diurnal mixed character reaching up to 2.77 m at Port Welshpool Pier. In southeastern Tasmania, tides are microtidal, semidiurnal at Hobart attaining 1.48 m. On the northwest coast of Tasmania between Burnie and Stanley, tides are mesotidal reaching up to between 3.3 m to 3.45 m. respectively. Between Hobart and Fraser Island, Queensland, the entire coastline is micro-tidal in character with a Spring tidal range up to 1.3 m along the coastline of New South Wales (Short, 2020). Tides are amplified in Bass Strait by the influx of tidal waters at the western and eastern entrances of the Strait onto the shallow shelf and reach up to 3.9 m at Launceston. Amplification of the tides is also evident on Flinders Island reaching 2.7 m.

Beach facies (lower foreshore) represented by planar cross-bedded bioclastic sands containing the cockle *Donax deltoides* are common along the modern open ocean coastlines of southeastern Australia. In this environment, the infaunal species characteristically burrows to 5–10 cm below the sediment-water interface of foreshore sediments and repeatedly emerge and reburrow in the lower intertidal sands up to 20 cm below present sea level (Prezant, 1998). *Donax deltoides* migrate laterally within the sediment profile in response to tidal movements but remain within the swash-zone and are most abundant just below low tide level. Thus, they may indicate a paleosea level within a range of ±0.5 m

The estuarine mollusc *Anadara trapezia* is a shallow-burrowing bivalve of semi-infaunal habit found on the surfaces of tidal flats within estuaries with good tidal exchange of waters (Murray-Wallace et al., 2000). The cockle *Katelysia* spp. occurs within many of the Last Interglacial estuarine successions of southeastern Australia as coquina accumulations of shells (Fig. 7). In modern environments, the genus occurs abundantly in protected, intertidal sandflats and represents the dominant mollusc in such settings (Harte, 1998; Ludbrook, 1984). *Katelysia*

682 *scalarina* characteristically occurs in intertidal to shallow subtidal habitats, while *Katelysia*
683 *rhytiphora* tends to frequent shallow subtidal waters immediately below low water limit of the
684 intertidal zone to a depth of approximately 1 m below low tidal datum (Nielsen, 1964; Roberts,
685 1984). The turreted gastropod *Batillaria* (*Zeacumantus*) *diemenensis* is also common in the
686 Last Interglacial successions of southeastern Australia. The species grazes just below the
687 sediment-water interface on sand and mud flats and occurs most prolifically in intertidal
688 environments (Ludbrook, 1984; Macpherson and Gabriel, 1962).
689
690 **4.2. Regional dataset**
691 The age, spatial distribution, and paleosea levels inferred from Last Interglacial coastal
692 landforms and sedimentary successions in southeastern Australia have been sufficiently well-
693 defined that their wider significance for understanding the long-term behaviour of the
694 lithosphere-mantle couplet and its role in geodetic changes since MIS 5e can be undertaken.
695 MIS 5e shoreline elevations and paleosea levels from southeastern Australia were compiled
696 from 47 locations (Fig. 1 and Table 1). The age uncertainty of the data is generally in the order
697 of ±2–3 ka for uranium-series ages by MC-ICP-MS, and up to ±10 ka for earlier measurements
698 by α-counting. Luminescence ages typically have uncertainties ranging from ±5 to ±10% (±4–
699 11 ka), that increase with age (see Table 6.1 in Murray-Wallace, 2018). Uncertainties in
700 inferred paleosea levels vary with the reliability of paleosea level indicators but are generally
701 in the range of ±0.5–1 m (Table 1). The inferred vertical surface displacement *SD* (m) of the
702 relict shoreline successions is taken as $SD = h + WD - SL$, where h is the maximum elevation
703 of the shoreline succession, WD the paleowater depth and SL is the elevation of the MIS 5e sea
704 surface in southeastern Australia. A value of 4±1 m APSL is adopted, based on the paleosea-
705 level observations from western Eyre Peninsula, and southern Yorke Peninsula, part of the
706 tectonically highly stable Gawler Craton in South Australia (Murray-Wallace et al., 2016; Pan

et al., 2018; see Section 3.1). Uncertainties associated with WD and SL were propagated as $E = \sqrt{e_{\mathrm{h}}^2 + e_{\mathrm{WD}}^2 + e_{\mathrm{SL}}^2}$, where e_{h} = 0.05 m (except for the New River Lagoon Sea Caves, SW Tasmania, for which it was equal to one metre) was the uncertainty associated with present-day elevation, e_{WD} was the uncertainty associated with paleosea level (Table 1) and e_{SL} = 1 m was the uncertainty associated with global sea level (Fig. 8b).

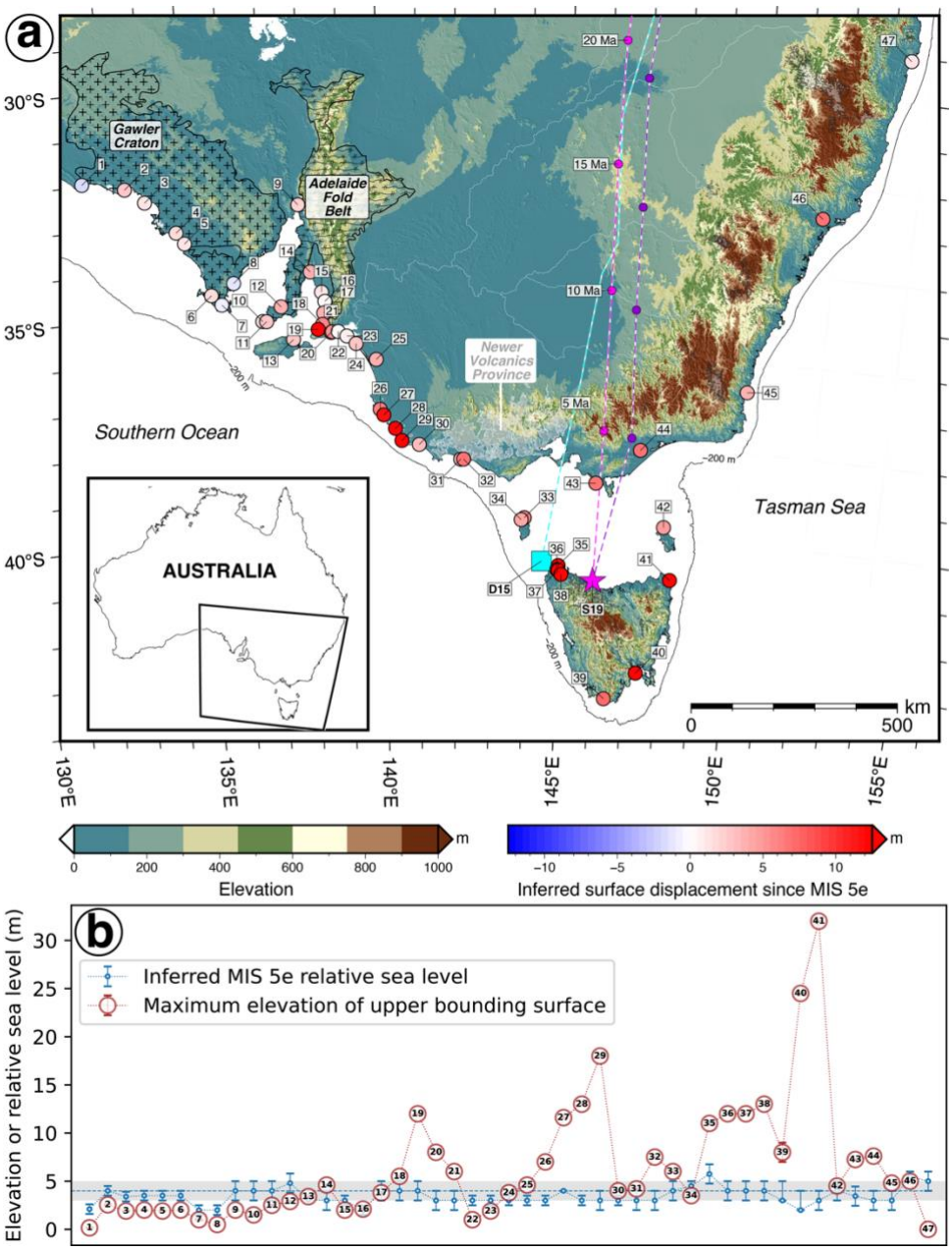

Figure 8. Inferred surface displacement of Last Interglacial shoreline successions in southeastern Australia. a, Digital Elevation Model (Geoscience Australia, 2019) and Last Interglacial shoreline successions at 47 locations (Table 1), shown as disks coloured by inferred surface displacement assuming sea level was 4 m higher during the Last Interglacial. Quaternary volcanic formations (Geoscience Australia, 2012) are shown as transparent grey polygons with a white outline, and earlier Cenozoic volcanic formations are shown as transparent grey polygons with a black outline. The reconstructed Cosgrove hotspot track is shown as a cyan dashed line and a cyan square labelled 'D15' for the inferred present-day location based on the original publication (Davies et al., 2015), and as magenta and purple dashed lines for two alternative reconstructions by Seton et al. (2019), ending at the inferred present-day location shown as a magenta star labelled 'S19'. Light shading from azimuth 225º. Main rivers are shown in white, and the -200 m isobath (GEBCO Compilation Group, 2020) is shown as a black line. **b-c**, Present-day maximum elevation and inferred paleowater depth for the considered MIS 5e paleoshoreline successions. The dashed line indicates a MIS 5e sea level 4 m higher than present-day for southern Australia (Murray-Wallace et al., 2016; Pan et al., 2018), with an uncertainty of ± 1 m (grey polygon). The Gawler Craton and Adelaide Fold Belt

at the 1:5 million scale (Blake, 1998) are shown as grey polygons. The inset shows the map area in the context of Australian coastlines.

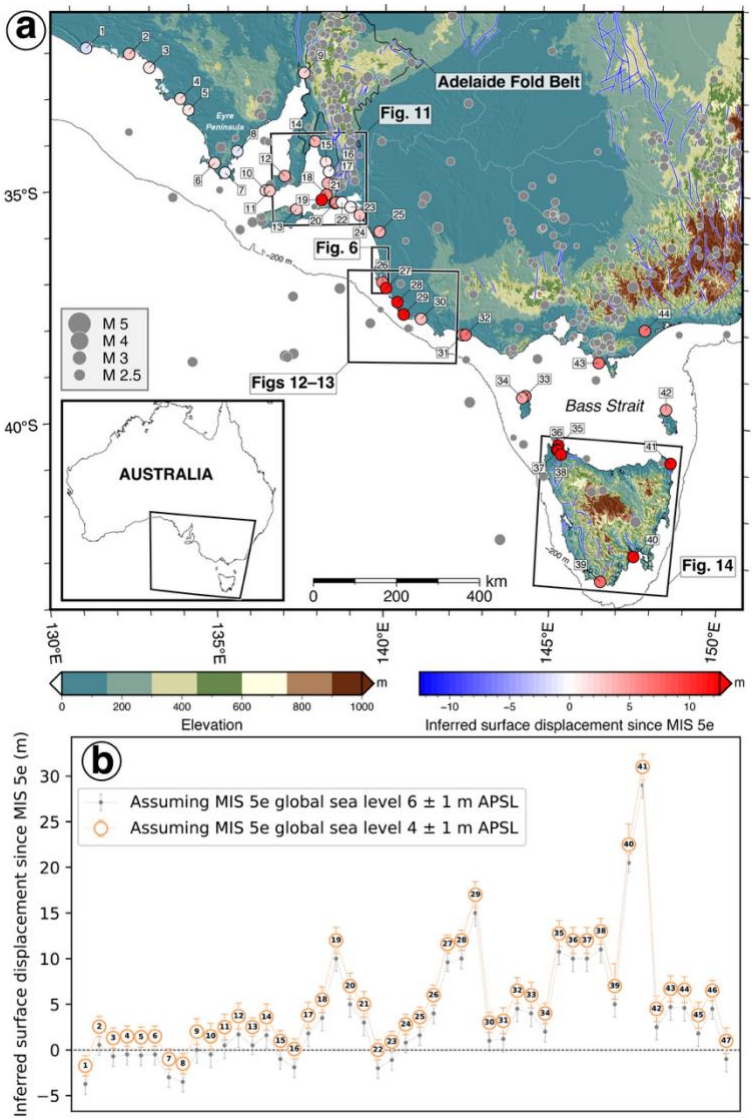

Figure 9. Inferred surface displacement of Last Interglacial shoreline successions, earthquakes, and major faults in southeastern Australia. a, Digital Elevation Model (Geoscience Australia, 2019) and Last Interglacial shoreline successions at 44 locations (Table 1), shown as disks coloured by inferred surface displacement assuming a 4 m higher sea level during MIS 5e than in the current, Holocene Interglacial. Earthquakes (Geoscience Australia, 2024) are shown as grey disks sized according to magnitude, and major faults (Raymond, 2023) are shown as blue lines. Light shading from azimuth 225º. Main rivers are shown in white, and the -200 m isobath (GEBCO Compilation Group, 2020) is shown as a black line. **b**, Inferred surface displacement at all 47 considered locations assuming MIS 5e global sea level to have been either 4 ± 1 m or 6 ± 1 m above present-day sea level (APSL).

5. Analysis

5.1. MIS 5e sea level in southern Australia and globally

MIS 5e ice-equivalent sea level relative to present-day for southern Australia can be estimated from three sites that, on first principles of geological setting, are considered tectonically highly stable. This has been documented at between 2.1 ± 0.5 m APSL (Fowlers Bay, location 1), at 4 ± 0.5 m APSL (Tourville Bay, location 2), Eyre Peninsula (Murray-Wallace et al., 2016) and at 4.8 ± 1 m APSL at Point Turton, Hardwicke Bay, southern Yorke Peninsula (location 12). Based on these estimates the average paleosea level for the considered sites is ~3.5 ± 0.7 m (Table 1), and a 4 ± 1 m APSL value for a MIS 5e sea surface is adopted in this study for southeastern Australia (Fig. 8b). This suggested MIS 5e sea surface is below the proposed global mean MIS 5e sea level of between 6–9 m APSL (Dutton et al., 2015). Models of glacial isostatic adjustment and evolution of dynamic topography since MIS 5e would make it possible to determine whether the southern Australian observations could be representative of an ice-equivalent sea level.

Uplift by more than 10 m since MIS 5e is inferred at ten locations (Figs 8-9), six of which are in Tasmania (locations 35–38 and 40–41), three on the Coorong Coastal Plain between Robe and Mount Gambier (locations 27-29), and one at Normanville, southern Fleurieu Peninsula (location 19, Fig. 1). Subsidence by less than 2 m (Figs 8-9) since MIS 5e time is inferred for Fowlers Bay, Port Lincoln, and Tumby Bay (locations 1, 7, and 8), all of which occur west of 139ºE and north of 35.6ºS, in the Gawler Craton (Figs 8-9).

Inferred surface displacement since MIS 5e appears to increase towards the east (Fig. 10a) and towards the south (Fig. 10b), as shown using Spearman's rank correlation coefficient, which assesses the monotonic relationship between two ranked variables (Spearman, 1904). There were statistically significant Spearman ranking correlations between inferred surface

displacements since MIS 5e and latitude (r = 0.74, Fig. 10b) as well as longitude (r = 0.63, Fig. 10a).

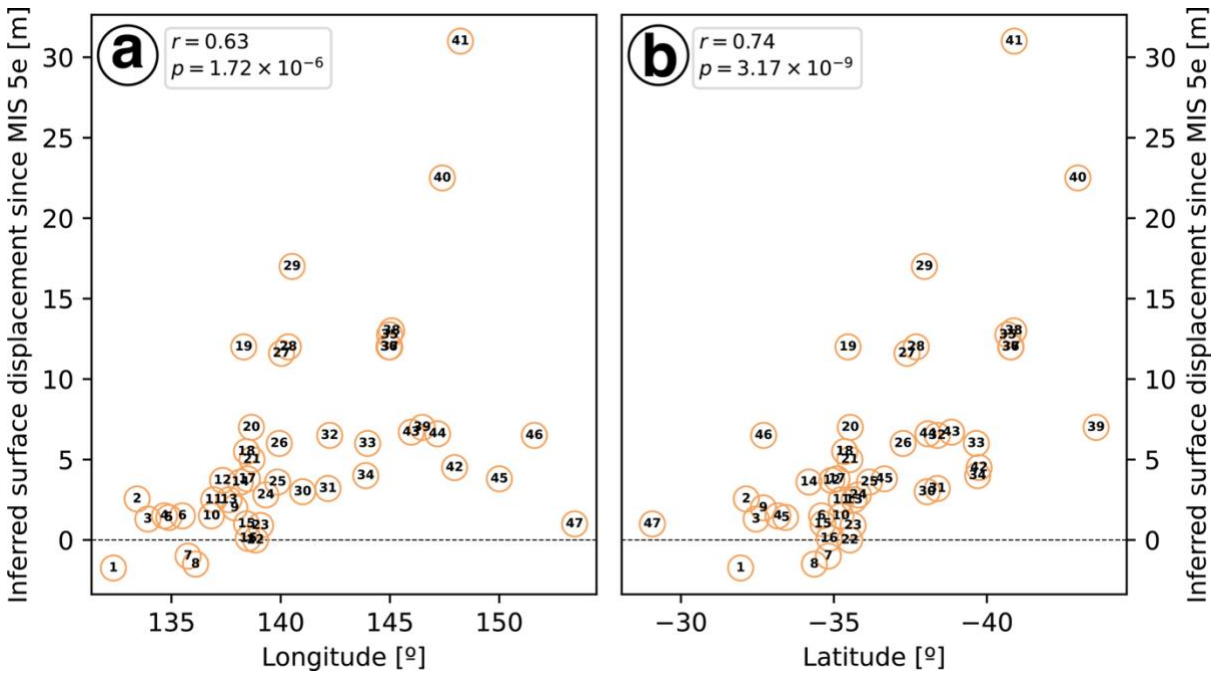

Figure 10. Inferred surface displacement of paleoshoreline successions since MIS 5e as a function of longitude (**a**) and latitude (**b**). r is the Spearman correlation coefficient, and p is the p-value for a Spearman ranking test with null hypothesis that two samples have no ordinal correlation.

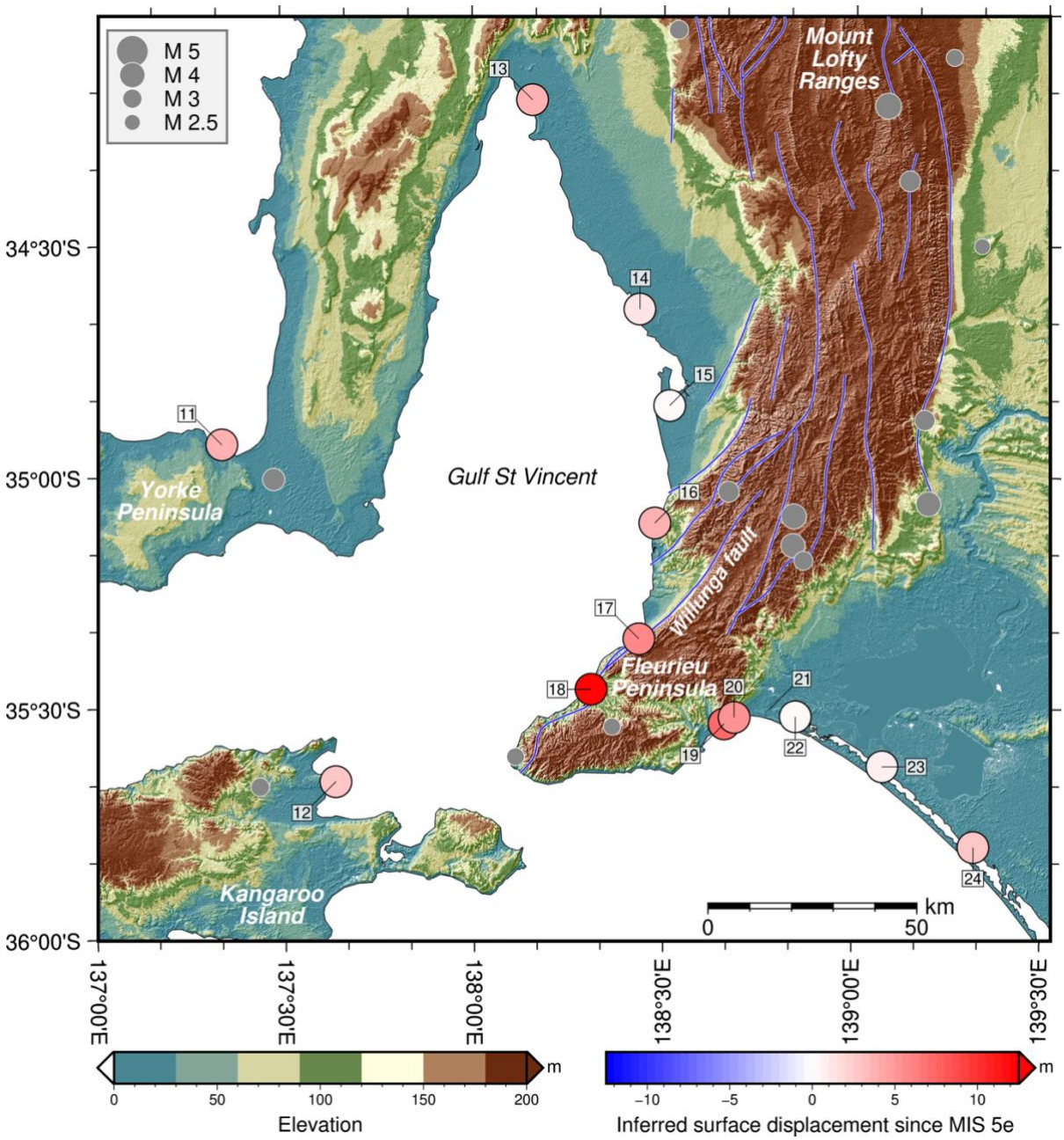

Figure 11. Inferred surface displacement of Last Interglacial shoreline successions, earthquakes, and major faults around Gulf St Vincent, Fleurieu Peninsula and the northern Coorong Coastal Plain. Digital Elevation Model (NASA JPL, 2013) and Last Interglacial coastal successions at 13 locations (Table 1), shown as disks coloured by inferred surface displacement assuming a 4 m APSL sea level during the Last Interglacial (MIS 5e). Earthquakes (Geoscience Australia, 2024) are shown as grey disks sized according to magnitude, and major faults (Raymond, 2023) are shown as blue lines. Light shading from azimuth 315º. The region is outlined in Figure 9a.

795 **5.2. MIS 5e shoreline elevations in the context of their tectonic setting**

796 The inferred surface displacement since MIS 5e at locations in the Gawler Craton region
797 (1-8 and 10-12, Figs 1, 8-9) is within -2 m and +4 m (Fig. 9b), suggests continued stability of
798 the Gawler Craton since MIS 5e, with local post-depositional subsidence at Fowlers Bay, Port
799 Lincoln, and Tumby Bay (locations 1, 7, and 8). The latter subsidence may be possibly due to
800 hydro-isostasy during the sea level highstand of MIS 5e as noted in the current Holocene
801 Interglacial (Belperio et al., 2002). It is also possible that paleoshoreline successions reflecting
802 minor subsidence represent only the later, lower sea level portion of MIS 5e highstand,
803 implying that a MIS 5e sea level highstand of lower than 4 m APSL is more appropriate to
804 infer vertical displacement at these locations.

805 Around Gulf St Vincent (Fig. 11), inferred surface displacement since MIS 5e time ranges
806 between 0 m and 12 m (average ~3.7 m) with Normanville standing out well above the range
807 (location 19, 12 m). Both Sellicks Beach and Normanville (locations 18 and 19) are close to
808 the Willunga Fault. The difference in inferred surface displacement since MIS 5e between these
809 two locations suggests up to 6.5 m of upward displacement of the block to the southeast of the
810 Willunga Fault (Fig. 11). Chiton Rocks and Victor Harbor (locations 20 and 21) are in the
811 foothills of the southern Mount Lofty Ranges on Fleurieu Peninsula, and close to the
812 seismically active Adelaide Fold Belt (Figs 9 and 11), suggesting that the modest inferred uplift
813 they experienced (7 m and 5 m, respectively) could also be affected by neotectonic motions.

814

815

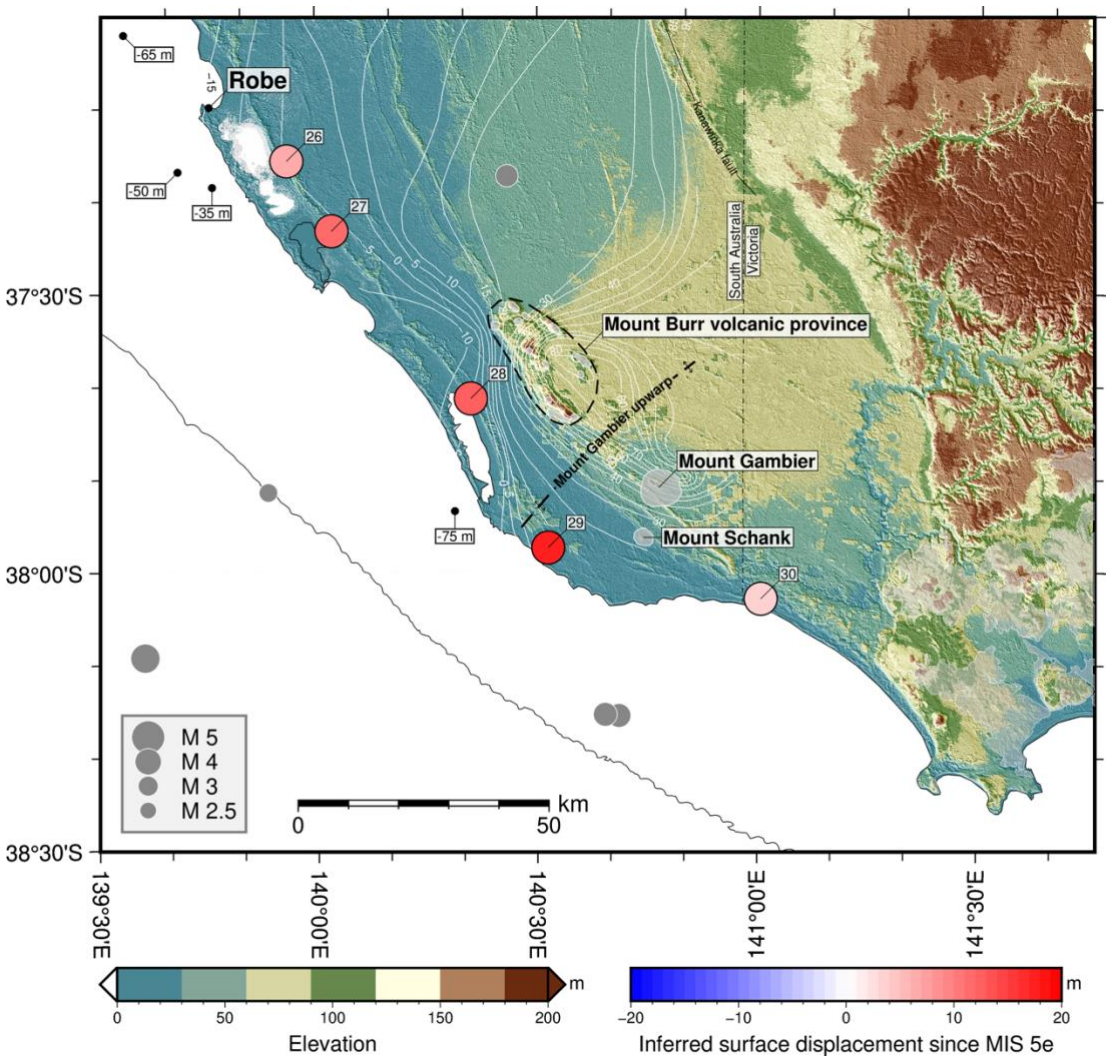

Figure 12. Inferred surface displacement of Last Interglacial shoreline successions, earthquakes, and Quaternary volcanic formations between Robe and Mount Gambier. a, Digital Elevation Model (NASA JPL, 2013) and Last Interglacial successions at five locations (Table 1), shown as disks coloured by inferred surface displacement assuming a 4 m APSL sea level during the Last Interglacial (MIS 5e). Quaternary volcanic formations (Geoscience Australia, 2012) are shown as transparent grey polygons with a white outline. White contours show the upper bounding surface of the Oligo-Miocene Gambier Limestone, with offshore values indicating the depth of the Gambier Limestone below present-day sea level. Light shading from azimuth 225º. The -200 m isobath (GEBCO Compilation Group, 2020) is shown as a black line. The region is outlined in Figure 9a.

Uplift by more than 10 m since MIS 5e time was inferred in the Coorong coastal plain in the vicinity of Quaternary volcanic formations, some 45 km to the west of the Newer Volcanic Province (Figs 8a and 12). The inferred uplift increases from west to east between Lake Hawdon South (location 26) and Nene Valley (location 29) from 6 m to 17 m over 120 km, then decreases down to 3 m at Nelson (location 30) over approximately 40 km (Figs 8a and

834 12). This increase by ~11 m between Lake Hawdon South and Nene Valley along the
835 Woakwine Range generally reflects the increase in the elevation of the upper-bounding surface
836 of the Oligo-Miocene Gambier Limestone by < 19 m between these locations, which is
837 associated with the upwarp of the Gambier Limestone in a dome structure around Mount
838 Gambier (Sprigg, 1952; Fig. 12). Given their spatial association with volcanic formations, the
839 Gambier upwarp and the trend in inferred uplift since MIS 5e are likely due to crustal doming
840 in response to shallow emplacement of magma at the Mount Burr Volcanic Complex during
841 Pleistocene time and at Mount Gambier and Mount Schank during Holocene times.
842 The Pleistocene Mount Burr Volcanic Complex represented an archipelago of volcanoes,
843 with the westernmost centres showing evidence of erosional modification during sea level
844 highstands and the deposition of calcarenite (aeolianite) of the Lower Bridgewater Formation
845 on the slopes of Mounts Graham, Muir, MacIntyre and Burr (Hossfeld, 1950; Sprigg, 1952). A
846 cuspate foreland developed, extending from the West Naracoorte Range (MIS 21-19) to the
847 Mount Burr Volcanic Complex. The coastal barriers Harper Range and Stewarts/Cave Range
848 nucleated against the volcanic centres commencing at least some 700 ka ago (MIS 17)
849 indicating a minimum age for the volcanism (Murray-Wallace, 2018; Fig. 13).
850 Although the pre-Quaternary bedrock of Tasmania is related to the eastern mainland of
851 Australia (e.g. Lachlan Fold Belt), Last Interglacial coastal successions occur at higher
852 landscape elevations in Tasmania (Bowden and Colhoun, 1984; Murray-Wallace and Goede,
853 1991; Murray-Wallace and Goede, 1995). Indeed, the inferred uplift since MIS 5e time is
854 largest in Tasmania (between 7 m and 31 m on the main island), in the absence of Quaternary
855 volcanic activity or of significant seismic activity (Figs 8, 9, and 14).

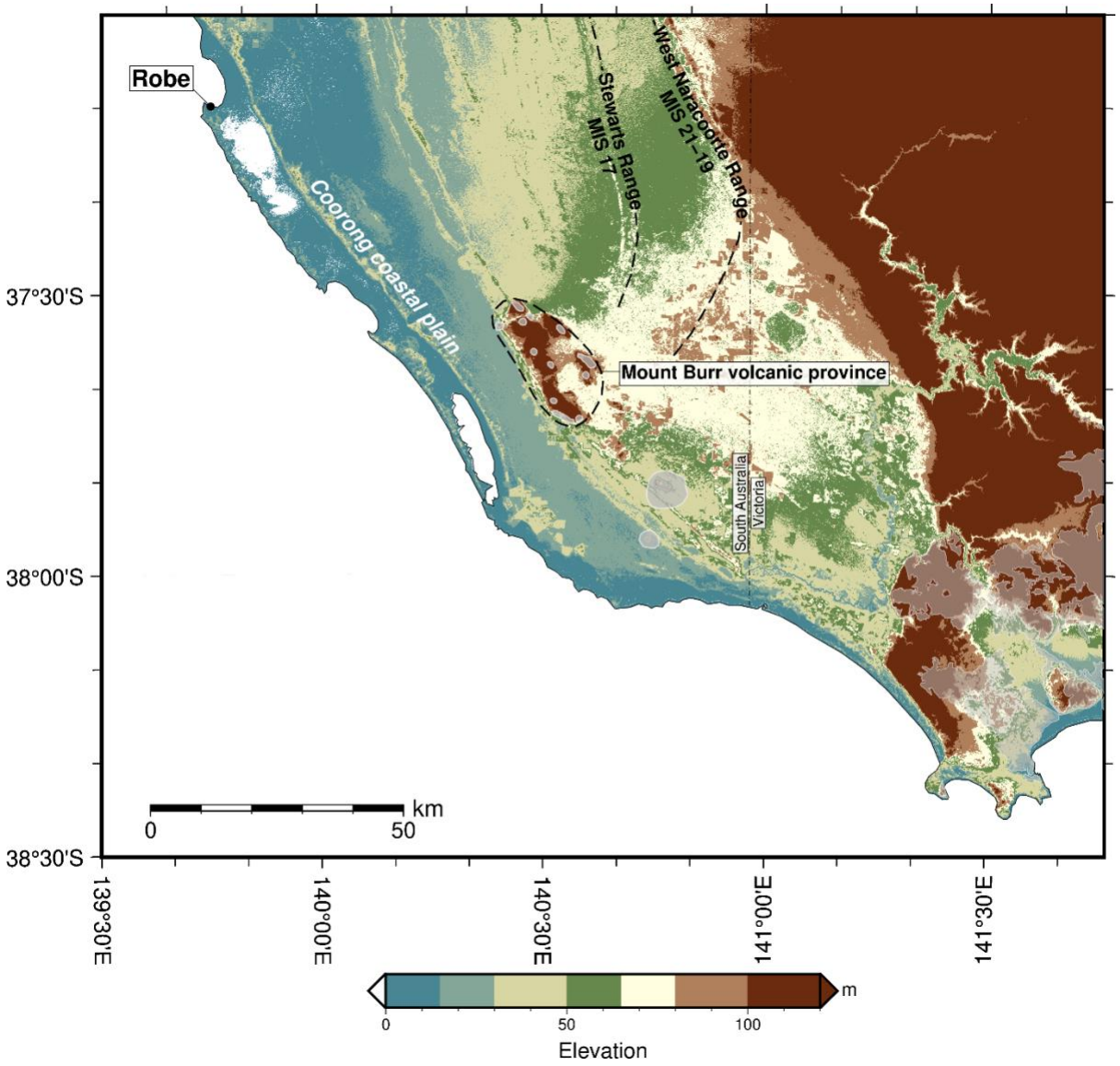

856

857 **Figure 13. Inferred minimum age of the Mount Burr volcanic province.** Digital Elevation
858 Model (JPL, 2013) with Quaternary volcanic formations (GA, 2012) shown as transparent grey
859 polygons with white outlines. The Naracoorte Range (MIS 21-19) and Stewarts Range
860 (MIS 17) are highlighted. Their cuspate shape suggest that they nucleated on the Mount Burr
861 volcanic province, which can be inferred to date back to MIS 17 times (~700 ka). Light shading
862 from azimuth 225º. The region is outlined in Figure 9a.

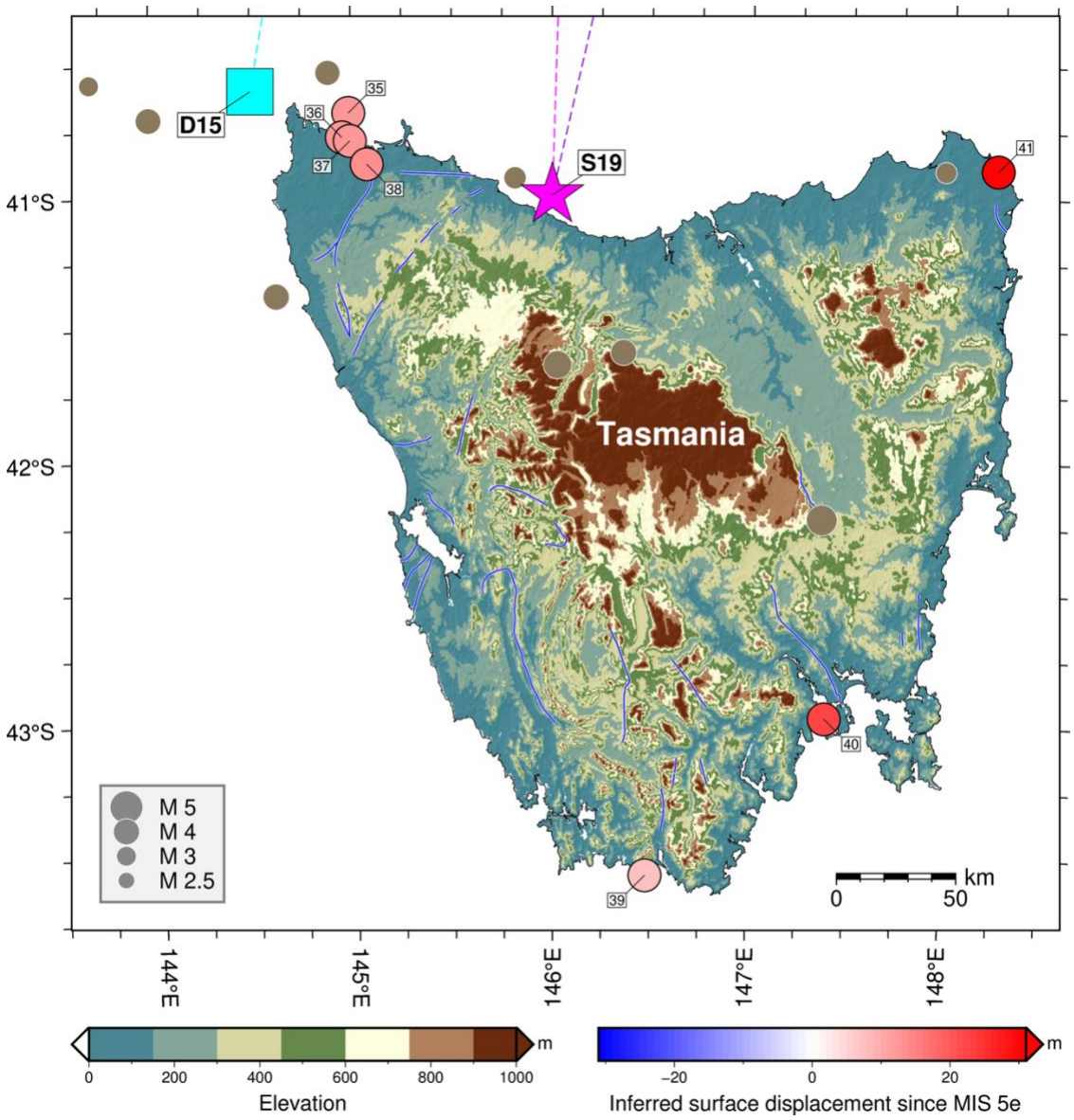

Figure 14. Inferred surface displacement of Last Interglacial shoreline successions, earthquakes, and major faults in Tasmania. Digital Elevation Model (Geoscience Australia, 2019) and Last Interglacial shoreline successions at seven locations (Table 1), shown as disks coloured by inferred surface displacement assuming a 4 m APSL sea level during MIS 5e. Earthquakes (Geoscience Australia, 2024) are shown as brown disks sized according to magnitude, and major faults (Raymond, 2023) are shown as blue lines. The reconstructed Cosgrove hotspot track is shown as a cyan dashed line and a cyan square labelled 'D15' for the inferred present-day location based on the original publication (Davies et al., 2015), and as magenta and purple dashed lines for two alternative reconstructions by Seton et al. (2019), ending at the inferred present-day location shown as a magenta star labelled 'S19'. Light shading from azimuth 315º. The region is outlined in Figure 9a.

879 **5.3. MIS 5e shoreline elevations in the context of their geodynamic setting**

880 *5.3.1. Seismic tomography*

881 A geodynamic process that does not result in seismicity or volcanism should explain the
882 uplift inferred since MIS 5e for Tasmania. Tasmania is at the end of the Cosgrove hotspot track,
883 with reconstructions by Davies et al. (2015) and Seton et al. (2019) both predicting the present-
884 day location of the hotspot to be just offshore and to the northwest (D19) or north (S19) of the
885 main Tasmanian island, respectively (Fig. 14). This suggests that active mantle upwelling could
886 be the driver for the uplift of Tasmania by 7 m to 31 m since MIS 5e time. Some seismic
887 tomographic models (Amaru, 2007; Montelli et al., 2006; Thrastarson et al., 2024) suggest that
888 seismic waves propagate more slowly through the mantle beneath Tasmania (Figs 15-17),
889 which implies that the mantle is hotter. This feature is most prominent in seismic tomographic
890 model PRI-S05 (Montelli et al., 2006), which was designed to image mantle plumes. In that
891 model, there is a clear slow S-wave velocity (Vs) anomaly at 200 km depth centred beneath the
892 northeastern part of Tasmania, which coincides with the largest inferred uplift since MIS 5e at
893 Stumpys Bay (31 m, location 41, Figs 8b, 9b, 14 and 15b). The anomaly appears to extend to
894 between ~100 km and ~500 km depths, and is most prominent between ~200 km and ~400 km
895 depth (Fig. 15b-e). The V_S anomaly is most pronounced and shallowest beneath Stumpys Bay,
896 and less pronounced and deeper beneath Mary Ann Bay (location 40, inferred uplift: 22.5 m).
897

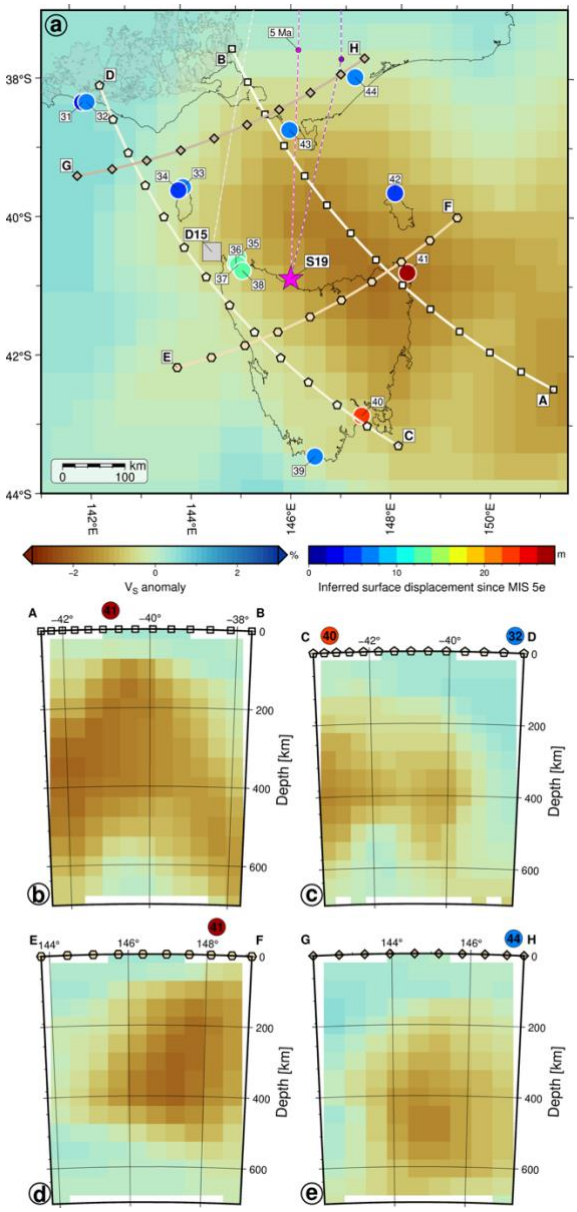

Figure 15. Inferred surface displacement of Last Interglacial shoreline successions and seismic tomography. a, Seismic tomography model PRI-S05 (Montelli et al., 2006) at 200 km depth, and Last Interglacial shoreline successions at 14 locations (Table 1) shown as disks coloured by inferred surface displacement assuming a 4 m APSL sea level during MIS 5e. Quaternary volcanic formations (Geoscience Australia, 2012) are shown as transparent grey polygons with a black outline. The reconstructed Cosgrove hotspot track is shown as a cyan dashed line and a grey square labelled 'D15' for the inferred present-day location based on the original publication (Davies et al., 2015), and as magenta and purple dashed lines for two alternative reconstructions by Seton et al. (2019), ending at the inferred present-day location shown as a magenta star labelled 'S19'. Cross-sections along small circles A-B, C-D, E-F, and G-H are shown with symbols matching panels **b-e.** Cross-sections of seismic topography model PRI-S05 down to 700 km depth along small-circle paths A-B (**b**), C-D (**c**), E-F (**d**) and G-H (**e**). Nearby shoreline succession locations are shown above the cross-sections.

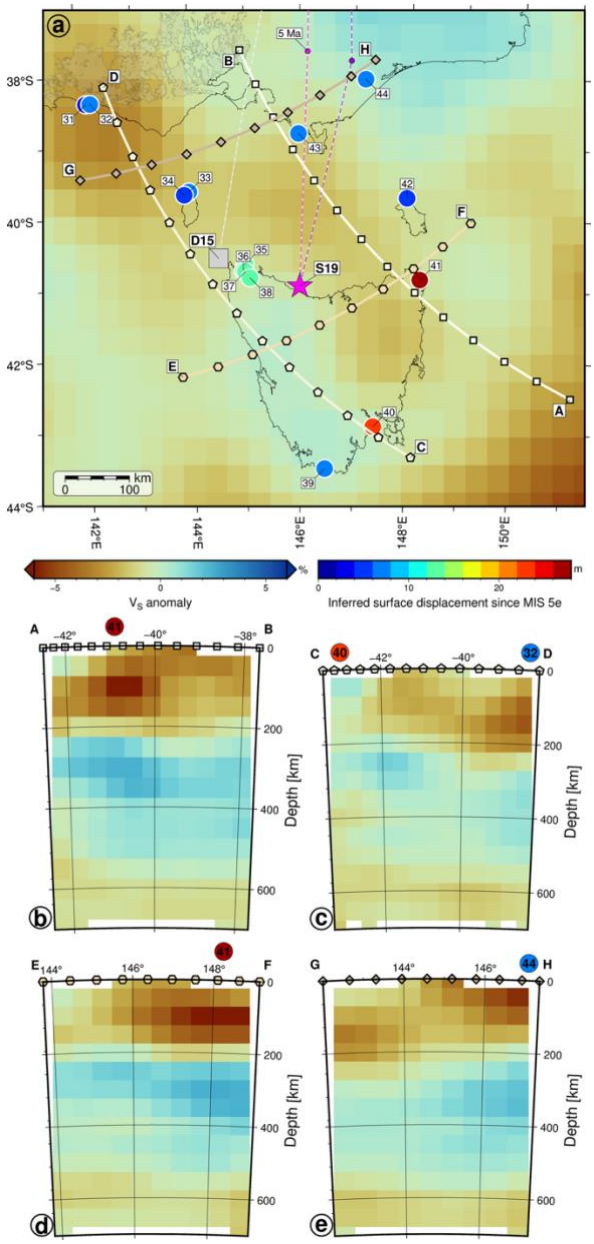

Figure 16. Inferred surface displacement of Last Interglacial shoreline successions and seismic tomography. a, Seismic tomography model REVEAL (Thrastarson et al., 2024) at 200 km depth, and Last Interglacial shoreline successions at 14 locations (Table 1) shown as disks coloured by inferred surface displacement assuming a 4 m APSL sea level during MIS 5e. Quaternary volcanic formations (GA, 2012) are shown as transparent grey polygons with a black outline. The reconstructed Cosgrove hotspot track is shown as a cyan dashed line and a grey square labelled 'D15' for the inferred present-day location based on the original publication (Davies et al., 2015), and as magenta and purple dashed lines for two alternative reconstructions by Seton et al. (2019), ending at the inferred present-day location shown as a magenta star labelled 'S19'. Cross-sections along small circles A-B, C-D, E-F, and G-H are shown with symbols matching panels b-e. Cross-sections of seismic topography model REVEAL down to 700 km depth along small-circle paths A-B (**b**), C-D (**c**), E-F (**d**) and G-H (**e**). Nearby shoreline succession locations are shown above the cross-sections.

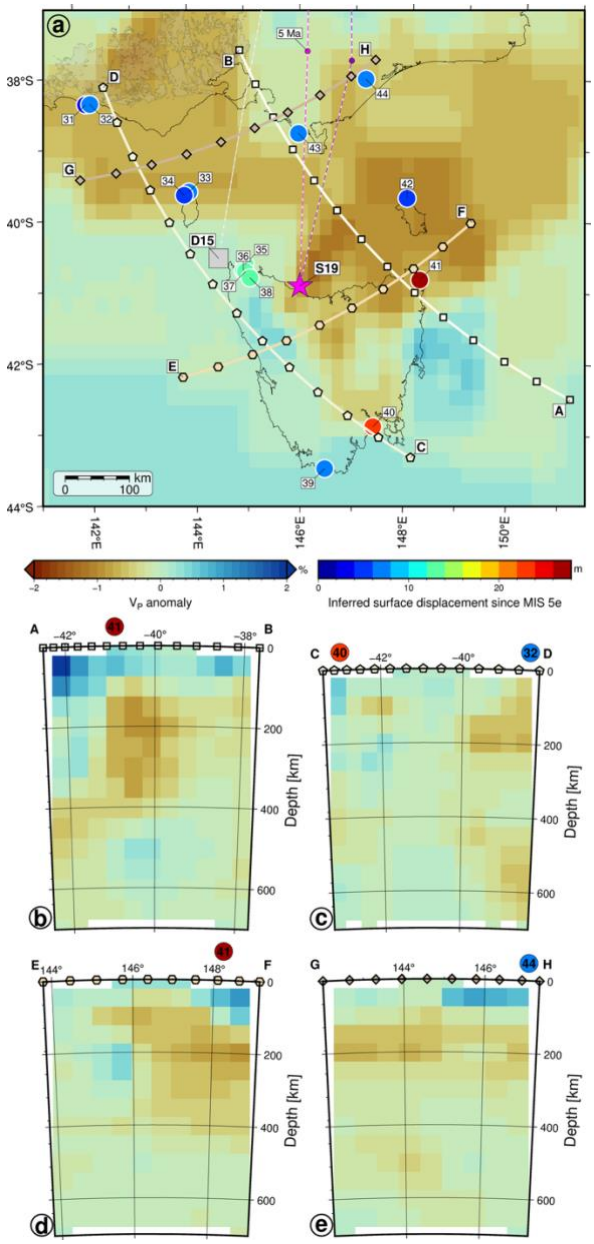

Figure 17. Last Interglacial shoreline elevation and seismic tomography. a, Seismic tomography model UU-P07 (Amaru, 2007) at 185 km depth, and Last Interglacial shoreline elevation at 14 locations (Table 1) shown as disks coloured by elevation. Disk outlines are black for paleoshorelines with present-day elevation greater than nine meters, and grey for other locations. Quaternary volcanic formations (Geoscience Australia, 2012) are shown as transparent grey polygons with a black outline. The reconstructed Cosgrove hotspot track is shown as a cyan dashed line and a grey square labelled 'D15' for the inferred present-day location based on the original publication (Davies et al., 2015), and as magenta and purple dashed lines for two alternative reconstructions by Seton et al. (2019), ending at the inferred present-day location shown as a magenta star labelled 'S19'. Cross-sections along small circles A-B, C-D, E-F, and G-H are shown with symbols matching panels **b-e.** Cross-sections of seismic topography model UU-P07 down to 700 km depth along small-circle paths A-B (**b**), C-D (**c**), E-F (**d**) and G-H (**e**). Nearby paleoshorelines locations are projected above the cross-sections and labelled with numbers.

Positive seismic velocity anomalies suggest that a relatively hot mantle could be the driver of uplift since MIS 5e in Tasmania, because hotter mantle is seismically slower and sources of buoyancy closer to the surface are expected to result in greater dynamic uplift (Hager and Clayton, 1989). In the S-wave tomographic model REVEAL (Thrastarson et al., 2024), the V_S anomaly is less pronounced under Tasmania and restricted to the uppermost 200 km (Fig. 16). While there is a pronounced anomaly at ~100 km beneath Mary Ann Bay (location 40) in that model, there is no V_S anomaly under Stumpys Bay (location 40; Figure 16b-e). Shallow anomalies beneath Warrnambool and Sale (locations 32 and 44, inferred uplift ~6.5 m) in the S-wave tomographic model REVEAL are probably in the lithosphere (Fig. 13). In the P-wave tomographic model UUP-7 (Amaru, 2007), there is a clear V_P anomaly beneath northeastern Tasmania at 185 km depth (Fig. 17a). There is a V_P anomaly between ~100–375 km depths close to Sale (location 44; Fig. 17b, d), no anomaly beneath Mary Ann Bay (location 40), and a possible shallow anomaly beneath Warrnambool (location 32). Overall, the three seismic tomographic models considered here suggest that hot mantle between ~100–400 km depth could explain inferred uplift since MIS 5e in Tasmania, particularly in the northeast part of the island.

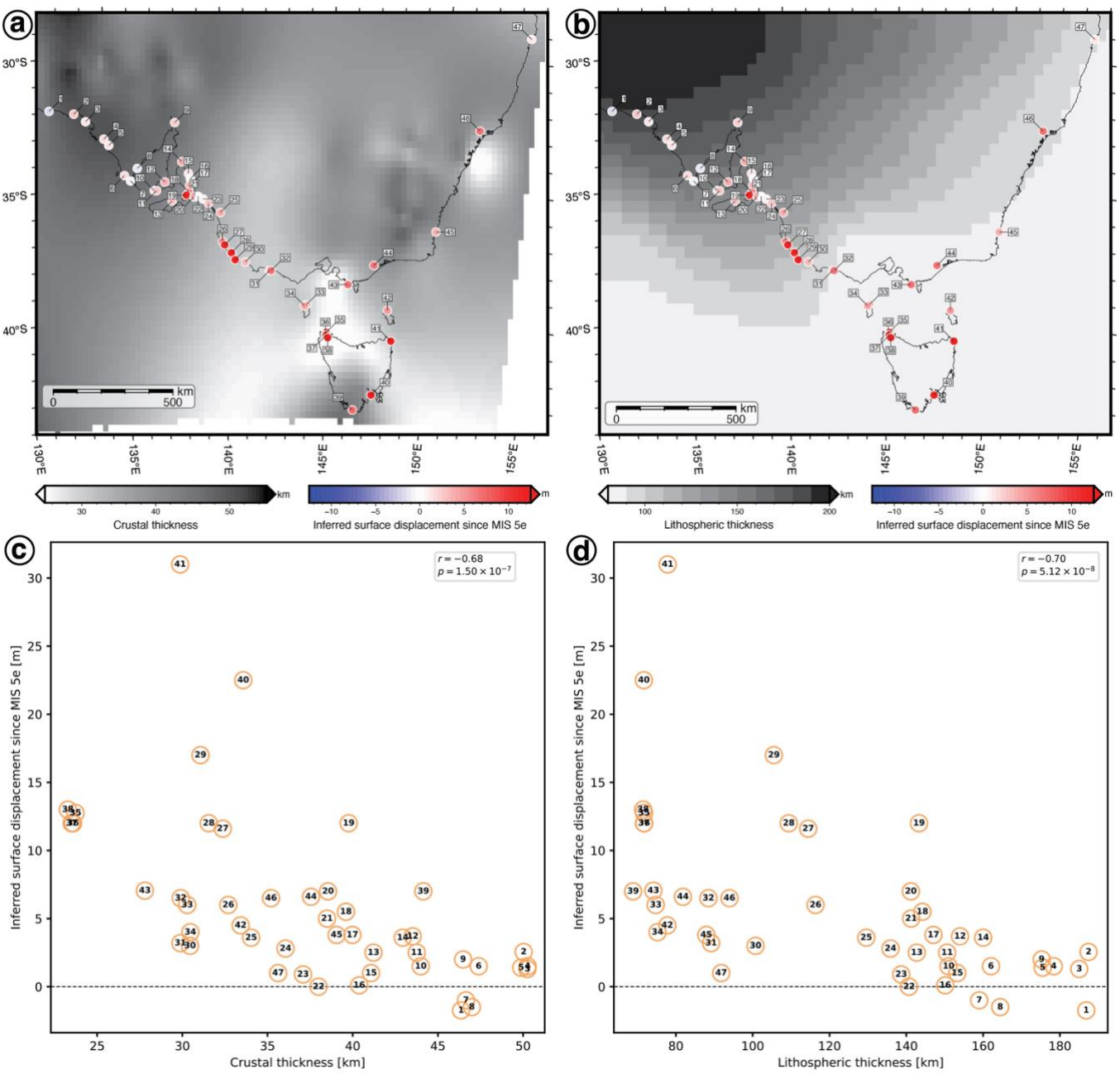

Figure 18. Inferred surface displacement of Last Interglacial shoreline successions, crustal thickness and lithospheric thickness. a, Crustal thickness (Stephenson et al., 2024), **b**, lithospheric thickness (Hoggard et al., 2020) and inferred surface displacement of Last Interglacial coastal successions at 47 locations (Table 1) shown as disks coloured by inferred surface displacement assuming a sea level 4 m higher during the Last Interglacial. **c-d**, Inferred surface displacement of Last Interglacial shoreline successions as a function of crustal (**c**) and lithosphere (**d**) thickness. *r* is the Spearman correlation coefficient, and *p* is the *p*-value for a Spearman ranking test with null hypothesis that two samples have no ordinal correlation.

979 *5.3.2. Crustal thickness*

980 A statistically significant Spearman anticorrelation (r = -0.68) indicates that inferred
981 surface displacement since MIS 5e time generally decreases as crustal thickness increases
982 (Fig. 18c). The thickness of the continental crust is less than ~34 km at the Tasmanian locations
983 of interest (Fig. 18a, c). In map view, the model of Stephenson et al. (2024) predicts the thinnest
984 crust beneath northwestern Tasmania, which could explain why inferred uplift since MIS 5e is
985 large there even though the area is not directly above slow seismic anomalies (Fig. 15):
986 dynamic uplift would be more significant because the convecting mantle would be closer to
987 the surface (Hager and Clayton, 1989). Significant uplift since MIS 5e time between the
988 McCourt Cutting and Nene Valley (locations 27-29, ~12-17 m) and at Normanville (location
989 19, 12 m) is not well explained by crustal thickness (~32-42 km thick, Fig. 18c).

990

991 *5.3.3. Lithospheric thickness*

992 In southeastern Australia, lithospheric thickness increases from the southeast to the
993 northwest (Fig. 18b). Thin (< 80 km thick) lithosphere occurs in Tasmania, where the largest
994 uplift since MIS 5e is inferred, and thick lithosphere occurs in the Gawler Craton, with
995 lithosphere thicker than 160 km at Fowlers Bay, Port Lincoln, and Tumby Bay (locations 1, 7,
996 and 8), where 1 m to 1.75 m of subsidence was inferred since MIS 5e (Figs 8b and 13d). There
997 is a statistically significant Spearman ranking anticorrelation (r = -0.70) between lithospheric
998 thickness and inferred surface displacement since MIS 5e (Fig. 18d). Overall, this general trend
999 suggests that lithospheric thickness influenced surface displacement since MIS 5e in the region,
1000 with mantle convection at shallower depths (i.e., in areas with thinner lithosphere) results in
1001 greater dynamic topography (Hager and Clayton, 1989). However, there are departures from
1002 this general trend, for example with significant uplift since MIS 5e time between McCourt

1003 Cutting and Nene Valley (locations 27-29, ~12-17 m) and at Normanville (location 19, 12 m)
1004 in areas where the lithosphere is ~110-145 km thick (Fig. 18b, d).
1005
1006 *5.3.4. Residual topography*
1007 Residual topography is the difference between observed topography and the topography
1008 expected from an isostatic model. Residual topography indicates the effect of mantle
1009 convection on topography, a limit being the uncertainty in the isostatic model. In the global
1010 continental residual topography model of Stephenson et al. (2024), residual topography
1011 (Fig. 19a) closely depends on crustal thickness (Fig. 18a), with more positive residual
1012 topography where the crust is thinner (Figs 18a and 19a). In southeastern Australia, there is a
1013 statistically significant Spearman ranking correlation (r = 0.62) indicating reasonable
1014 agreement between this residual topography model and inferred surface displacement since
1015 MIS 5e (Fig. 19c). Large (~800 m) residual topography could explain the inferred large uplift
1016 of MIS 5e shorelines (12–13 m) in northwest Tasmania, and negative residual topography
1017 (between approximately -650 m and approximately -20 m) is predicted for the three locations
1018 in the Gawler Craton, for which some subsidence was inferred (Fig. 19c). Significant uplift of
1019 MIS 5e shoreline successions between McCourt Cutting and Nene Valley (locations 27 and 29,
1020 ~12-17 m) also correspond with positive residual topography (~180–210 m). However,
1021 residual topography is predicted to be only ~200 m in northeast Tasmania, where the inferred
1022 uplift since MIS 5e time is largest (31 m). Residual topography is predicted to be negative
1023 (approximately -500 m) in southeast Tasmania, where the inferred uplift since MIS 5e time is
1024 large (22.5 m) and at Normanville (location 19, approximately -180 m), where the inferred
1025 uplift is 12 m (Fig. 19a,c).
1026 Stephenson et al. (2024) found that positive residual topography tends to be associated with
1027 lithosphere thinner than ~100 km. While positive residual topography tends to be associated

with thin lithosphere in southeastern Australia (Figs 18b and 19a), there are exceptions in southeastern Tasmania and to some extent in the area between Lake Hawdon South and Nene Valley (locations 26-29), which is above a steep gradient in lithospheric thickness (Fig. 18b).

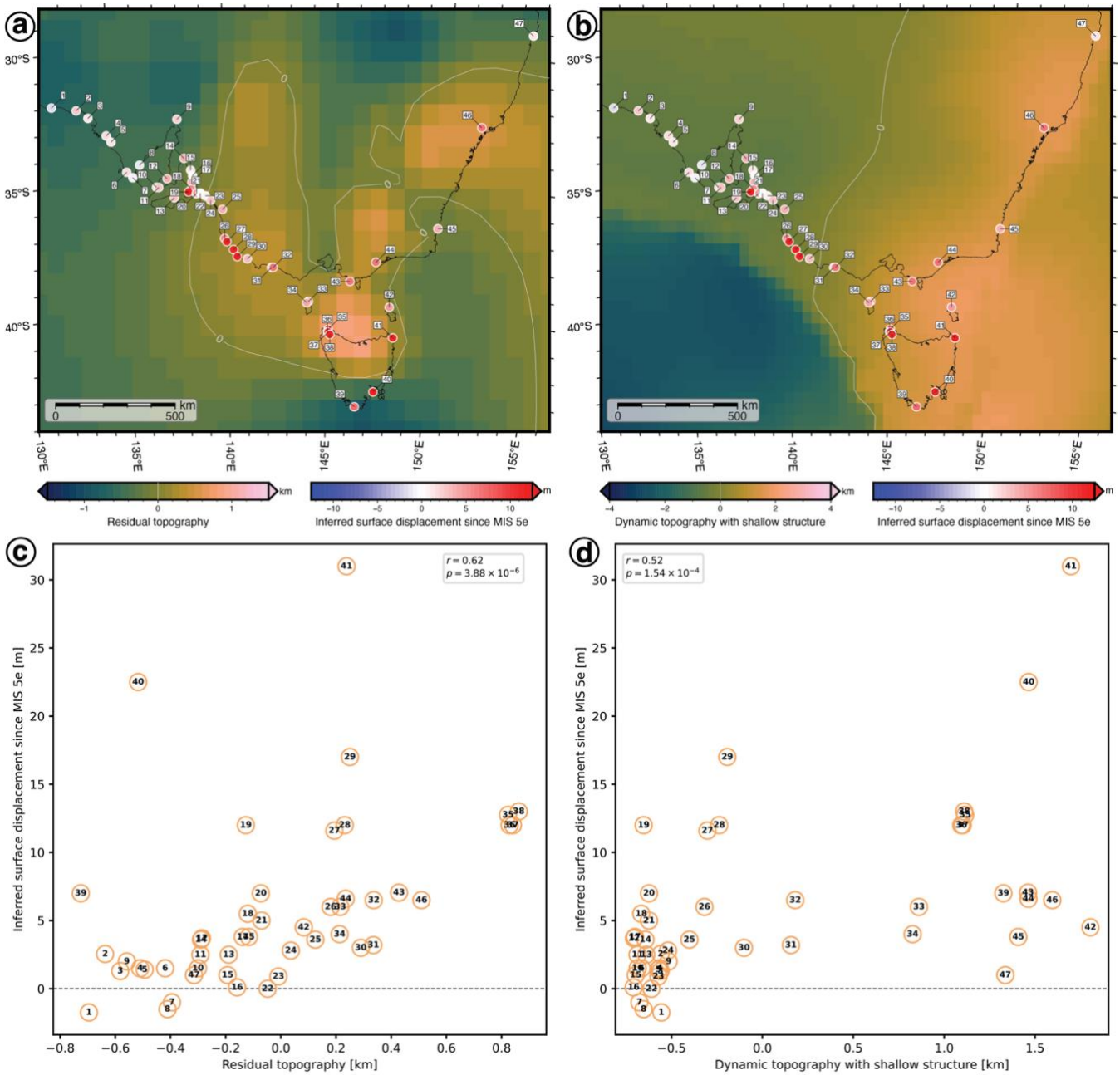

Figure 19. Inferred surface displacement of Last Interglacial shoreline successions, residual topography, and dynamic topography. a, Residual topography (Stephenson et al., 2024), **b**, dynamic topography (Davies et al., 2019), and Last Interglacial coastal successions at 47 locations (Table 1) shown as disks coloured by inferred surface displacement assuming a sea level 4 m higher during the Last Interglacial. **c-d**, Inferred surface displacement of Last Interglacial shoreline successions as a function of residual topography (**c**) and dynamic topography (**d**). *r* is the Spearman correlation coefficient, and *p* is the *p*-value for a Spearman ranking test with null hypothesis that two samples have no ordinal correlation.

5.3.5. Dynamic topography

Dynamic topography, which is the surface deflection predicted by a mantle flow model, depends on the distribution of sources of buoyancy and on the viscosity structure of the mantle (Flament et al., 2013; Hager and Clayton, 1989). A dynamic topography model that considers the structure of the lithosphere (Davies et al., 2019) presents some agreement with the inferred surface displacement of MIS 5e shoreline successions, with a statistically significant Spearman ranking correlation (r = 0.52, Fig. 19d). The model suggests that positive dynamic topography (> 1 km) could be contributing to the inferred uplift in Tasmania, and negative dynamic topography (< -0.5 km) is predicted for the three locations in the Gawler Craton for which subsidence was inferred (Fig. 19d). However, the predicted large positive dynamic topography (> 1.3 km) is at odds with limited inferred uplift in Bass Strait and on the East coast of Australia, and negative dynamic topography (<-0.5 km) is at odds with the inferred uplift between McCourt Cutting and Nene Valley (locations 27-29, ~12-17 m) and at location Normanville (location 19, 12 m, Fig. 19b,d).

6. Discussion: global, regional and local drivers of MIS 5e paleoshoreline elevations

6.1. MIS 5e sea level in southeastern Australia and globally

6.1.1. Inferred amplitude of MIS 5e peak sea level: globally and in southeastern Australia

There has been much discussion about the height of the sea surface during the MIS 5e highstand. In a compilation of paleosea level observations from Indo-Pacific coralline successions remote from plate boundaries, Veeh (1966) documented relative sea levels of 2–9 m APSL. From these observations a *de facto* value of 6 m APSL emerged in the literature for the MIS 5e highstand, which was consolidated by observations by Neumann and Moore (1975) in the northern Bahamas and by Ku et al. (1974) in Hawaii. Studies of neotectonism at plate

1067 boundaries consolidated the 6 m APSL value which was used commonly in calculations of
1068 uplift rates (Murray-Wallace and Woodroffe, 2014).

1069 Based on statistical modelling, Kopp et al. (2009) concluded that there is a 95% probability
1070 that global sea level reached at least 6.6 m APSL during MIS 5e, as distinct from local sea
1071 levels. The highstand is an indication of global mean sea level, which is proposed to have
1072 ranged between 6 and 9 m during MIS 5e (Creveling et al., 2015; Dutton et al., 2015; Lambeck
1073 et al., 2012). Even in tectonically highly stable areas, sea level observations are affected by
1074 evolving dynamic topography and glacial isostatic adjustments (Dutton et al., 2015), reducing
1075 the overall resolution in quantifying ice-equivalent sea level at a global scale. Whilst
1076 observations of peak sea level may be useful to infer the peak in global mean sea level, the
1077 range in sea level proxies for a given area and period may contain information about climatic
1078 or tectonic influences on sea level. The MIS 5e sea level range of 4 ± 1 m adopted in this study
1079 (Murray-Wallace, 2018; Murray-Wallace et al., 2016; Pan et al., 2018) is slightly below the
1080 MIS 5e eustatic sea level peak (> 6 m) proposed by Dutton et al. (2015). Modelling of glacial
1081 isostatic adjustment and dynamic topography since MIS 5e could determine whether southern
1082 Australian observations are representative of an ice-equivalent sea level. The dynamic
1083 topography history of southern Australia could also explain why MIS 5e sea level is inferred
1084 to have peaked at around 4 m in southeast Australia as opposed to 6 m. Keeping in mind that
1085 models are uncertain, at present-day, continental residual topography could be negative west
1086 of Bonney Reserve (location 24, Fig. 19a), oceanic residual topography could be negative west
1087 of Tasmania (Hoggard et al., 2017), and continental and dynamic topography could be negative
1088 west of Nelson (location 30, Fig. 19b). This negative residual and dynamic topography could
1089 explain why the inferred surface displacement in the Gawler Craton region is systematically
1090 less than in Western Australia (Murray-Wallace, 2002; O'Leary et al., 2013), where both
1091 oceanic and continental residual topography are presently positive (Hoggard et al., 2017;

1092 Stephenson et al., 2024) and neotectonic uplift is evident in the Cape Range region (Whitney
1093 and Hengesh, 2015).
1094
1095 *6.1.2. Two sea level highstands during the Last Interglacial (MIS 5e)?*
1096 The notion of a bipartite sea level highstand during the Last Interglacial (MIS 5e) was first
1097 documented from rapidly uplifting coastlines such as the Huon Peninsula in Papua New Guinea
1098 and eastern Indonesia, where well-dated coral reef successions are physically separated (Bloom
1099 et al., 1974; Chappell, 1974; Chappell and Thom, 1977; Chappell and Veeh, 1978; Stein et al.,
1100 1993). On Atauro Island, two distinct reef crests were noted of Last Interglacial age (Chappell
1101 and Veeh, 1978). On the Huon Peninsula, an early phase of reef development (Fringing reef:
1102 Reef VIIa; 138±5 ka) was distinguished from a late phase (Barrier reef: Reef VIIb; 118±2 ka),
1103 corresponding with uplift-corrected high sea level culminations of 5±5 m and 6.5±4 m APSL
1104 respectively (Aharon and Chappell, 1986). Subsequent uranium-series ages for corals from the
1105 Last Interglacial reef complex at Sialum on the Huon Peninsula, spanned 133±4 ka to 112±5
1106 ka for Reef VIIa and 117±7 ka to 103±4 ka for Reef VIIb (Stein et al., 1993). A continuous
1107 sea-level rise from 134 ka to 118 ka would represent a parsimonious interpretation of these
1108 results rather than a bipartite sea level highstand. The absence of ages between 132 ka and
1109 120 ka may relate to the combined effects of episodic co-seismic uplift of the region and
1110 associated erosion of the stratigraphical record. It is noted that corals of the two age groups
1111 occur within the barrier reef VIIb, with the younger corals having grown on an erosional surface
1112 on the barrier reef structure. A compound sea-level peak, however, is not evident in higher
1113 resolution oxygen isotope records from deep sea cores (Lisiecki and Raymo, 2005; Shackleton,
1114 1987) or the EPICA Dome C ice-core record from Antarctica which reveals a single peak for
1115 MIS 5e (Masson-Delmotte et al., 2010). In a similar manner, a compound sea level highstand

is not evident in the coastal sedimentary records of Florida or in California, USA (Muhs, 2022; Muhs et al., 2011).

A compound sea level highstand is also not evident in Last Interglacial sedimentary successions in southeastern Australia, where exposures of facies architecture are sufficiently clear for detailed assessment. Two exposures of the Glanville and Upper Bridgewater Formations provide insights about the late-stage relative sea level history during MIS 5e in southeastern Australia. The sites show that sea level rose during MIS 5e, in the absence of two sea level highstands (Murray-Wallace et al., 2016; Pan et al., 2018).

In a 3-km-long coastal cliff at Point Turton, Hardwicke Bay, southern Yorke Peninsula (location 12), the section reveals a single, upward deepening succession of bioclastic sediments, passing upwards from a basal unit of intertidal sand flat facies with abundant *Batillaria* (*Zeacumantus*) *diemenensis*, into richly fossiliferous shelly sands (coquina) of shallow subtidal origin, dominated by the bivalve mollusc *Katelysia* spp., and *Amesodesma angusta* (Pan et al., 2018). A bipartite sea level highstand is not evident from this sedimentary succession. At the time of deposition of the Glanville Formation at this locality, a seaway (Peesey Swamp) existed across southern Yorke Peninsula linking southern Spencer Gulf with Gulf St Vincent (Pan et al., 2021; Fig. 20).

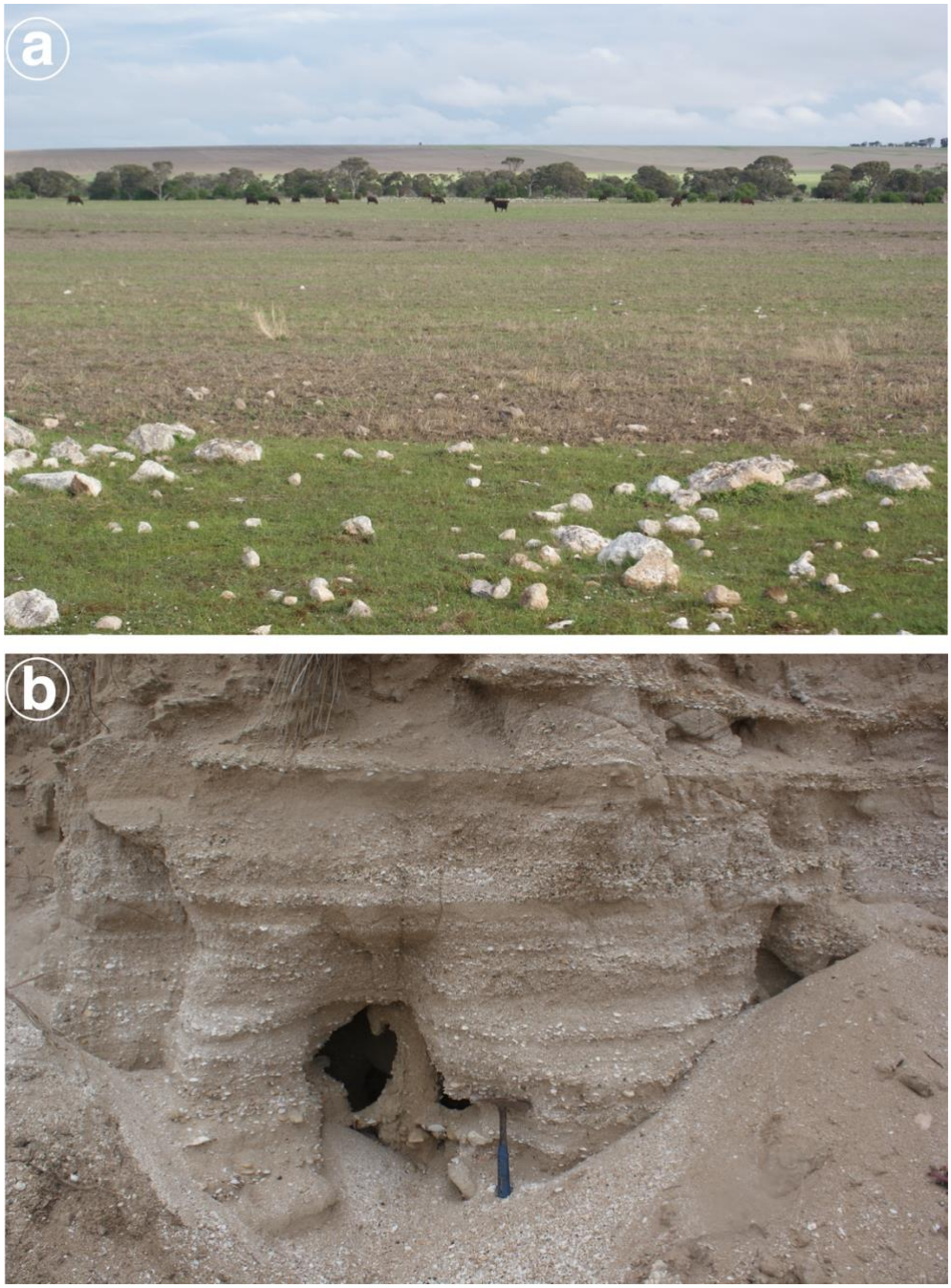

Figure 20. a, View looking southwest across Peesey Swamp, a landscape depression across southern Yorke Peninsula, southern Australia. The graded hillslope in the horizon extends up to 30 m APSL. Peesey Swamp is approximately 30 km long and represented a seaway during the Last Interglacial (MIS 5e) connecting southern Spencer Gulf and Gulf St Vincent. Detached calcrete blocks of the Last Interglacial Glanville Formation, containing fossil shells can be seen in the foreground and relate to deposition at the margin of the former seaway. **b**, Shell-rich bioclastic sand of the Last Interglacial (MIS 5e) Glanville Formation at Point Turton, southern Yorke Peninsula. The sedimentary succession, which crops out for 3 km was deposited when Peesey Swamp represented a seaway across Yorke Peninsula. The shelly assemblage is dominated by transported, disarticulated values of the mollusc *Amesodesma angusta*. The site is approximately 2.5 km from the entrance to the former seaway.

In the McCourt Cutting (location 27), a 1 km long drainage channel across the Last Interglacial Woakwine Range (Fig. 5d), near Robe in southern South Australia, a basal transgressive facies rises progressively landward, resting unconformably on an erosion surface formed on an older calcarenite of MIS 7 age (Murray-Wallace et al., 1999). The laterally persistent transgressive unit, comprising bioclastic sand and stringers of flint pebbles, extends up to 11.6 m APSL representing a relative sea-level rise, uncorrected for tectonic uplift, from 6.4 m to 11.6 m APSL. At the culmination of post-MIS 6 sea-level rise, an accumulation of indurated calcarenite clasts up to 40 cm (long-axis) were deposited on the seaward side of a relict sea stack in the core of the Woakwine Range (Murray-Wallace et al., 1999). Separated by an irregular scour surface, the transgressive unit is overlain by a progradational succession of subtidal and overlying intertidal sediments which formed during the sea level highstand of MIS 5e. The contact between subtidal and intertidal facies dips in a seaward direction, falling steadily from 11.5 m to 6.2 m APSL uncorrected for neotectonic uplift, over a horizontal distance of 200 m within the McCourt Cutting, indicating a relative sea level fall of 5.3 m following the culmination of MIS 5e sea-level rise. No subsequent relative sea-level rise in MIS 5e is evident in the facies architecture of this barrier landform complex.

The Woakwine Range back-barrier estuarine-lagoonal facies with articulated intertidal cockles (*Katelysia rhytiphora* and *K. scalarina*) is overlain by landward-advancing dune facies (Fig. 5e) and indicate a palaeosea-level of 9.2 m APSL, uncorrected for neotectonic uplift (Murray-Wallace et al., 1999). The back-barrier facies provides a more reliable paleosea-level estimate in view of the lower energy conditions at the time of sedimentation, in contrast to the higher wave energy that would have prevailed on the open ocean coastline. We assume an ice-equivalent sea level of 4±1 m APSL during the Last Interglacial based on data from Eyre and Yorke peninsulas (Murray-Wallace et al., 2016; Pan et al., 2018) and note that the landward limit of modern shelly gravel beaches occurs up to 2 m APSL. This in turn implies 5.6 m of

1170 uplift of the Woakwine Range at the site of McCourt Cutting since the Last Interglacial. A
1171 bipartite sea level highstand is not evident from this sedimentary succession, which tracks the
1172 culmination of the post-MIS 6 sea-level rise and the history of the MIS 5e highstand (Murray-
1173 Wallace et al., 1999).

1174 The observations from the Glanville Formation about relative sea-level trends during the
1175 Last Interglacial are corroborated by a sedimentary succession at the North East River on
1176 northern Flinders Island, Bass Strait. Here, a Last Interglacial upward shoaling estuarine
1177 succession reveals a transition from a basal accumulation of subtidal oyster bioherms, passing
1178 upwards through depauperate sands, culminating in three distinct shell beds (coquina –
1179 packstones) interbedded with bioclastic sand and minor shell fragments (Murray-Wallace and
1180 Goede, 1995; Fig. 5g, Fig. 7a,b). The mollusc packstones comprise mixed assemblages of
1181 articulated and disarticulated *Katelysia rhytiphora*, *Fulvia tenuicostata* and *Brachidontes* sp.,
1182 representing shallow subtidal to intertidal facies. The succession represents a relatively quiet-
1183 water depositional environment within an estuary with good tidal exchange, and continued
1184 sediment aggradation during MIS 5e. The interbedded sand and coquina units represent lateral
1185 facies changes associated with sandflat development and sediment aggradation with the
1186 progressive loss of accommodation space within the North East River paleoestuary. A bipartite
1187 sea level high stand is not evident from the succession.

1188 The beach ridge plain on Robbins Island, northwestern Tasmania, also does not indicate a
1189 bipartite sea level highstand during MIS 5e. The relative sea level record during MIS 5e is
1190 represented by three discrete phases: a sea level fall from 7 m to 6 m APSL between 130–
1191 126 ka, a stillstand at 5.75 ± 0.5 m APSL between 126–121 ka, and a subsequent fall in sea
1192 level between 119–114 ka (Goodwin et al., 2023). The overall pattern of sea level behaviour
1193 for the Robbins Island beach ridge succession is a progressive fall in sea level (forced
1194 regression) in accord with hydro-isostasy as noted from Last Interglacial and Holocene relative

sea level records (Belperio et al., 2002; Lambeck et al., 2012; Nakada and Lambeck, 1989; Stirling et al., 1995). In summary, a bipartite sea level highstand for MIS 5e is not evident from four geographically widely separated sites in southeastern Australia at which a continuous record of MIS 5e sea-level change is preserved.

6.2. A waning mantle upwelling at the end of the longest continental hotspot track

6.2.1. Inferring the location of the Cosgrove upwelling from MIS 5e shoreline elevations

Our main finding is that the inferred uplift since MIS 5e by 7 m to 31 m on the main island of Tasmania (Figs 8–9) could be explained by seismically slow (and therefore hot) mantle beneath Tasmania (Figs 15–17). This model fits to first order with reconstructions of the Cosgrove track, from which the hotspot is inferred to be presently located under northern Tasmania (Figs 8, 14–17). The absence of Quaternary volcanism in Tasmania (Fig. 8) suggests a waning Cosgrove mantle upwelling in which temperature anomalies are no longer large enough to trigger melting and volcanic eruptions. However, the Cosgrove mantle upwelling may still be buoyant enough to result in positive residual and dynamic topography (Fig. 19) above thin continental crust and lithospheric mantle (Fig. 18), and to drive the inferred uplift of MIS 5e shorelines by up to 31 m (Fig. 8b). A continental-scale compilation of temperature at 5 km depth (Geoscience Australia, 2021) reveals elevated temperatures in northeastern Tasmania, suggesting that the waning Cosgrove upwelling may still be hot enough to result in large geothermal gradients, which is reminiscent of a waning plume model previously proposed for eastern Europe (Ismail-Zadeh et al., 2024).

The inferred uplift on King Island and Flinders Island (locations 33, 34 and 42) in Bass Strait is relatively low (4.5 m to 6 m), even though these islands tend to be above seismically slow mantle (Figs 15-17). This discrepancy might be explained by continuing subsidence in Bass Basin (Middleton, 1982). Alternatively, these elevations may suggest that the waning

1220 Cosgrove mantle upwelling could have been located beneath Bass Strait before MIS 5e times,
1221 and that the continued northward motion of the Australian plate resulted in the present location
1222 of the upwelling being farther south under the main island of Tasmania.

1223 Tomographic models and geothermal gradients suggest that the waning Cosgrove
1224 upwelling could be further east than previously inferred from hotspot tracks (Figs 8, 14–17;
1225 Davies et al., 2019; Seton et al., 2019), keeping in mind that the location of a mantle upwelling
1226 is better characterised by a region than by discrete points that are most convenient to represent
1227 hotspot tracks. A related question is the spatio-temporal relationship between the Newer
1228 Volcanic Province and the Cosgrove upwelling. While early volcanic activity (between 7.9 Ma
1229 and ~4 Ma) in the Newer Volcanic Province (Heath et al., 2020) would temporally fit with the
1230 inferred latitude of the Cosgrove upwelling at these times (Fig. 8a). Indeed, the complex age
1231 distribution of eruptions in the Newer Volcanics Province is consistent with an influence of the
1232 Cosgrove mantle upwelling until ~4 Ma (Oostingh et al., 2017). Nevertheless, the eastern edge
1233 of the Newer Volcanic Province is ~200 km west from the western-most reconstructed
1234 Cosgrove hotspot track (Fig. 8a; Seton et al., 2019), which would require asthenospheric flow
1235 over 200 km without surface expression. Volcanic activity in the Newer Volcanic Province
1236 between 7.9 Ma and 0.8 Ma (Heath et al., 2020) has been linked to edge-driven convection at
1237 the trailing edge of a fast moving plate (Farrington et al., 2010), with a heat source restricted
1238 to the upper mantle (Davies and Rawlinson, 2014). Volcanic activity from ~700 ka at the
1239 Mount Burr Volcanic Complex and in the past 5,000 years at Mount Gambier and Mount
1240 Schank (Barbetti and Sheard, 1981; Robertson et al., 1996) is within 70 km of the Newer
1241 Volcanic Province (Fig. 12), and could be a continuation of edge-driven convection, favoured
1242 by crustal enrichment in CO_2 (Chivas et al., 1987). Volcanic activity is inferred to have
1243 migrated ~20 km to the southeast from the Mount Burr Volcanic Complex at ~700 ka to Mount
1244 Gambier at ~5 ka (Figs 12–13). This trend is opposite the to the reported diffuse age trend from

east to west in the last 1 Myr in the Newer Volcanics Province, which has been attributed to the orientation of lithospheric stress (Oostingh et al., 2017). Future research could compare the patterns of eruptions predicted by models of edge-driven convection to the age distribution of volcanoes younger than ~4 Ma in the Newer Volcanics Province.

6.2.2. Some remarks on Eastern Australian volcanism

Age progressive volcanism. The age distribution of 15 shield volcanoes and leucitite fields along the Cosgrove hotspot track (Davies et al., 2019) and of offshore seamounts along the Tasmantid and Lord Howe hotspot tracks (Seton et al., 2019) are consistent with the reconstruction of the Australian plate over stationary mantle upwelling for more than 30 Myr. Slow velocity anomalies extending into the lower mantle are not apparent at the inferred present-day location of the Cosgrove upwelling (Figs 15–17) or of the Tasmantid and Lord Howe tracks (Jackson et al., 2021). This is consistent with the proposed enriched mantle source of the Tasmantid and Lord Howe tracks (Eggins et al., 1991; Rogers et al., 2023), in the absence of a primitive helium mantle signature (Farley et al., 1992) that is used to geochemically fingerprint deep mantle plumes (Courtillot et al., 2003). The three hotspot tracks are roughly subparallel to one another. The Cosgrove and Tasmantid hotspot are about 700–1,000 km apart and the Tasmantid and Lord Howe hotspot tracks are about 300–500 km apart. While two 18–15 Myr old volcanoes ~300 km apart either side of the Great Dividing Range have been proposed to have originated from the same source (Crossingham et al., 2018), it seems unlikely that a stationary upper mantle source (less than 670 km deep) could trigger three hotspot tracks more than ~1,000 km apart. As another example, the well-documented Loa and Kea sub-parallel trends in Hawaiian volcanoes are only about ~30 km apart (Frey et al., 2016; Jones et al., 2017). While it is geochemically possible for the Tasmantid and Lord Howe tracks to be from the same mantle source (Eggins et al., 1991; Rogers et al., 2023), it seems likely that at

least two distinct stationary upper mantle sources would have needed to persist for at least 30 Myr to account for the three sub-parallel hotspots tracks along eastern Australia.

Non-age progressive volcanism. Even though Cenozoic age progressive volcanism has long been proposed in eastern Australia (Wellman and McDougall, 1974), most eastern Australian volcanoes do not follow an age progressive trend (Davies et al., 2015; Mather et al., 2020; Seton et al., 2019). A recent model proposes that eastern Australian mantle upwelling could be restricted to the upper mantle, with fluctuations in upwelling and magmatic activity from 60 Ma occurring as a response to changes in slab flux along the western Pacific margin (Mather et al., 2020).

6.3. Local drivers of MIS 5e shoreline elevations

The elevated MIS 5e shoreline at Normanville, Fleurieu Peninsula (location 19) can be explained by uplift of the Kangarilla Fault Block to the southeast of the Willunga Fault (Fig. 11). The Willunga Fault is a Cambrian rift fault reactivated as a thrust fault during the Delamerian Orogeny (c. 510–490 Ma; Foden et al., 2006), and again in compression from Eocene times (Preiss, 2019). Movement on the Willunga Fault is also evident from the deposition of the Ochre Cove Formation, a succession of proximal alluvial gravels at Sellicks Beach, which have been dated to Early-Middle Pleistocene age based on magnetostratigraphy (Pillans and Bourman, 2001). This suggests that the uplift of the Normanville location could be driven by reactivation of the Willunga Fault under the current thrust-strike slip fault local stress regime (Rajabi et al., 2017).

The increase in MIS 5e shoreline elevations between Lake Hawdon South to Nene Valley (locations 26-29) could be linked to volcanic activity at Mount Schank and Mount Gambier (Murray-Wallace, 2018; Sprigg, 1952). It is noted that the decrease in inferred uplift since MIS 5e times between Nene Valley and Nelson (locations 29 and 30, 14 m over 40 km) is more

rapid than the increase between Lake Hawdon South and Nene Valley (locations 26-29, 11 m over 100 km). Sprigg (1952) defined an axis separating opposing slopes, which he termed the Mt Gambier Upwarp (Fig. 12). The broadly linear axis trends northeast-southwest and truncates the mid-point of a dome on the upper surface of the Oligo-Miocene Gambier Limestone. According to Sprigg (1952), the Mt Gambier Upwarp is situated mid-way between the Pleistocene and Holocene volcanic centres, approximately 10 km west of Mount Gambier. The origin of this asymmetry could be elucidated by further mapping of geological structures including the upper surface of the Gambier limestone, and by the characterisation of further MIS 5e shoreline successions between Nene Valley and Nelson.

7. Conclusions

1. The present-day elevation and paleosea levels of 47 shoreline successions in southeastern Australia make it possible to infer surface displacement since their deposition during MIS 5e times. The paleosea levels suggest that sea level was 4 ± 1 m higher during the Last Interglacial than at present. This sea level is approximately two metres lower than the commonly assumed global MIS 5e sea level peak. Future research could quantify the effects of glacial isostatic adjustment and dynamic topography on sea level change since MIS 5e in the region to determine whether southern Australian observations are representative of an ice-equivalent sea level. There is no evidence for two MIS 5e sea-level peaks from the four distant sites at which a continuous record of MIS 5e sea-level change is preserved.
2. The inferred uplift since MIS 5e is largest in Tasmania, where it is likely caused by the waning Cosgrove mantle upwelling. Seismic tomographic models and the locations with largest inferred uplift of MIS 5e shoreline successions in Tasmania suggest that the Cosgrove hotspot could be farther east than previously proposed.

Volcanic activity from ~700 ka at the Mount Burr volcanic complex and ~5 ka at Mount Gambier and Mount Schank caused tilting of the Coorong coastal plain by up to ~10 m to the southeast since MIS 5e times. This volcanic activity is favoured by crustal enrichment in CO_2, and it could be driven by mantle convection along a steep lithospheric thickness gradient at the trailing edge of a fast-moving plate.

3. Fleurieu Peninsula is tectonically active, and the inferred surface displacements suggest reactivation of the Willunga Fault accommodating 6.5 m of upward displacement of the block to its southeast since MIS 5e times. In contrast, the Gawler craton is inferred to have been stable since MIS 5e times, with possible limited local subsidence.

Acknowledgments

NF and CVM-W were supported by ARC DP200101591. NF was supported by ARC FT230100001. The underlying basis for this research commenced in the early 1990s when CVM-W started field investigations on the Quaternary geological history of the Coorong Coastal Plain in southern South Australia, involving many field investigations. CVM-W acknowledges research support from the Australian Research Council over many years that made this work possible. We thank Dan Muhs and an anonymous reviewer for their constructive comments which have enhanced this work. Python Jupyter Notebooks to reproduce Figures 1, 6, and 8–19 are available at https://doi.org/10.5281/zenodo.18831341. Figures 1, 6, 8a, 9a, 11–17, 18a,b, and 19a,b were created using the open-source Python library PyGMT (Uieda et al., 2021; Wessel et al., 2019) and Figures 8b, 9b, 10, 18c,d and 19c,d were created using the open-source Python library Matplotlib (Hunter, 2007).

Author contributions (CRediT author statement)

Both authors contributed equally to the work. **Nicolas Flament:** Conceptualization, Methodology, Validation, Formal Analysis, Investigation, Writing – Original Draft, Visualization, Funding Acquisition. **Colin V. Murray-Wallace:** Conceptualization, Methodology, Validation, Formal Analysis, Investigation, Writing – Original Draft, Visualization, Funding Acquisition.

References

Aharon, P. and Chappell, J., 1986. Oxygen isotopes, sea level changes and the temperature history of a coral reef environment in New Guinea over the last 10^5 years. Palaeogeography, palaeoclimatology, palaeoecology, 56(3-4): 337-379.

Amaru, M., 2007. Global travel time tomography with 3-D reference models.

Barbetti, M. and Sheard, M., 1981. Palaeomagnetic results from Mounts Gambier and Schank, South Australia. Journal of the Geological Society of Australia, 28(3-4): 385-394.

Belperio, A., 1985. Quaternary geology of the Sandy Point and Outer Harbor-St. Kilda areas, Gulf St. Vincent, Quarterly Geological Notes. The Geological Survey of South Australia, pp. 2-6.

Belperio, A., 1993. Land subsidence and sea level rise in the Port Adelaide estuary: implications for monitoring the greenhouse effect. Australian Journal of Earth Sciences, 40(4): 359-368.

Belperio, A., Harvey, N. and Bourman, R., 2002. Spatial and temporal variability in the Holocene sea-level record of the South Australian coastline. Sedimentary Geology, 150(1-2): 153-169.

Belperio, A., Murray-Wallace, C. and Cann, J., 1995. The last interglacial shoreline in southern Australia: morphostratigraphic variations in a temperate carbonate setting. Quaternary International, 26: 7-19.

Blake, D.H., Kilgour, B., 1998. Geological Regions of Australia, 1:5 000 000 scale. In: G. Australia (Editor).

Blakemore, A., Murray-Wallace, C. and Lachlan, T., 2014. First recorded evidence of subaqueously-deposited late Pleistocene interstadial (MIS 5c) coastal strata above present sea level in Australia. Marine Geology, 355: 377-383.

Blakemore, A., Murray-Wallace, C.V., Westaway, K.E. and Lachlan, T.J., 2015. Aminostratigraphy and sea-level history of the Pleistocene Bridgewater Formation, Mount Gambier region, southern Australia. Australian Journal of Earth Sciences, 62(2): 151-169.

Bloom, A., Broecker, W., Chappell, J., Matthews, R. and Mesolella, K., 1974. Quaternary sea level fluctuations on a tectonic coast: New 230Th/234U dates from the Huon Peninsula, New Guinea. Quaternary research, 4(2): 185-205.

Bordoni, P. and Valensise, G., 1999. Deformation of the 125 ka marine terrace in Italy: tectonic implications. In: I. Stewart and C. Vita-Finzi (Editors), Coastal Tectonics. Geological Society, London, Special Publications, pp. 71-110.

1387 Bourman, R. and Lindsay, J., 1989. Timing, extent and character of late Cainozoic faulting on
1388 the eastern margin of the Mt Lofty Ranges, South Australia. Transactions of the Royal
1389 Society of South Australia, 113(1-2): 63-67.
1390 Bourman, R., Prescott, J., Banerjee, D., Alley, N. and Buckman, S., 2010. Age and origin of
1391 alluvial sediments within and flanking the Mt Lofty Ranges, southern South Australia:
1392 a Late Quaternary archive of climate and environmental change. Australian Journal of
1393 Earth Sciences, 57(2): 175-192.
1394 Bourman, R.P., Belperio, A., Murray-Wallace, C. and Cann, J., 1999. A last interglacial
1395 embayment fill at Normanville, South Australia, and its neotectonic implications.
1396 Transactions of the Royal Society of South Australia, 123: 1-15.
1397 Bourman, R.P., Murray-Wallace, C., Belperio, A. and Harvey, N., 2000. Rapid coastal
1398 geomorphic change in the River Murray Estuary of Australia. Marine Geology, 170(1-
1399 2): 141-168.
1400 Bourman, R.P., Murray-Wallace, C.V. and Harvey, N., 2016. Coastal Landscapes of South
1401 Australia. University of Adelaide Press.
1402 Bowden, A. and Colhoun, E., 1984. Quaternary emergent shorelines of Tasmania. In: B.
1403 Thom (Editor), Coastal Geomorphology in Australia. Academic Press, Sydney, pp.
1404 313–342.
1405 Bowen, D., 1985. Quaternary Geology. Pergamon, Oxford, 237 pp.
1406 Bryant, E., Young, R. and Price, D., 1997. Late Pleistocene marine deposition and TL
1407 chronology of the New South Wales, Australian coastline. Zeitschrift für
1408 Geomorphologie: 205-227.
1409 Cann, J. and Gostin, V., 1985. Coastal sedimentary facies and foraminiferal biofacies of the
1410 St Kilda Formation at Port Gawler, South Australia. Transactions of the Royal Society
1411 of South Australia, 109(4): 121-142.
1412 Chappell, J., 1974. Geology of coral terraces, Huon Peninsula, New Guinea: a study of
1413 Quaternary tectonic movements and sea-level changes. Geological Society of America
1414 Bulletin, 85(4): 553-570.
1415 Chappell, J. and Thom, B.G., 1977. Sea levels and coasts. In: J. Allen, J. Golson and B. Thom
1416 (Editors), Sunda and Sahul, pp. 275-291.
1417 Chappell, J. and Veeh, H., 1978. Late Quaternary tectonic movements and sea-level changes
1418 at Timor and Atauro Island. Geological Society of America Bulletin, 89(3): 356-368.
1419 Chivas, A.R., Barnes, I., Evans, W.C., Lupton, J.E. and Stone, J.O., 1987. Liquid carbon
1420 dioxide of magmatic origin and its role in volcanic eruptions. Nature, 326(6113): 587-
1421 589.
1422 Coe, A.L., 2003. The sedimentary record of sea-level change. Cambridge University Press.
1423 Colhoun, E., Turner, E. and Van de Geer, G., 1982a. Late Pleistocene marine molluscan
1424 faunas from four sites in Tasmania. Papers and Proceedings of the Royal Society of
1425 Tasmania, 116: 91-96.
1426 Colhoun, E., Van de Geer, G. and Mook, W., 1982b. Stratigraphy, pollen analysis, and
1427 paleoclimatic interpretation of Pulbeena Swamp, northwestern Tasmania. Quaternary
1428 research, 18(1): 108-126.
1429 Courtillot, V., Davaille, A., Besse, J. and Stock, J., 2003. Three distinct types of hotspots in
1430 the Earth's mantle. Earth and Planetary Science Letters, 205(3-4): 295-308.
1431 Creveling, J.R., Mitrovica, J.X., Hay, C.C., Austermann, J. and Kopp, R.E., 2015. Revisiting
1432 tectonic corrections applied to Pleistocene sea-level highstands. Quaternary Science
1433 Reviews, 111: 72-80.
1434 Crocker, R.L. and Cotton, B.C., 1946. Some raised beaches of the lower south-east of South
1435 Australia and their significance. Transactions of the Royal Society of South Australia,
1436 70: 64-82.

1437 Crossingham, T.J., Ubide, T., Vasconcelos, P.M. and Mallmann, G., 2018. Parallel plumbing
1438 systems feeding a pair of coeval volcanoes in eastern Australia. Journal of Petrology,
1439 59(6): 1035-1066.
1440 Daniel, R., 2002. Carbonate sediments of a cool water embayment, Streaky Bay, South
1441 Australia. PhD Thesis., University of Adelaide.
1442 Davies, D., Rawlinson, N., Iaffaldano, G. and Campbell, I.H., 2015. Lithospheric controls on
1443 magma composition along Earth's longest continental hotspot track. Nature,
1444 525(7570): 511-514.
1445 Davies, D.R. and Rawlinson, N., 2014. On the origin of recent intraplate volcanism in
1446 Australia. Geology, 42(12): 1031-1034.
1447 Davies, D.R., Valentine, A., Kramer, S.C., Rawlinson, N., Hoggard, M., Eakin, C. and
1448 Wilson, C.R., 2019. Earth's multi-scale topographic response to global mantle flow.
1449 Nature Geoscience, 12(10): 845-850.
1450 De Mooy, C., 1959. Notes on the geomorphic history of the area surrounding Lakes
1451 Alexandrina and Albert, South Australia. Transactions of the Royal Society of South
1452 Australia, 82: 99-118.
1453 Dutton, A., Carlson, A.E., Long, A.J., Milne, G.A., Clark, P.U., DeConto, R., Horton, B.P.,
1454 Rahmstorf, S. and Raymo, M.E., 2015. Sea-level rise due to polar ice-sheet mass loss
1455 during past warm periods. Science, 349(6244): aaa4019.
1456 Eggins, S., Green, D.H. and Falloon, T.J., 1991. The Tasmantid seamounts: Shallow melting
1457 and contamination of an EM1 mantle plume. Earth and Planetary Science Letters,
1458 107(3-4): 448-462.
1459 Eggins, S.M., Grün, R., McCulloch, M.T., Pike, A.W., Chappell, J., Kinsley, L., Mortimer, G.,
1460 Shelley, M., Murray-Wallace, C.V. and Spötl, C., 2005. In situ U-series dating by
1461 laser-ablation multi-collector ICPMS: new prospects for Quaternary geochronology.
1462 Quaternary Science Reviews, 24(23-24): 2523-2538.
1463 England, P. and Molnar, P., 1990. Surface uplift, uplift of rocks, and exhumation of rocks.
1464 Geology, 18(12): 1173-1177.
1465 Fanning, C.M., Reid, A. and Teale, G., 2007. A geochronological framework for the Gawler
1466 Craton, South Australia. Bulletin, 55. Geological Survey of South Australia, 258 pp.
1467 Farley, K., Natland, J. and Craig, H., 1992. Binary mixing of enriched and undegassed
1468 (primitive?) mantle components (He, Sr, Nd, Pb) in Samoan lavas. Earth and
1469 Planetary Science Letters, 111(1): 183-199.
1470 Farrington, R., Stegman, D.R., Moresi, L.-N., Sandiford, M. and May, D.A., 2010.
1471 Interactions of 3D mantle flow and continental lithosphere near passive margins.
1472 Tectonophysics, 483(1-2): 20-28.
1473 Firman, J., 1966. Stratigraphic units of Late Cainozoic age in the St Vincent Basin, South
1474 Australia. Quarterly Geological Notes, Geological Survey of South Australia, 17: 6-9.
1475 Flament, N., Gurnis, M. and Müller, R.D., 2013. A review of observations and models of
1476 dynamic topography. Lithosphere, 5(2): 189-210.
1477 Foden, J., Elburg, M.A., Dougherty-Page, J. and Burtt, A., 2006. The timing and duration of
1478 the Delamerian Orogeny: correlation with the Ross Orogen and implications for
1479 Gondwana assembly. The Journal of Geology, 114(2): 189-210.
1480 Frey, F.A., Huang, S., Xu, G. and Jochum, K.P., 2016. The geochemical components that
1481 distinguish Loa-and Kea-trend Hawaiian shield lavas. Geochimica et Cosmochimica
1482 Acta, 185: 160-181.
1483 Gardner, T., Webb, J., Pezzia, C., Amborn, T., Tunnell, R., Flanagan, S., Merritts, D.,
1484 Marshall, J., Fabel, D. and Cupper, M.L., 2009. Episodic intraplate deformation of
1485 stable continental margins: evidence from Late Neogene and Quaternary marine

terraces, Cape Liptrap, Southeastern Australia. Quaternary Science Reviews, 28(1-2): 39-53.
GEBCO Compilation Group, 2020. The GEBCO_2020 Grid – a continuous terrain model of the global oceans and land. British Oceanographic Data Centre, National Oceanography Centre, NERC.
Geoscience Australia, 2012. Surface Geology of Australia. In: Geoscience Australia (Editor). Geoscience Australia,.
Geoscience Australia, 2019. National Gravity Compilation 2019 ground elevation ellipsoid image (hillshade HSI). In: Geoscience Australia (Editor).
Geoscience Australia, 2021. Australian (OZTemp) Well Temperature Data Collection. In: Geoscience Australia (Editor).
Geoscience Australia, 2024. Geoscience Australia Earthquake Catalogue. In: Geoscience Australia (Editor).
Gill, E., 1988. Warrnambool-Port Fairy district. In: J.G. Douglas and J.A. Ferguson (Editors), Geology of Victoria. Geological Society of Australia pp. 374-379.
Gill, E.D. and Banks, M.R., 1956. Cainozoic history of Mowbray Swamp and other areas of north-western Tasmania. Records of the Queen Victoria Museum, 6. Museum committee, Launceston City Council, Launceston, 41 pp.
Goodwin, I.D., Mortlock, T.R., Ribo, M., Mitrovica, J.X., O'Leary, M. and Williams, R., 2023. Robbins Island: The index site for regional Last Interglacial sea level, wave climate and the subtropical ridge around Bass Strait, Australia. Quaternary Science Reviews, 305: 107996.
Greenway, T. and Phillipps, H., 1902. Notes on the geological features of southern Yorke Peninsula. Transactions of the Royal Society of South Australia, 26: 268-277.
Hager, B.H. and Clayton, R.W., 1989. Constraints on the structure of mantle convection using seismic observations, flow models, and the geoid. Mantle convection, 657.
Hails, J., Belperio, A., Gostin, V. and Sargent, G., 1984. The submarine Quaternary stratigraphy of northern Spencer Gulf, South Australia. Marine Geology, 61(2-4): 345-372.
Hallmann, N., Camoin, G., Webster, J.M. and Humblet, M., 2021. A standardized database of Marine Isotopic Stage 5e sea-level proxies on tropical Pacific islands. Earth Syst. Sci. Data, 13(6): 2651-2699.
Harte, M., 1998. Superfamily Veneroidea. In: P. Beesley, G. Ross and A. Wells (Editors), Mollusca: The Southern Synthesis. Fauna of Australia. CSIRO Publishing, Melbourne.
Heath, M., Phillips, D. and Matchan, E., 2020. Basalt lava flows of the intraplate Newer Volcanic Province in south-east Australia (Melbourne region): 40Ar/39Ar geochronology reveals~ 8 Ma of episodic activity. Journal of Volcanology and Geothermal Research, 389: 106730.
Hoggard, M.J., Czarnota, K., Richards, F.D., Huston, D.L., Jaques, A.L. and Ghelichkhan, S., 2020. Global distribution of sediment-hosted metals controlled by craton edge stability. Nature Geoscience, 13(7): 504-510.
Hoggard, M.J., Winterbourne, J., Czarnota, K. and White, N., 2017. Oceanic residual depth measurements, the plate cooling model, and global dynamic topography. Journal of Geophysical Research: Solid Earth, 122(3): 2328-2372.
Hossfeld, P.S., 1950. The Late Cainozoic history of the south-east of South Australia. Transactions of the Royal Society of South Australia, 73(2): 232-279.
Howchin, W., 1888. Remarks on a geological section at the new graving dock, Glanville, with special reference to a supposed old land surface now below sea level. Transactions of the Royal Society of South Australia, 10: 31-35.

Hunter, J.D., 2007. Matplotlib: A 2D graphics environment. Computing in science & engineering, 9(3): 90-95.
Ismail-Zadeh, A., Davaille, A., Besse, J. and Volozh, Y., 2024. East European sedimentary basins long heated by a fading mantle upwelling. Nature Communications, 15(1): 3915.
Jackson, M., Becker, T. and Steinberger, B., 2021. Spatial characteristics of recycled and primordial reservoirs in the deep mantle. Geochemistry, Geophysics, Geosystems, 22(3): e2020GC009525.
Jenkin, J.J., 1968. The geomorphology and Upper Cainozoic geology of south-east Gippsland, Victoria. Memoir, 27. Mines Department.
Jenkin, J.J., 1988. Western Port and Southern Gippsland. In: J.G. Douglas and J.A. Ferguson (Editors), Geology of Victoria. Geological Society of Australia pp. 392-402.
Jennings, J.N., 1959. The coastal geomorphology of King Island, Bass Strait, in relation to changes in the relative level of land and sea. Records of the Queen Victoria Museum, Launceston, 11. Museum Committee, Launceston City Council.
Jones, T., Davies, D.R., Campbell, I., Iaffaldano, G., Yaxley, G., Kramer, S.C. and Wilson, C.R., 2017. The concurrent emergence and causes of double volcanic hotspot tracks on the Pacific plate. Nature, 545(7655): 472-476.
Kaufman, A., Broecker, W., Ku, T.-L. and Thurber, D., 1971. The status of U-series methods of mollusk dating. Geochimica et Cosmochimica Acta, 35(11): 1155-1183.
Kiernan, K. and Lauritzen, S.-E., 2001. Dated speleothem evidence for uplift rates and terrace ages on the Tasmanian south coast. Zeitschrift für Geomorphologie, 45(6): 159–176.
Kopp, R.E., Simons, F.J., Mitrovica, J.X., Maloof, A.C. and Oppenheimer, M., 2009. Probabilistic assessment of sea level during the last interglacial stage. Nature, 462(7275): 863-867.
Kopp, R.E., Simons, F.J., Mitrovica, J.X., Maloof, A.C. and Oppenheimer, M., 2013. A probabilistic assessment of sea level variations within the last interglacial stage. Geophysical Journal International, 193(2): 711-716.
Ku, T.-L., Kimmel, M.A., Easton, W.H. and O'Neil, T.J., 1974. Eustatic sea level 120,000 years ago on Oahu, Hawaii. Science, 183(4128): 959-962.
Lambeck, K. and Chappell, J., 2001. Sea level change through the last glacial cycle. Science, 292(5517): 679-686.
Lambeck, K., Purcell, A. and Dutton, A., 2012. The anatomy of interglacial sea levels: the relationship between sea levels and ice volumes during the Last Interglacial. Earth and Planetary Science Letters, 315: 4-11.
Lewis, D. and Quilty, P.G., 2009. Foraminifera and palaeoenvironment of elevated late Pleistocene sands, White Rock Point, southeastern Tasmania.
Lisiecki, L.E. and Raymo, M.E., 2005. A Pliocene-Pleistocene stack of 57 globally distributed benthic δ18O records. Paleoceanography, 20(1).
Ludbrook, N., 1976. The Glanville Formation at Port Adelaide, Quarterly Geological Notes. The Geological Survey of South Australia.
Ludbrook, N., 1984. Quaternary molluscs of South Australia. Handbook, 9. Department of Mines and Energy, South Australia, 327 pp.
Macpherson, J. and Gabriel, C., 1962. Marine molluscs of Victoria. Melbourne University Press, Melbourne.
Marshall, J. and Thom, B., 1976. The sea level in the last interglacial. Nature, 263(5573): 120-121.
Masson-Delmotte, V., Stenni, B., Pol, K., Braconnot, P., Cattani, O., Falourd, S., Kageyama, M., Jouzel, J., Landais, A. and Minster, B., 2010. EPICA Dome C record of glacial and interglacial intensities. Quaternary Science Reviews, 29(1-2): 113-128.

Mather, B.R., Müller, R.D., Seton, M., Ruttor, S., Nebel, O. and Mortimer, N., 2020. Intraplate volcanism triggered by bursts in slab flux. Science Advances, 6(51): eabd0953.

McIntosh, P., Price, D., Grove, S. and Slee, A., 2013. Reply to Murray-Wallace et al.(2013): Comments on a paper by Slee et al.(2012). A reassessment of Last Interglacial deposits at Mary Ann Bay, Tasmania. Quaternary Australasia, 30(1): 6-8.

McLaren, S. and Rowe, P., 1996. The reliability of uranium-series mollusc dates from the western Mediterranean basin. Quaternary Science Reviews, 15(7): 709-717.

Middleton, M., 1982. The subsidence and thermal history of the Bass basin, Southeastern Australia. Tectonophysics, 87(1-4): 383-397.

Montelli, R., Nolet, G., Dahlen, F. and Masters, G., 2006. A catalogue of deep mantle plumes: New results from finite-frequency tomography. Geochemistry, Geophysics, Geosystems, 7(11).

Muhs, D.R., 2022. MIS 5e sea-level history along the Pacific coast of North America. Earth System Science Data, 14(3): 1271-1330.

Muhs, D.R., Simmons, K.R., Schumann, R.R. and Halley, R.B., 2011. Sea-level history of the past two interglacial periods: new evidence from U-series dating of reef corals from south Florida. Quaternary Science Reviews, 30(5-6): 570-590.

Murray-Wallace, C. and Belperio, A., 1991. The last interglacial shoreline in Australia—a review. Quaternary Science Reviews, 10(5): 441-461.

Murray-Wallace, C., Belperio, A., Cann, J., Huntley, D. and Prescott, J., 1996a. Late Quaternary uplift history, Mount Gambier region, South Australia. Zeitschrift für Geomorphologie. Supplement Band(106): 41-56.

Murray-Wallace, C., Beu, A., Kendrick, G., Brown, L., Belperio, A. and Sherwood, J., 2000. Palaeoclimatic implications of the occurrence of the arcoid bivalve *Anadara trapezia* (Deshayes) in the Quaternary of Australasia. Quaternary Science Reviews, 19(6): 559-590.

Murray-Wallace, C. and Bourman, R., 2002. Amino acid racemisation dating of a raised gravel beach deposit, Sellicks Beach, South Australia. Transactions of the Royal Society of South Australia, 126: 21-28.

Murray-Wallace, C., Goede, A. and Picker, K., 1990. Last Interglacial coastal sediments at Mary Ann Bay, Tasmania, and their neotectonic significance. Quaternary Australasia, 8: 26-32.

Murray-Wallace, C., Leary, S. and Kimber, R., 1996b. Amino acid racemisation dating of a last interglacial estuarine deposit at Largs, New South Wales, Proceedings-Linnean Society of New South Wales. Linnean Society Of New South Wales, pp. 213-222.

Murray-Wallace, C.V., 2000. 20. Quaternary coastal aminostratigraphy: Australian data in a global context. In: G.A. Goodfriend, M.J. Collins, M.L. Fogel, S.A. Macko and J.F. Wehmiller (Editors), Perspectives in amino acid and protein geochemistry. Oxford University Press, New York, pp. 279-300.

Murray-Wallace, C.V., 2011. Comment on:" New 40 Ar/39 Ar ages for selected young (< 1 Ma) basalt flows of the Newer Volcanic Province, southeastern Australia" by E. Matchan & D. Phillips. Quaternary Geochronology, 6(6): 598-599.

Murray-Wallace, C.V., 2018. Quaternary history of the Coorong coastal plain, southern Australia. Springer.

Murray-Wallace, C.V., Belperio, A., Bourman, R., Cann, J. and Price, D., 1999. Facies architecture of a last interglacial barrier: a model for Quaternary barrier development from the Coorong to Mount Gambier Coastal Plain, southeastern Australia. Marine Geology, 158(1-4): 177-195.

Murray-Wallace, C.V., Belperio, A., Dosseto, A., Nicholas, W.A., Mitchell, C., Bourman, R.P., Eggins, S.M. and Grün, R., 2016. Last interglacial (MIS 5e) sea-level determined from a tectonically stable, far-field location, Eyre Peninsula, southern Australia. Australian Journal of Earth Sciences, 63(5): 611-630.

Murray-Wallace, C.V., Bourman, R.P., Prescott, J.R., Williams, F., Price, D.M. and Belperio, A.P., 2010. Aminostratigraphy and thermoluminescence dating of coastal aeolianites and the later Quaternary history of a failed delta: The River Murray mouth region, South Australia. Quaternary Geochronology, 5(1): 28-49.

Murray-Wallace, C.V. and Cann, J., 2007. Quaternary history of the Coorong Coastal Plain, South Australia. XVII INQUA Congress, Excursion Guide A6. School of Earth & Environmental Sciences, University of Wollongong.

Murray-Wallace, C.V., Cann, J.H., Yokoyama, Y., Nicholas, W.A., Lachlan, T.J., Pan, T.-Y., Dosseto, A., Belperio, A.P. and Gostin, V.A., 2021. Late Pleistocene interstadial sea-levels (MIS 5a) in Gulf St Vincent, southern Australia, constrained by amino acid racemization dating of the benthic foraminifer Elphidium macelliforme. Quaternary Science Reviews, 259: 106899.

Murray-Wallace, C.V., Colhoun, E.A., Goede, A. and Quilty, P.G., 2013. Comments on slee et al.(2012). A reassessment of last interglacial deposits at Mary Ann Bay, Tasmania. Quaternary Australasia 29: 4-11. Quaternary Australasia, 30(1): 4-6.

Murray-Wallace, C.V. and Goede, A., 1991. Aminostratigraphy and electron spin resonance studies of late Quaternary sea level change and coastal neotectonics in Tasmania, Australia. Zeitschrift für Geomorphologie, 35(2): 129-149.

Murray-Wallace, C.V. and Woodroffe, C.D., 2014. Quaternary sea-level changes: a global perspective. Cambridge University Press.

Murray-Wallace, C. and Goede, A., 1995. Aminostratigraphy and electron spin resonance dating of Quaternary coastal neotectonism in Tasmania and the Bass Strait islands. Australian Journal of Earth Sciences, 42(1): 51-67.

Murray-Wallace, C.V., 2002. Pleistocene coastal stratigraphy, sea-level highstands and neotectonism of the southern Australian passive continental margin—a review. Journal of Quaternary Science, 17(5-6): 469-489.

Nakada, M. and Lambeck, K., 1989. Late Pleistocene and Holocene sea-level change in the Australian region and mantle rheology. Geophysical Journal International, 96(3): 497-517.

NASA JPL, 2013. NASA Shuttle Radar Topography Mission Global 3 arc second. In: N.L.P.D.A.A. Center (Editor).

Neumann, A.C. and Moore, W.S., 1975. Sea level events and Pleistocene coral ages in the northern Bahamas. Quaternary Research, 5(2): 215-224.

Nichol, S. and Murray-Wallace, C.V., 1992. A partially preserved last interglacial estuarine fill: Narrawallee Inlet, New South Wales. Australian Journal of Earth Sciences, 39(4): 545-553.

Nicholas, W., Lachlan, T., Murray-Wallace, C.V. and Price, G.J., 2019. Amino acid racemisation and uranium-series dating of a last interglacial raised beach, Kingscote, Kangaroo Island, southern Australia. Transactions of the Royal Society of South Australia, 143(1): 1-26.

Nielsen, B.J., 1964. Studies of the genus Katelysia Romer 1857 (Mollusca, Lamellibranchiata). Memoirs of the National Museum of Victoria, Melbourne, 26: 219-257.

O'Leary, M.J., Hearty, P.J., Thompson, W.G., Raymo, M.E., Mitrovica, J.X. and Webster, J.M., 2013. Ice sheet collapse following a prolonged period of stable sea level during the last interglacial. Nature Geoscience, 6(9): 796-800.

Ollier, C., 1978. Tectonics and geomorphology of the Eastern Highlands. In: J. Davies and M. Williams (Editors), Landform evolution in Australia. Australian National University Press, Canberra, pp. 5-47.
Ollier, C., 1986. Early landform evolution. In: D. Jeans (Editor), The Natural Environment. Sydney University Press, Sydney, pp. 97-116.
Oostingh, K., Jourdan, F., Matchan, E. and Phillips, D., 2017. 40Ar/39Ar geochronology reveals rapid change from plume-assisted to stress-dependent volcanism in the Newer Volcanic Province, SE Australia. Geochemistry, Geophysics, Geosystems, 18(3): 1065-1089.
Pan, T.-Y., Chivas, A.R., Murray-Wallace, C.V., Wheeler, D.J. and Bourman, R.P., 2026. Last Interglacial (MIS 5e) and Holocene Sea surface temperature and environmental reconstructions from Yorke Peninsula, southern Australia. Marine Geology, 494: 107731.
Pan, T.-Y., Murray-Wallace, C., Bourman, R. and García, A., 2021. Peesey Swamp—a Last Interglacial (MIS 5e) marine corridor across southern Yorke Peninsula, southern Australia. Australian Journal of Earth Sciences, 68(7): 952-967.
Pan, T.-Y., Murray-Wallace, C.V., Dosseto, A. and Bourman, R.P., 2018. The last interglacial (MIS 5e) sea level highstand from a tectonically stable far-field setting, Yorke Peninsula, southern Australia. Marine Geology, 398: 126-136.
Pedoja, K., Husson, L., Johnson, M.E., Melnick, D., Witt, C., Pochat, S., Nexer, M., Delcaillau, B., Pinegina, T. and Poprawski, Y., 2014. Coastal staircase sequences reflecting sea-level oscillations and tectonic uplift during the Quaternary and Neogene. Earth-Science Reviews, 132: 13-38.
Pillans, B. and Bourman, R., 2001. Mid Pleistocene arid shift in southern Australia, dated by magnetostratigraphy. Australian Journal of Soil Research, 39(1): 89-98.
Preiss, W., 2019. The tectonic history of Adelaide's scarp-forming faults. Australian Journal of Earth Sciences, 66(3): 305-365.
Preiss, W., Alexander, E., Cowley, W. and Schwarz, M., 2002. Towards defining South Australia's geological provinces and sedimentary basins. MESA Journal, 27: 39-52.
Prezant, R., 1998. Introduction – Subclass Heterodonta. In: P. Beesley, G. Ross and A. Wells (Editors), Mollusca: The Southern Synthesis, Fauna of Australia. CSIRO Publishing, Melbourne, pp. 301–307.
Quigley, M.C., Clark, D. and Sandiford, M., 2010. Tectonic geomorphology of Australia. In: P. Bishop and B. Pillans (Editors), Australian Landscapes. Geological Society, London, Special Publication, pp. 243-265.
Rajabi, M., Tingay, M., Heidbach, O., Hillis, R. and Reynolds, S., 2017. The present-day stress field of Australia. Earth-Science Reviews, 168: 165-189.
Raymond, O.L.e., Gallagher, R. (editor), Shaw, R., Yeates, A.N., Doutch, H.F., Palfreyman, W.D., Blake, D.H., Highet, L., 2023. Surface Geology of Australia 2012, 1:2.5 Million Scale - Faults. In: Geoscience Australia (Editor).
Roberts, D., 1984. The genus Katelysia (Bivalvia: Veneridae) in southern Australia. Journal of the Malacological Society of Australia, 6(3-4): 191-204.
Robertson, G., Prescott, J. and Hutton, J., 1996. Thermoluminescence dating of volcanic activity at Mount Gambier, South Australia. Transactions of the Royal Society of South Australia, 120: 7-12.
Rogers, A., Flanigan, M., Nebel, O., Nebel-Jacobsen, Y., Wang, X., Arculus, R.J., Miller, L., Smith, I., Mather, B.R. and Kendrick, M., 2023. The isotopic origin of Lord Howe Island reveals secondary mantle plume twinning in the Tasman Sea. Chemical Geology, 622: 121374.

Rovere, A., Ryan, D.D., Vacchi, M., Dutton, A., Simms, A.R. and Murray-Wallace, C.V., 2023. The World Atlas of Last Interglacial Shorelines (version 1.0). Earth Syst. Sci. Data, 15(1): 1-23.
Ryan, D.D., 2015. The Quaternary geomorphological evolution of the River Murray mouth and lakes region, southern Australia, University of Wollongong, 460 pp.
Sandiford, M., 2003. Neotectonics of southeastern Australia: linking the Quaternary faulting record with seismicity and in situ stress. In: R.R. Hillis and R.D. Müller (Editors), Evolution and Dynamics of the Australian Plate. Geological Society of Australia and Geological Society of America Special Publication, pp. 107-199.
Saputra, S.E.A., Fergusson, C.L., Dosseto, A., Dougherty, A. and Murray-Wallace, C.V., 2022. Late Quaternary neotectonics in the Bird's Head Peninsula (West Papua), Indonesia: implications for plate motions in northwestern New Guinea, western Pacific. Journal of Asian Earth Sciences, 236: 105336.
Schornick, J., 1973. Th-230/U-234 geochronology of marine shells from near Sale, E. Victoria, Australia. Proceedings of the Royal Society of Victoria, 86: 35-37.
Schwebel, D., 1984. Quaternary stratigraphy and sea-level variation in the southeast of South Australia. In: B. Thom (Editor), Coastal geomorphology in Australia, pp. 291-311.
Seton, M., Williams, S., Mortimer, N., Meffre, S., Micklethwaite, S. and Zahirovic, S., 2019. Magma production along the Lord Howe seamount chain, northern Zealandia. Geological Magazine, 156(9): 1605-1617.
Shackleton, N., 1987. Oxygen isotopes, ice volume and sea level. Quaternary Science Reviews, 6(3-4): 183-190.
Shackleton, N.J., Chapman, M., Sánchez-Goñi, M.F., Pailler, D. and Lancelot, Y., 2002. The classic marine isotope substage 5e. Quaternary Research, 58(1): 14-16.
Shennan, I., 2015. Handbook of sea-level research: framing research questions. Handbook of sea-level research: 3-25.
Sherwood, J., Barbetti, M., Ditchburn, R., Kimber, R., McCabe, W., Murray-Wallace, C., Prescott, J. and Whitehead, N., 1994. A comparative study of Quaternary dating techniques applied to sedimentary deposits in southwest Victoria, Australia. Quaternary Science Reviews, 13(2): 95-110.
Shin, J., 2013. Stratigraphy and geochronology of Quaternary marine terraces of Tasmania, southeastern Australia: implications on neotectonism. Geosciences Journal, 17(4): 429-443.
Short, A.D., 2020. Australian Coastal Systems: Beaches, Barriers and Sediment Compartments. Springer, Cham, 1241 pp.
Slee, A.J., McIntosh, P.D., Price, D.M. and Groved, S., 2012. A reassessment of last interglacial deposits at Mary Ann Bay, Tasmania. Quaternary Australasia, 29(2): 4-11.
Spearman, C., 1904. The Proof and Measurement of Association between Two Things. The American Journal of Psychology, 15(1): 72-101.
Sprigg, R., 1959. Stranded sea beaches and associated sand accumulations of the upper southeast. Transactions of the Royal Society of South Australia, 82: 183-193.
Sprigg, R. and Boutakoff, N., 1953. Summary report on the petroleum possibilities of the Gambier Sunklands. Mining Review, Adelaide, 95: 41-62.
Sprigg, R.C., 1952. The Geology of the South-East Province of South Australia: With Special Reference to Quaternary Coast-line Migrations and Modern Beach Developments. Bulletin, 29. Government Printer, South Australia.
Stein, M., Wasserburg, G., Aharon, P., Chen, J., Zhu, Z., Bloom, A. and Chappell, J., 1993. TIMS U-series dating and stable isotopes of the last interglacial event in Papua New Guinea. Geochimica et Cosmochimica Acta, 57(11): 2541-2554.

Stephenson, S.N., Hoggard, M.J., Holdt, M.C. and White, N., 2024. Continental residual topography extracted from global analysis of crustal structure. Journal of Geophysical Research: Solid Earth, 129(4): e2023JB026735.

Stirling, C., Esat, T., McCulloch, M. and Lambeck, K., 1995. High-precision U-series dating of corals from Western Australia and implications for the timing and duration of the Last Interglacial. Earth and Planetary Science Letters, 135(1-4): 115-130.

Sutherland, F. and Kershaw, R., 1971. The Cainozoic geology of Flinders Island, Bass Strait, Papers and Proceedings of the Royal Society of Tasmania, pp. 151-178.

Tate, R., 1879a. The Anniversary address of the President, Transactions and Proceedings and Report of the Philosophical Society of Adelaide, South Australia, for 1878-1879, pp. XXXIX–IXXV.

Tate, R., 1879b. The natural history of the country around the head of the Great Australian Bight, Transactions and Proceedings and Report of the Philosophical Society of Adelaide, South Australia, for 1878-1879, 1–2.

Tate, R., 1882. The geology about Port Wakefield. Transactions and Proceedings and Report of the Royal Society of South Australia, 4: 45-46.

Thom, B. and Murray-Wallace, C., 1988. Geological note: last Interglacial (Stage 5e) estuarine sediments at Largs. New South Wales. Australian Journal of Earth Sciences, 35: 571-574.

Thrastarson, S., van Herwaarden, D.P., Noe, S., Josef Schiller, C. and Fichtner, A., 2024. REVEAL: A global full-waveform inversion model. Bulletin of the Seismological Society of America, 114(3): 1392-1406.

Twidale, C., 2007. Ancient Australian Landscapes. Rosenberg, Sydney, 144 pp.

Uieda, L., Tian, D., Leong, W.J., Jones, M., Schlitzer, W., Toney, L., Grund, M., Yao, J., Magen, Y. and Materna, K., 2021. PyGMT: A Python interface for the generic mapping tools. Zenodo.

Van de Geer, G., Colhoun, E. and Mook, W., 1986. Stratigraphy, pollen analysis and paleoclimatic interpretation of Mowbray and Broadmeadows Swamps, North Western Tasmania. Australian Geographer, 17(2): 121-133.

Veeh, H.H., 1966. Th230/U238 and U234/U238 ages of Pleistocene high sea level stand. Journal of Geophysical Research, 71(14): 3379-3386.

Wellman, P. and McDougall, I., 1974. Cainozoic igneous activity in eastern Australia. Tectonophysics, 23(1-2): 49-65.

Wessel, P., Luis, J.F., Uieda, L.a., Scharroo, R., Wobbe, F., Smith, W.H. and Tian, D., 2019. The generic mapping tools version 6. Geochemistry, Geophysics, Geosystems, 20(11): 5556-5564.

Whitney, B.B. and Hengesh, J.V., 2015. Geomorphological evidence for late Quaternary tectonic deformation of the Cape Region, coastal west central Australia. Geomorphology, 241: 160-174.

Woods, J.E., 1862. Geological observations in South Australia: principally in the district south-east of Adelaide. Longman, Green, Longman, Roberts, & Green.

Young, R., Bryant, E. and Price, D., 1993. Last interglacial sea levels on the south coast of New South Wales. The Australian Geographer, 24(2): 72-75.